SSD

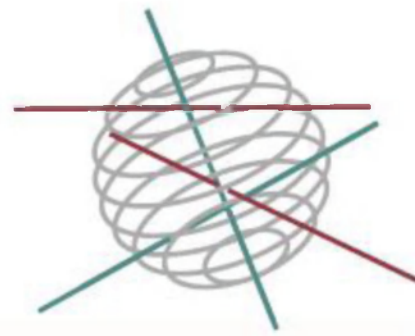## SCIENCE FOR A SUSTAINABLE DEVELOPMENT

ATMOSPHERIC DEPOSITION FLUXES TO THE BELGIAN MARINE WATERS ORIGINATING FROM SHIP EMISSIONS

«SHIPFLUX»

L. Bencs, B. Horemans, A. Jolanta Buczyńska,
R. Van Grieken, P. Viaene, N. Veldeman, F. Deutsch,
B. Degraeuwe, M. Van Poppel, D. Lauwaet, K. De Ridder,
L. Janssen, B. Maiheu, M. Vanhulsel, S. Janssen, L. Blyth,
C. Mensink

ENERGY

TRANSPORT AND MOBILITY

AGRO-FOOD
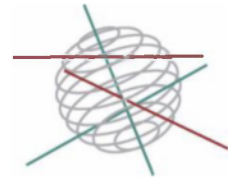
HEALTH AND ENVIRONMENT

CLIMATE

BIODIVERSITY

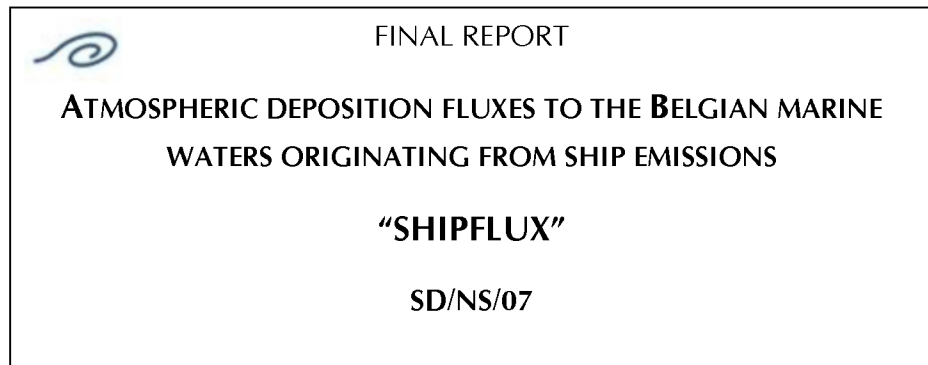ATMOSPHERE AND TERRESTRIAL AND MARINE ECOSYSTEMS

TRANSVERSAL ACTIONS

.be

SCIENCE FOR A SUSTAINABLE DEVELOPMENT

(SSD)

North Sea

FINAL REPORT

ATMOSPHERIC DEPOSITION FLUXES TO THE BELGIAN MARINE WATERS ORIGINATING FROM SHIP EMISSIONS

"SHIPFLUX"

SD/NS/07

Promotors

René Van Grieken
University of Antwerp (UA)
Universiteitsplein 1
BE-2610 Antwerp, Belgium

Clemens Mensink
Flemish Institute for Technological Research (VITO)
Boeretang 200
BE-2400 Mol, Belgium

Authors

László Bencs, Benjamin Horemans, René Van Grieken (UA)
Anna Jolanta Buczyńska
(UA, Joint Research Centre IRMM, Retieseweg 111, BE-2440 Geel)

Peter Viaene, Nele Veldeman, Felix Deutsch, Bart Degraeuwe,
Martine Van Poppel, Dirk Lauwaet, Koen De Ridder, Liliane Janssen,
Bino Maiheu, Marlies Vanhulsel, Stijn Janssen, Lisa Blyth, Clemens Mensink
(VITO)

Universiteit Antwerpen

vito
vision on technology

L. Bencs, B. Horemans, R. Van Grieken, A. Jolanta Buczyńska, P. Viaene, N. Veldeman, F. Deutsch, B. Degraeuwe, M. Van Poppel, D. Lauwaet, K. De Ridder, L. Janssen, B. Maiheu, M. Vanhulsel, S. Janssen, L. Blyth, C. Mensink. *Atmospheric deposition fluxes to the Belgian marine waters originating from ship emissions - SHIPFLUX*. Final Report. Brussels : Belgian Science Policy Office 2012 – 109 p. (Research Programme Science for a Sustainable Development)

TABLE OF CONTENT

Scope and aims

Anthropogenic pollution by atmospheric and riverine inputs triggers the phenomenon of coastal eutrophication (i.e., increased bio-productivity) in the Southern Bight of the North Sea, which is a serious environmental concern in present years. For the past decades, the atmospheric input has increased to an extent that it is commensurable to that of the riverine inputs (Rendell et al., 1993). Consequently, the contribution of atmospheric pollutants to coastal eutrophication initiates an increasing scientific and policy-related interest at intra and intergovernmental levels.

Besides terrestrial inputs through industry, traffic and agriculture, an additional and very important source of atmospheric pollutants is the international ship traffic (Cooper et al., 1996; Bartnicki and Fagerli, 2006). Ship emission related mortality has just recently been estimated to be considerable in populated areas located at nearby marine environments (Corbett et al., 2007). Although it has not yet been studied before, ship emissions are also believed to be a source of several kinds of persistent organic pollutants (POPs). POPs are those pollutants, which stay permanent (without any changes) in environmental compartments, bio-accumulate through the food chain, and pose a risk of causing adverse effects to human health and the environment. POPs include a wide range of xenobiotic chemicals, for instance, polycyclic aromatic hydrocarbons (PAHs), which are reported to be present in ship exhaust fumes (Moldanová et al., 2009). Consequently, their determination/mapping over marine areas, besides inorganic tracers, would be important for the identification and characterization of ship-emission related pollution.

Estimation of annual ship emission from the Belgian part of the North Sea, which has a water surface of 3600 km^2, has already been done for SO_2, NO_x, and CO_2 by taking into account national and international traffic on these waters, and also power and fuel usage of ships/boats (De Meyer et al., 2008). These ship emission estimates are based on a bottom-up, activity based methodology, covering more than 90 % of the ship activity, complemented with a top-down fuel consumption methodology for the rest activities. Compared to the Belgian national inventory data, the obtained emissions of SO_2 and NO_x correspond to 30 % and 22 % of the total national emission, hence a significant contribution (De Meyer et al., 2008). It should be mentioned that the study focuses on only a few gaseous pollutants, which rather limits the knowledge about the overall atmospheric impact of shipping emissions in terms of other, emission-related gaseous compounds (e.g., nitric acid) and aerosols.

According to the ship emission related literature, there is a certain gap of knowledge regarding the gaseous and aerosol phase related pollutant identification, quantification, and characterization of their fate (transport/transformation/deposition) over North Sea waters. Especially the role of pollutants released from the large cargo/ferry boats taking part in the national and international ship-traffic has not yet been characterized. Atmospheric nutrients and toxic substances deposited to the marine environment can be accumulated and amplified in the food chain, and might contribute to coastal eutrophication. Therefore, their influence on marine ecosystems certainly needs to be systematically studied. Apparently, the first stage of such a multi-disciplinary investigation is to map the concentrations and deposition of anthropogenic pollutants over marine areas with the assistance of experimental/model approaches, which is the main aim of this study.

Work Package 1: Sampling and analysis of gaseous and particulate air pollutants

1.1. Methodology and equipment

1.1.1. Sampling campaigns and areas

In this two-year-long project, a total of seven, about ten-day-long sampling campaigns has been organized concurrently onboard Belgian research vessels and at a coastal research station in De Haan. One sampling campaign was conducted onboard the research vessel Zeeleeuw and the other campaigns onboard the research vessel (R/V) Belgica (Figure 1), according to the following schedule:

Campaign 1:   March 17-30, 2010 (Zeeleeuw)
Campaign 2:   May 3-7, 2010 (Belgica-1)
                       May 10-12, 2010 (Belgica-2)
Campaign 3:   September 6-9, 2010 (Belgica-3)
                       September 10-16, 2010 (Belgica-4)
Campaign 4:   October 4-8, 2010 (Belgica-5)
                       October 11-15, 2010 (Belgica-6)
Campaign 5:   January 31-February 4, 2011 (Belgica-7)
                       February 7-February 11, 2011 (Belgica-8)
Campaign 6:   March 14-18, 2011 (Belgica-9)
                       March 21-25, 2011 (Belgica-10)
Campaign 7:   May 14-18, 2011 (Belgica-11)
                       May 21-25, 2011 (Belgica-12)

Figure 1. The research vessel Belgica

The coastal sampling site selected for this study as a terrestrial background site, De Haan, Belgium, is a small village at the coast of the Belgian North Sea located at coordinates of 51.28688° N and 3.06098° E. The area at which the sampling equipment was deployed is a small research station of the Flanders Marine Institute (Vlaams Instituut voor de Zee - VLIZ), located around 500 m of the coast among the sand-dunes, it being characteristic for this coastal region under study.

Figure 2. The Belgian Continental Shelf and the shipping lanes (source: C-Power, www.c-power.be)

During the onboard sampling campaigns, various marine areas of the Southern Bight of the North Sea have been visited. The sampled areas were in and around the main international shipping route of the Southern North Sea (Figure 2), the shipping routes to Zeebrugge, and the Schelde estuary, or out of the shipping lanes to acquire marine background pollution data. Detailed description of the routes covered by the Belgica have been recorded by the ODAS system and the visited maritime areas are also presented in the Belgica cruise reports on campaigns 2010/12, 2010/13, 2010/22, 2010/23, 2010/25c, 2010/26, 2011/2, 2011/3, 2011/7, 2011/8, 2011/15 and 2011/16.

1.1.2. Meteorological data

The meteorological parameters, such as air temperature (T_a), air pressure (p_a), relative humidity (RH), wind-speed, wind direction and precipitation were logged during the onboard campaigns and also at the coastal sampling site. During the Zeeleeuw and De Haan campaigns, the weather data were received from a meteorological database (IVA MDK - afdeling Kust - Meetnet Vlaamse Banken), and also from a small meteorological weather-station deployed at the sampling site by colleagues from VLIZ. The weather data at this station were logged every second by a computer. For the cruises onboard the Belgica, the data were acquired from the ODAS database, along the exact geo-coordinates of the vessel during the cruises.

1.1.3. Monitoring of criteria gaseous pollutants

The gaseous pollutants, NO, NO_2, NOx, O_3 and SO_2, were measured on-line using a 1 min-averaging time. The instrumentation used was a mobile measurement platform using reference analysers. The integrated platform, called "Airpointer" uses standard analysis techniques for different pollutants (NOx: chemiluminescence; O_3: UV photometry; SO_2: UV chemiluminescence). Measurements were carried out using two identical measurement units.

Airpointers (see below for a description) were installed onboard of the R/V Zeeleeuw or the Belgica and at a coastal location in De Haan. Measurements were carried out during the first sampling campaign from 18/3/2010 to 30/3/2010 and during the second sampling campaign from 4/10/2010 to 15/10/2010. Sampling was carried out continuously and the results for the concentrations of gaseous pollutants were combined with the exact position of the Zeeleeuw or the Belgica (via GPS) as a function of time. In this way pollutant concentrations could be attributed to the location where they were measured.

As concentration changes can be expected to occur on a small lateral scale (and hence on a short timescale, e.g. when the Zeeleeuw is crossing a major shipping route), fastly responding measurement techniques are needed to map these changes in pollutant concentrations. Additionally, in order to know the difference between concentrations above the North Sea and above land, the concentrations were measured both onboard of the Zeeleeuw/Belgica and at a fixed location located at the coast (De Haan).

It must be noted that the measurement results of a single crossing of a shipping route are probably strongly influenced by the number of ships present at that moment and also by the emissions of the individual ships present. As the aim of the project is not to measure/calculate the contribution of individual ship emissions to the deposition of nutrients, but rather to investigate the total or mean contribution of ship emissions, a sufficiently large number of observations has to be mapped in order for them to be representative for the emissions of all ships travelling through the Belgian marine waters.

Datapoints that have been collected when the sampling instrumentation probably was under influence of the emissions of the Zeeleeuw/Belgica itself have been removed. This can be the case when the wind was blowing from the exhaust of the ship to the instruments and when the ship has not been cruising (speed of 0 m/h). When the ship is cruising, the measured concentrations are not influenced by the ship emissions because the instrumentation had been placed in front of the exhaust.

For model validation purposes, the recorded short-term highly elevated concentrations of NO_2 and SO_2 above a certain threshold value have been flagged in the database and were not used for the comparison between observations and model results. As most of these high peak values occurred for a very short period of time, they do not play an important role for the overall concentrations during the sampling campaigns anyway. Hence, in order not to count them for the model validation, this pragmatic approach had been followed.

1.1.4. Sampling procedures

Gaseous nitric acid, nitrous acid and ammonia were sampled actively with an URG-2000-01K annular denuder during each sampling campaign. The denuder tubes were coated with a 1:1 diluted methanol solution of 1% (m/v) sodium carbonate plus 1% (v/v) glycerol and 1% (m/v) citric acid plus 1 % (v/v) glycerol in methanol for the collection of acidic and alkaline gases, respectively. The air flow rate was set at 10 dm^3/min.

Size-segregated particulate matter was collected with Harvard-impactors at aerosol size-ranges of PM_1, $PM_{2.5}$ and PM_{10}. Pallflex type TK15-G3M membrane filters (Pall Life Sciences, Ann Arbor, MI, USA) with 0.3 μm pore-size were applied. Each filter unit was attached to a vacuum pump.

The pumps maintained a constant air-flow rate of 10 or 23 L/min. The sampled aerosol filters were subjected to ion chromatography (IC) and EDXRF analysis.

A Graseby&Andersen (Atlanta, GA, USA) Model GMW high volume aerosol sampler was applied in campaigns 1-3, whereas in the other campaigns a Digitel Model DHA-80 (Hegnau, Switzerland) automated high volume sampler was used, for the collection of aerosols (total PM), and PM_{10}, respectively, on Whatmann quartz fibre filters (QFFs). The filters were preheated at 550 °C for at least 6 h before sampling; this was done in order to remove the organic contaminants and lower the blank levels.

1.1.5. Ion-chromatography (IC) sample preparation and analysis

Water-soluble fraction of aerosols (ionic compounds, e.g., ammonium, nitrate and nitrite salts) were quantitatively analysed by means of IC. Filters were exposed to ultrasonic aided leaching in 5 ml ultrapure water (Milli-Q) and the leachate solutions were analysed for their cationic and anionic content.

For the analysis of gaseous nitric acid, nitrous acid and ammonia, the absorber-tubes of the denuders were eluted with 10 ml Milli-Q and the leachate solutions were analyzed with IC for their NO_2^-, NO_3^- and NH_4^+ content, from which the air concentration of the corresponding pollutant was calculated.

A Dionex Model DX-120 ion chromatograph, equipped with Dionex IonPack CS16 cation and AS14 anion exchanger columns and a CDM-3 conductivity detector, was applied for the determination of various ionic species. For sample introduction, both the standard and sample solutions were injected through a 20 µl loop. The eluents applied for the anion and cation exchangers were 3.5 mM Na_2CO_3 plus 1.0 mM $NaHCO_3$, and 17 mM H_2SO_4, respectively, with flow rates of 1.2 and 1.0 ml/min. For the detection of ions, the conductivity of the sample/standard solutions was monitored. For the suppression of the conductivity of the eluent, the ASRS-300 ULTRA and CSRS-300 ULTRA suppression columns were applied for the anion and cation exchanger, respectively. The retention times of the peaks were used for the assignment of diverse ions in the sample solutions. Calibration was made against two sets of standard solutions, each consisting of five solutions of the measured anions and cations, respectively. Two replicate measurements were performed for each sample/standard solution, from which data the average and the standard deviation (SD) values were calculated.

1.1.6. Elemental analysis of aerosol content

The heavy metal content of the various aerosol fractions was determined by energy dispersive X-ray fluorescence (EDXRF) spectrometry. For this analysis, a Model Epsilon 5 high-energy EDXRF spectrometer (PANalytical, Almelo, The Netherlands) was applied. This instrument uses a polarized X-ray beam, and is equipped with a 600 W Gd-anode with an adjustable voltage, in the range from 25 to 100 kV and a current from 0.5 to 24 mA. There are 13 secondary fluorescencers (Al, CaF_2, Ti, Fe, Co, Ge, KBr, Zr, Mo, Ag, CsI, CeO_2 and W) and two Barkla-scatterers (Al_2O_3 and B_4C). There is also the possibility for using a primary beam filter between tube and target; the following filter materials are present: Al 100 μm, Al 500 μm, Cu 250 μm, Zr 125 μm and Mo 250 μm. Detection is performed with a high purity Ge-detector (HPGe) in the energy range from 0.7 to 200 keV and a resolution at Mn $K\alpha$ of < 165 eV and it needs cooling to the temperature of liquid nitrogen. Tube, target, sample and detector are arranged in a Cartesian geometry in order to obtain polarization. For the determinations, a vacuum atmosphere was applied in the measurement chamber. To compensate for possible problems with sample inhomogeneity, a spinner was used to rotate the samples during measurements. The spectrometer is equipped with an autosampler consisting of four trays, each containing 8 racks for sample cups; two additional trays can be added if necessary. The complete measuring process is computer controlled. In the software

package (Epsilon 5 software) the complete sample quantification process is built in; including the acquisition of the spectrum, the spectrum fitting over to the calibration and the quantification.

The measurement conditions for each element are summarized in Table 1. For each target an access (measurement) time of 300 s was applied, hence the total time for the analysis of one sample was around 40 min. Up to 20 elements can be quantified, including several heavy metals such as Cd, Pb and Sb. The calibration is made in $\mu g/cm^2$, when taking in account the deposited filter area (in this case a circle with a diameter of 29 mm), this can be converted to μg per filter. Since volume of air-mass passed through the filter is being recorded by the gas-counter, this can again be converted to ng/m^3, which is the regular unit of air pollution. These values were used in further data processing. More information about the optimization of this EDXRF method can be found elsewhere (Spolnik et al., 2005).

Table 1. Measurement conditions for the EDXRF analysis

Element	Secondary target	Accelerating voltage (kV)	Current (mA)	Analytical line
Al-Ca	Ti	35	17	$K\alpha$
Ti-V	Fe	50	12	$K\alpha$
Cr-Zn	Ge	100	6	$K\alpha$
Se, Pb	Zr	100	6	$K\alpha$, $L\beta$
Sr	Mo	100	6	$K\alpha$
As	KBr	100	6	$K\alpha$
Cd	CsI	100	6	$K\alpha$
Sb	CeO_2	100	6	$K\alpha$

1.1.7. Black carbon (BC) monitoring and gravimetry of aerosols

Black carbon (soot) content of atmospheric air was monitored with the application of an AE-42 Aethalometer (Magee Scientific, Berkeley, CA, USA). This instrument facilitates the combination of optical absorption measurements at wavelengths of 880 nm for black carbon and of 370 nm designated as 'UVPM', interpreted as an indicator of "UV-active" aromatic organic compounds (e.g., PAHs).

BC concentrations were monitored semi-continuously (i.e., in 1 minute intervals) during each sampling cruise. The instrument was synchronized with the computer of the onboard data acquisition system (ODAS), which logged every 10 seconds the key parameters of the boat, such as the geographical coordinates, ship heading, relative wind speed and relative wind direction. The output data files of the ODAS and AE42 were aligned manually in a PC. Each BC concentration obtained from relative wind direction between 90 and 270 degrees, e.g., from the chimney of the boat, was omitted from the evaluations. In this way, even the smallest influence of the combustion plume of the Belgica on these measurements was excluded. The BC concentrations were averaged over all sampling cruises according to the geographical location, using a grid of 0.01 by 0.01 degrees.

The filters used for aerosol sampling were weighed on a micro-balance (Sartorius model M5P-000V001, Göttingen, Germany) before and after sampling according to the EN12341 protocol. The masses (concentrations) for the $PM_{10-2.5}$ and $PM_{2.5-1}$ (coarse and median size fractions) were calculated from the masses of the three aerosol fractions sampled.

1.1.8. Instrumentation and methods for PAH analysis

The particulate matter and gases sampled by the HiVol samplers were extracted by accelerated solvent extraction (ASE-200, Dionex), or ultrasonic extraction. The ultrasonic extracts were subsequently cleaned up with the use of SPE silica gel cartridges and concentrated by rotary

evaporation and nitrogen blow-down techniques. The levels of PAHs were determined by GC-MS with the use of internal standards (hexamethyl benzene and *p*-terphenyl). The mass selective detector (MSD) was operated in electron impact mode. The temperature of the GC-MS transferline and source were 300 °C and 250 °C, respectively. The GC oven temperature program was as follows: 50 °C held for 1.5 min, increased to 180 °C at 20 °C/min, and then increased to 300 °C at the rate of 1.5 °C/min and held for 20 min. The ASE extracts were evaporated to 1 ml by Zymark evaporator and analysed with the use of HPLC-MSD-APPI measurement.

1.1.9. Installation of the sampling equipment

The most pieces of the sampling equipment onboard the Belgica were deployed on the fore-deck, in front of the bridge (Figure 3). For the carbon monitor, the inlet of the sampling tube was fixed at the monkey-bridge, whereas the instrument was placed on one of the desks inside the bridge. For the Zeeleeuw, all the sampling equipment was installed on the monkey bridge. The sampling equipment was switched off for certain, short periods when the ships' own plumes were supposed to affect the sampling (e.g., during manoeuvres).

Figure 3. Picture of the sampling equipment deployed onboard; the front of the Belgica's bridge with the denuder, the HiVol and low volume aerosol samplers (left), the BC monitor and particulate counter installed on a desk inside the bridge(right)

1.2. Results and discussion

1.2.1. Monitoring of NO2, SO2 and O3 criteria gaseous pollutants

Figure 4 shows the travel routes during the sampling campaign in March 2010. Different days are shown with different colours.

Figure 4. Travel routes during the first sampling campaign between March 18-30, 2010
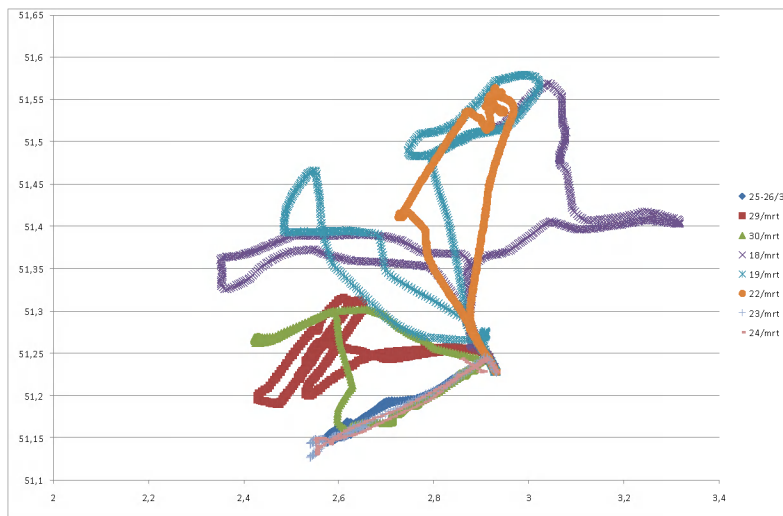
Figures 5-7 show the observed concentrations as function of time. It is clear that increased concentrations were measured onboard of the Zeeleeuw compared to the concentrations measured at the coast. This coastal site is not directly influenced by nearby shipping emissions.

Figure 5. NOx concentrations measured onboard the Zeeleeuw compared to concentrations measured at the coastal station De Haan during March 2010 (a); same figure with zoom on Y-axis (b)
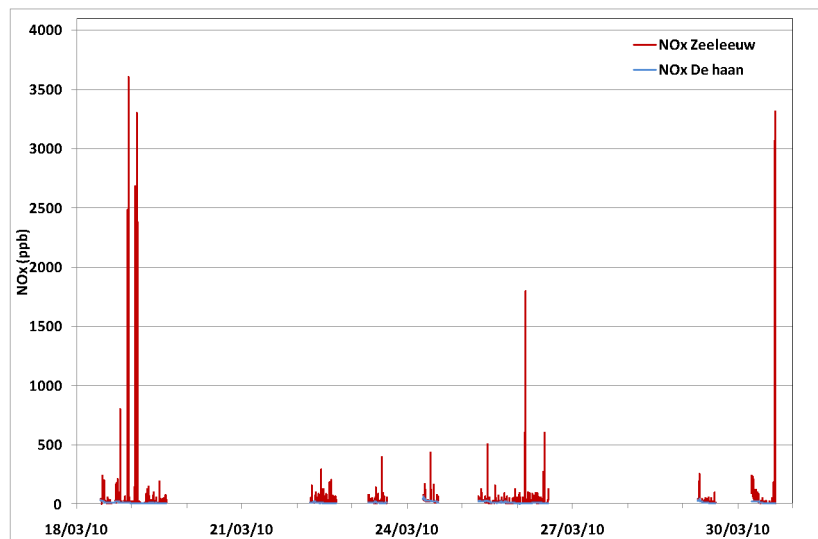
(a)

(continue Figure 5)
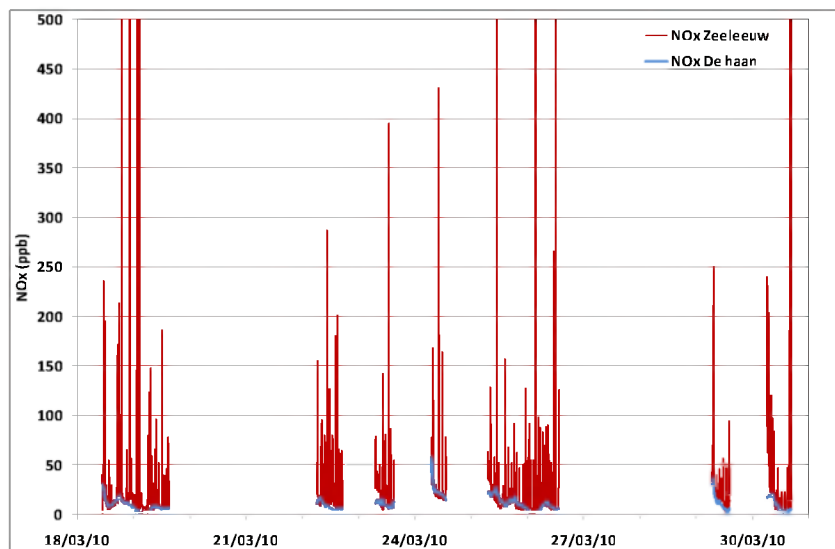
(b)

The observed NOx concentrations reached short-term values of up to 3000 ppb. As pointed out earlier, these data points were probably influenced by the emissions of the research vessel itself. The "background concentrations" (the lower values) observed on the ship and at the coastal station in De Haan usually follow the same trend.

The SO$_2$ pollutant concentrations observed onboard the Zeeleeuw during the first sampling campaign in March 2010 were also increased compared to the concentrations measured at the coast. In a lot of cases, peak coincidence with NOx peaks was observed, indicating that NOx and SO$_2$ are originating from the same sources.

Figure 6. SO$_2$ concentrations measured onboard the Zeeleeuw compared to concentrations measured at the coast (De Haan) during March 2010
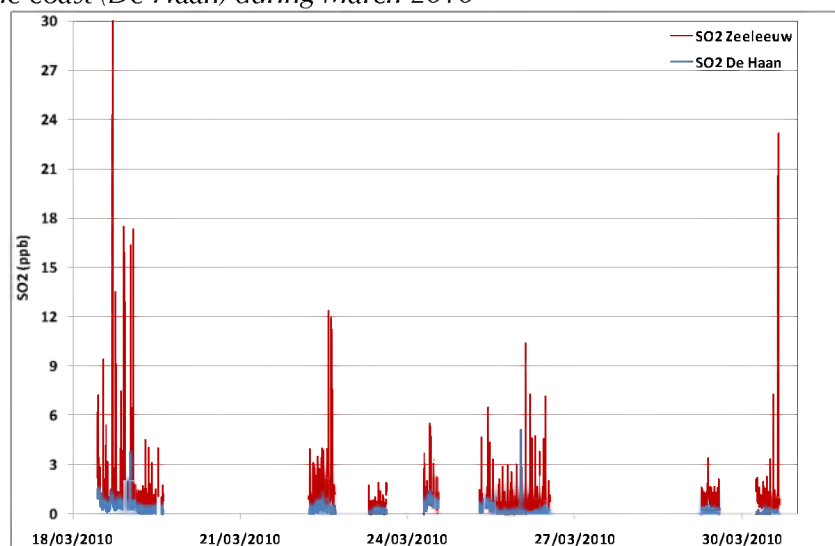
In contrast to the other pollutants, ozone concentrations followed the same trend at the coast and onboard the ship. Ozone concentrations measured onboard the Zeeleeuw showed somewhat lower values, corresponding to periods of high NOx emissions. Some ozone peaks had been measured at the coast that were not recorded at the Zeeleeuw (e.g. on 18/03/2010). Also in the case of SO$_2$, high short-term peak concentrations may be due to the influence of the emissions of the Zeeleeuw itself.

Figure 7. O₃ concentrations measured onboard the Zeeleeuw compared to concentrations measured at the coast (De Haan) during March 2010
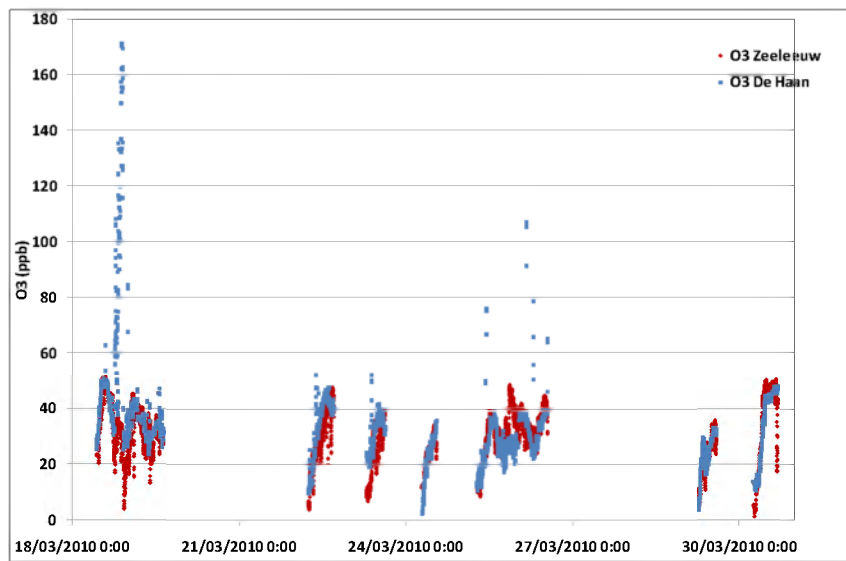
Figures 8-10 show the observed concentrations during the sampling campaign in October 2010 as function of time. Again, NOx concentrations observed onboard the Belgica were significantly higher than the concentrations observed at the coastal station in De Haan. SO_2 pollutant concentrations were also significantly increased compared to concentrations measured at the coast. Again, peak coincidence between SO_2 and NOx peaks indicates common sources for both pollutants. In contrast, ozone concentrations followed the same trend at the coast and onboard the ship.

Figure 8. NOx concentrations observed onboard the Belgica and at the coastal station De Haan during October 2010 (a); same figure with zoom on Y-axis (b)
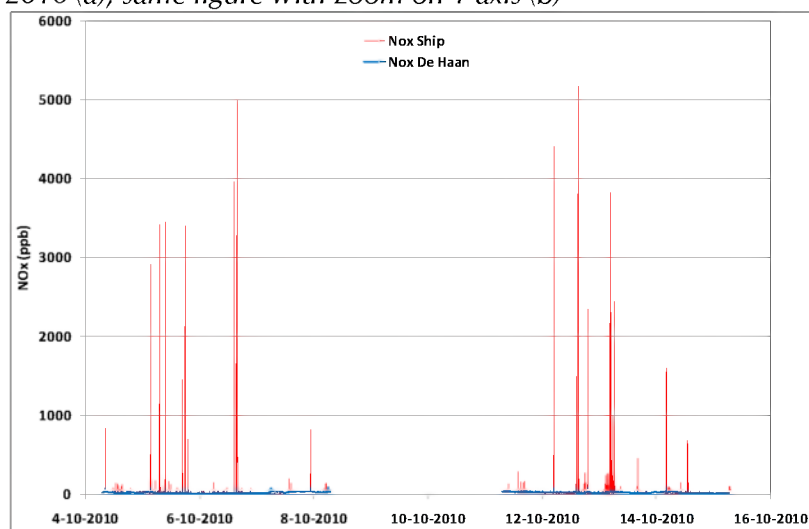
(a)

(continue Figure 8)
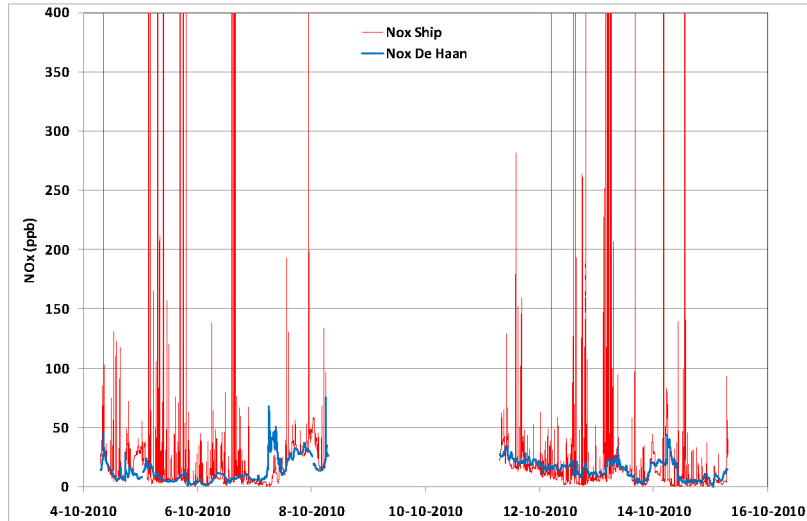
(b)

Figure 9. SO₂ concentrations observed onboard the Belgica compared to concentrations observed at the coast (De Haan) during October 2010
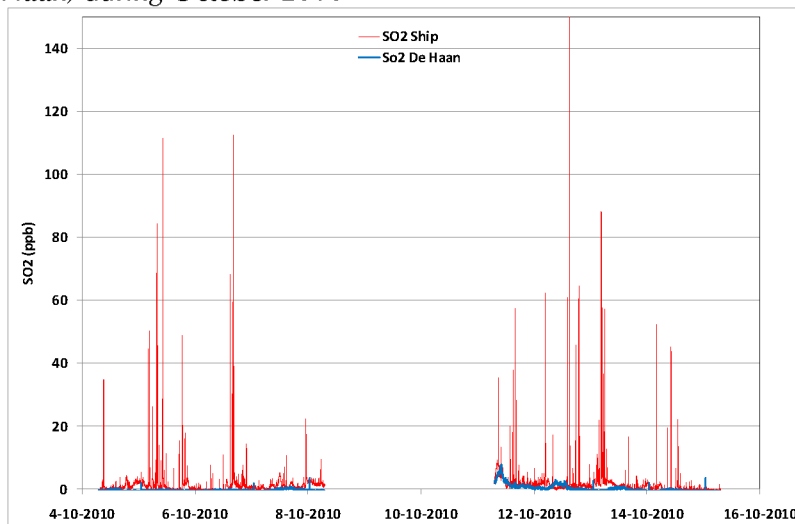
Figure 10. O₃ concentrations observed onboard the Belgica compared to concentrations observed at the coast (De Haan) during October 2010
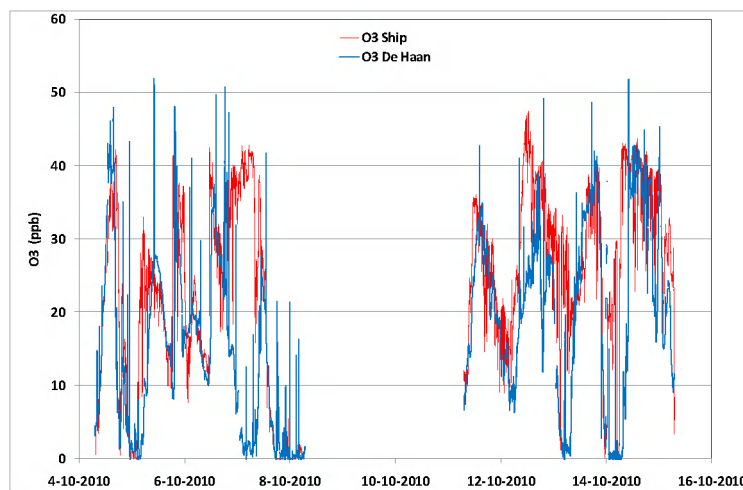
For further analyses using the NO_2 and SO_2 observations we refer to the chapter dealing with the validation of the air quality model results using the observations during the SHIPFLUX sampling campaigns.

1.2.2. Mass concentrations and distribution of atmospheric aerosols

An overview of the gravimetry results obtained for various size-ranges of aerosols for the spring 2010 campaigns are presented in Table 2. In the March 2010 campaigns, the PMx showed lower median concentrations for De Haan in the fine and coarse fractions (i.e., 7.7 and 6.8 $\mu g/m^3$ for PM_1 and $PM_{10-2.5}$, respectively) than those observed for the samples taken onboard the Zeeleeuw over the sea. During the May 2010 campaign, both at the sea-side and over the sea (onboard Belgica), lower PM concentrations were found in each aerosol fraction (i.e., 5.0, 3.5, and 7.6 $\mu g/m^3$ for PM_1, $PM_{2.5-1}$ and $PM_{10-2.5}$, respectively) compared to those of the March 2010 campaign. Moreover, there was not any significant mass difference between the median concentrations of sea-side and marine aerosols in any of the three fractions in the March and May campaigns, respectively. This was possibly due to meteorological conditions, i.e., the northern/northeastern winds from the open sea were prevailing during these sampling periods. It appears that they keep the pollutant concentrations at equally low levels at coastal and marine areas as well.

Table 2. Overview of the concentrations of various aerosol size fractions in spring 2010

Campaign/PM fraction	Concentration ($\mu g/m^3$)				
	Min	Max	Median	Average	SD
Zeeleeuw (March 2010)					
PM_1	5.7	20.5	11.1	12.4	5.7
$PM_{2.5-1}$	1.6	9.3	5.3	5.4	2.5
$PM_{10-2.5}$	3.6	19.6	8.2	9.8	5.2
De Haan (March 2010)					
PM_1	1.9	28.2	7.7	11.5	8.8
$PM_{2.5-1}$	2.9	13.2	7.6	8.0	3.4
$PM_{10-2.5}$	n.d.	10.0	6.8	3.4	8.9
Belgica (May 2010)					
PM_1	2.8	6.8	5.0	4.9	1.4
$PM_{2.5-1}$	2.6	6.9	3.5	4.5	2.0
$PM_{10-2.5}$	4.2	16.2	7.6	8.5	4.5
De Haan (May 2010)					
PM_1	2.2	12.8	4.4	5.1	3.5
$PM_{2.5-1}$	1.2	6.1	3.0	3.2	1.5
$PM_{10-2.5}$	3.7	17.2	8.0	8.4	3.6

n.d. − not detectable, i.e., the concentration of the species was below
the detection limit of the method

The data of PM mass analysis for the 2010 autumn campaigns are listed in Table 3. As can be seen, the trend is that the coarser fraction dominates over the medium and the fine fractions. The PM_1 size-fractions for the over-sea and coastal aerosols showed similar median values in September and October, respectively. The coarse (PM_{10}) and the medium ($PM_{2.5-1}$) size fractions in September

showed lower mass for the coastal aerosols than for marine aerosols. On the other hand, the trend is opposite for the October campaign. This is likely due to the different weather pattern of the two campaigns (i.e., the September campaign was with high wind speed and thus low atmospheric stability, whereas the October campaigns were with relatively low wind-speed, i.e., up to 3 B°.

Interestingly, in October, the coastal site at De Haan showed an even distribution of the three fractions, which can also be explained with the relative atmospheric stability during this period. However, the distribution of PMx mass between the three aerosol-fractions observed over the sea follows the same trend as the ones for other campaigns. Interestingly, and unexpectedly, some seasonality can be noticed when comparing the spring and autumn campaigns in 2010, in terms of increased PM masses at each aerosol fractions of autumn samples.

Table 3. Concentrations of various aerosol size fractions sampled during autumn in 2010

Campaign/PM fraction	Concentration ($\mu g/m^3$)				
	Min	Max	Median	Average	SD
Belgica (September 2010)					
PM_1	2.1	12.8	4.8	5.9	3.9
$PM_{2.5-1}$	3.0	10.0	5.4	6.0	2.6
$PM_{10-2.5}$	9.9	22.2	17.2	16.9	4.2
De Haan (September 2010)					
PM_1	3.8	7.3	5.6	5.6	1.5
$PM_{2.5-1}$	n.d.	6.4	4.0	3.5	2.9
$PM_{10-2.5}$	6.3	19.7	11.7	12.3	6.0
Belgica (October 2010)					
PM_1	2.8	21.9	6.0	8.3	5.8
$PM_{2.5-1}$	n.d.	12.8	3.7	4.7	3.6
$PM_{10-2.5}$	3.4	19.4	8.4	9.8	4.7
De Haan (October 2010)					
PM_1	3.5	18.2	6.5	7.9	4.8
$PM_{2.5-1}$	0.21	14.8	7.9	7.3	5.1
$PM_{10-2.5}$	n.d.	13.7	9.8	8.7	4.8

n.d. – not detectable

An overview of the data of aerosol masses for the 2011 spring campaigns are listed in Table 4. As can be seen from the median PMx concentrations, the aerosol mass is almost evenly distributed between the three aerosol fractions of the February campaigns, both at the seaside and over the sea. This period of the year was with fairly calm weather, and as a consequence with high atmospheric pollution (e.g., smog alert over Belgium), thus the atmospheric stability promoted the coagulation and even distribution of aerosols over the size-range studied. On the other hand, approximately twice higher PM1 concentration of the marine air is observed in the March campaign than for medium and coarse fractions, while the coastal site showed increased medium concentrations. For the May campaign onboard the Belgica, the three times higher coarse fraction dominated over the finer fractions.

Table 4. Concentrations of various aerosol size fractions during the 2011 campaigns

Campaign/PM fraction	Concentration ($\mu g/m^3$)				
	Min	Max	Median	Average	SD
Belgica (February 2011)					
PM_1	3.0	20.6	9.3	11.4	5.5
$PM_{2.5-1}$	n.d.	12.2	4.8	5.1	4.8
$PM_{10-2.5}$	3.0	29.0	11.2	13.7	7.2
De Haan (February 2011)					
PM_1	n.d.	17.6	8.2	8.6	6.0
$PM_{2.5-1}$	1.57	22.8	8.4	9.8	7.1
$PM_{10-2.5}$	n.d.	22.8	11.9	9.7	9.9
Belgica (March 2011)					
PM_1	9.1	44.3	19.4	21.6	11.5
$PM_{2.5-1}$	3.4	23.2	8.9	12.4	8.1
$PM_{10-2.5}$	n.d.	22.2	11.0	10.2	6.8
De Haan (March 2011)					
PM_1	2.6	18.0	9.9	11.0	5.0
$PM_{2.5-1}$	6.5	31.1	14.3	17.5	8.9
$PM_{10-2.5}$	0.3	12.8	6.7	6.9	4.0
Belgica (May 2011)					
PM_1	1.9	21.7	6.3	7.2	5.5
$PM_{2.5-1}$	n.d.	10.3	5.9	5.0	5.3
$PM_{10-2.5}$	5.7	34.3	23.5	23.0	9.7
De Haan (May 2011)					
PM_1	3.1	20.6	6.3	7.5	5.3
$PM_{2.5-1}$	2.4	62.5	8.9	13.3	18.7
$PM_{10-2.5}$	n.d.	24.5	15.6	11.6	13.2

n.d. – not detectable

The distribution of the PM aerosol mass for the three size fractions observed on all the Belgica campaigns over the North Sea is visualized on Figure 11. It should be mentioned that due to the low resolution of the presently applied aerosol sampling equipment, the tracks represent the averaged PM mass values collected over the sections sampled (as described in the section Experimental). However, the results are fairly interesting and respond to the expectations. As can be seen on Figure 11b, the fine aerosol (PM_1) levels are the highest (20-35 $\mu g/m^3$) near the anchoring area (pilot station), which is used as a waiting area for the ships for pilots, for entering the Schelde-estuary and/or the Belgian harbours. Similarly high PM_1 values can be observed over the W-E shipping routes to the estuary of the Schelde river and at sites close to the coast/large harbours. On the other hand, when diverting from these sites towards marine areas of low or no traffic intensity, one can see a steep drop of the PM_1 concentration, e.g., to 3-6 $\mu g/m^3$, which values one can assume that it corresponds to the "close-to-coast" or „continental shelf" marine background level. Similar to the behaviour of PM_1, the medium ($PM_{2.5-1}$) and the $PM_{10-2.5}$ aerosols showed similar distribution over the marine areas studied as seen on Figures 11c and 11d, respectively. However, the coarse aerosols were found at higher concentrations (especially over the international and W-E shipping routes and the anchoring area) than the fine ones, while the medium sized aerosols were present at lower level than the fine. Overall, the PM mass trend over the Belgian North Sea is

obvious, increased atmospheric levels of fine, medium and coarse particulates are experienced, mostly localized at/near the marine areas with high ship traffic density.

Figure 11. Average background concentration ($\mu g/m^3$) of airborne particulate mass; (a) map visualizing the borders (solid black lines) and the major shipping routes (pink shaded areas) of the Belgian continental shelf, (b) PM$_1$, (c) PM$_{2.5-1}$ and (d) PM$_{10-2.5}$
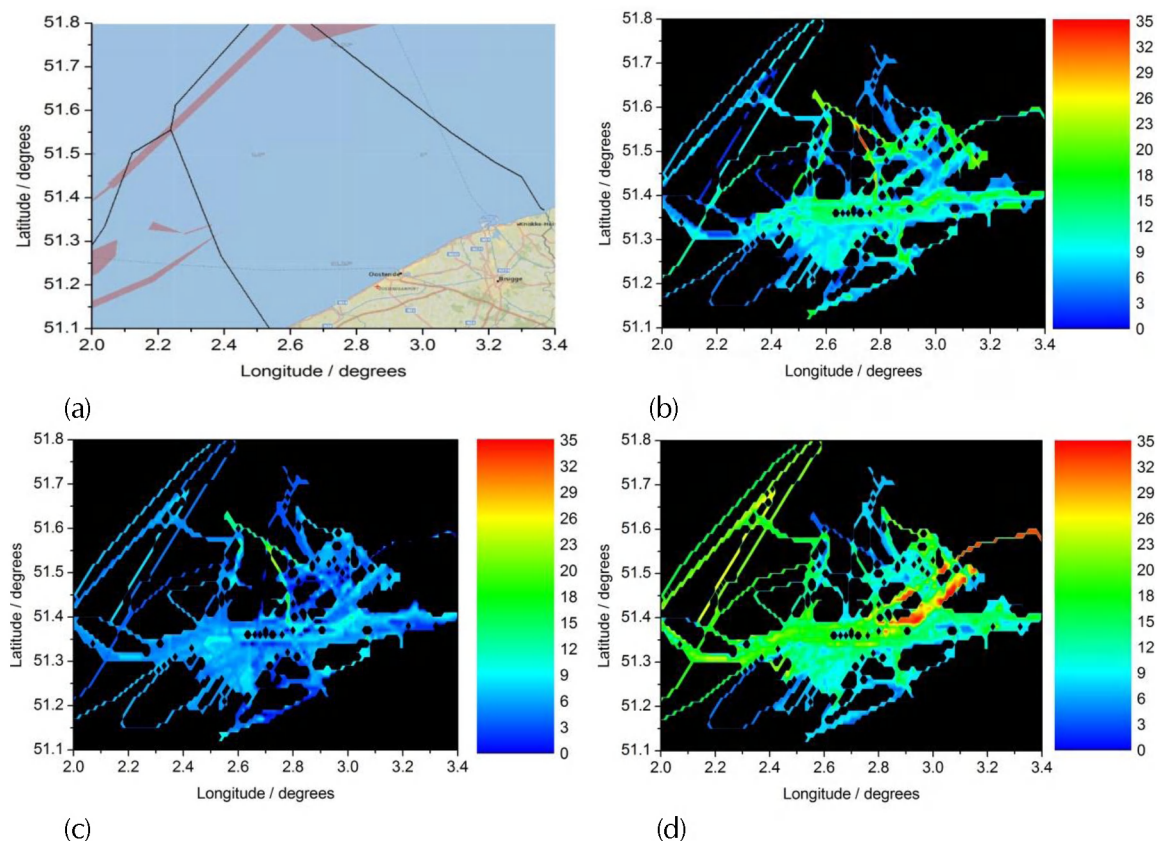
1.2.3. Elemental content of size-segregated aerosols

Several metallic (Si, K, Ca, Ti, V, Fe, Ni, Mn, Cu, Zn, Al and Pb) and non-metallic (S, Cl) elements were detected by EDXRF during the campaigns, onboard as well as at the sea-side sampling station. However, a few metals, like Se, Cr, As, Cd and Sb, could either not well or even not at all be detected with the EDXRF method applied in this study. The results for metals show that generally lower values were observed at the sea-side (background site) than over the sea. Na is one of the main components of marine aerosols, which could not properly be detected by EDXRF, but IC (see Section 1.2.5.).

The elemental composition of three size fractions of atmospheric aerosols sampled during the May 2010 campaign onboard Belgica and at the coastal site are depicted on Figures 12a and 12b, respectively. For marine samples (Figure 12a), the higher the aerosol size, the higher the elemental content of the fraction. The highest concentrations were observed for Cl, S, Si, Al, K and Ca, mostly in the coarse and medium sized particulate fractions, apart from S, which was found at higher amounts in fine particulate. The highest (total) elemental concentration was certainly observed at the main international shipping route, and followed by the W-E shipping lanes/Schelde-estuary. As can be seen on Figure 12b, lower total elemental concentrations of metals were observed at the coastal site than in the marine samples of the same campaign (Figure 12a). The total concentration distribution was mostly similar in the fine and coarse particulate fractions, while the medium

fraction generally showed lower elemental content (Figure 12b). K and S were mostly present in the finer, whereas Si, Ca and Cl in the coarser fractions.

Figure 12. Elemental composition of three size fractions of atmospheric aerosols obtained for May 2010 campaign onboard Belgica (a) and at the coastal site (b); (the x-axis indicates the sampled marine area, the prevailing wind direction and the average wind speed in m/s.

(a)
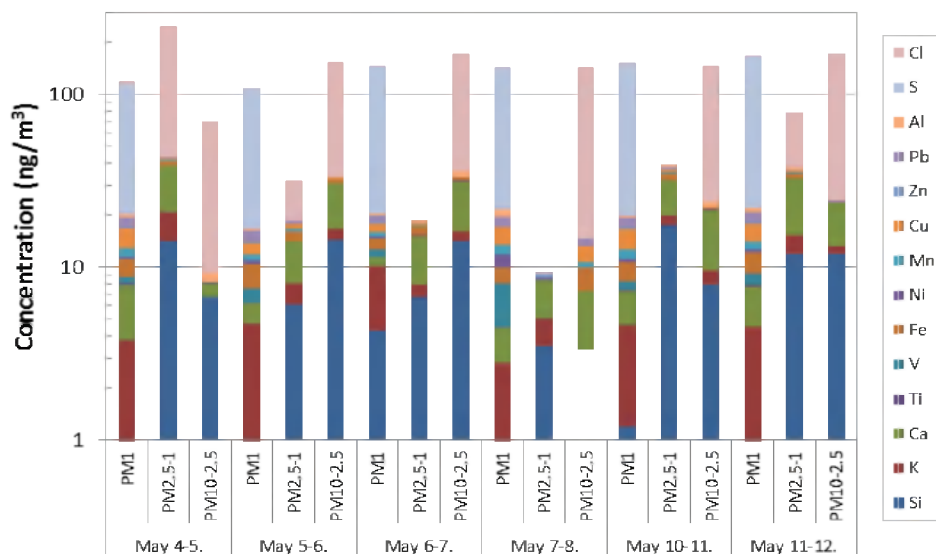
(b)

The elemental composition of three size fractions of atmospheric aerosols in the February 2011 campaign onboard Belgica and at the coastal site are depicted on Figures 13a and 13b, respectively. For marine samples (Figure 13a), the highest levels are generally observed for Cl, mainly in the medium and the coarse particulate fractions. High concentrations of S were found in the medium and fine fractions. Ca, Fe and Al were present at increased amounts in the medium/coarse fractions. Increased amounts of elements/metals (e.g., V) were detected at the shipping lanes and near the Wandelaar pilot station. These marine areas are all with high ship traffic density. Both V and Ni are markers of diesel combustion, so their detection is important to make

distinction between sources of pollutants in aerosols. V and Ni are present in the diesel oil of large ships, called "heavy fuel oil" (HFO).

Figure 13. Elemental composition of three size fractions of atmospheric aerosols obtained in the first week of the February 2011 campaign onboard Belgica (a) and at the coastal site (b); the x-axis indicates the sampled marine area, the prevailing wind direction and the average wind speed in m/s
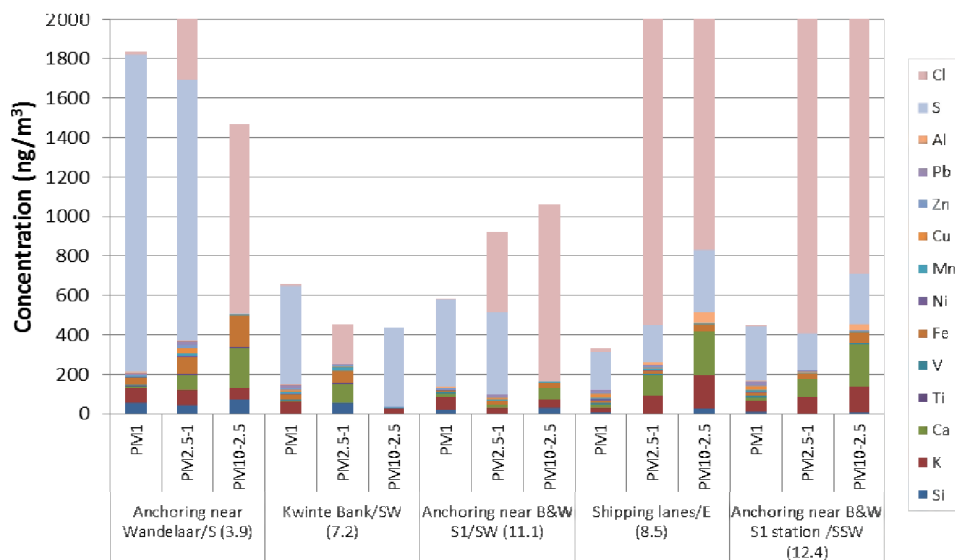
(a)
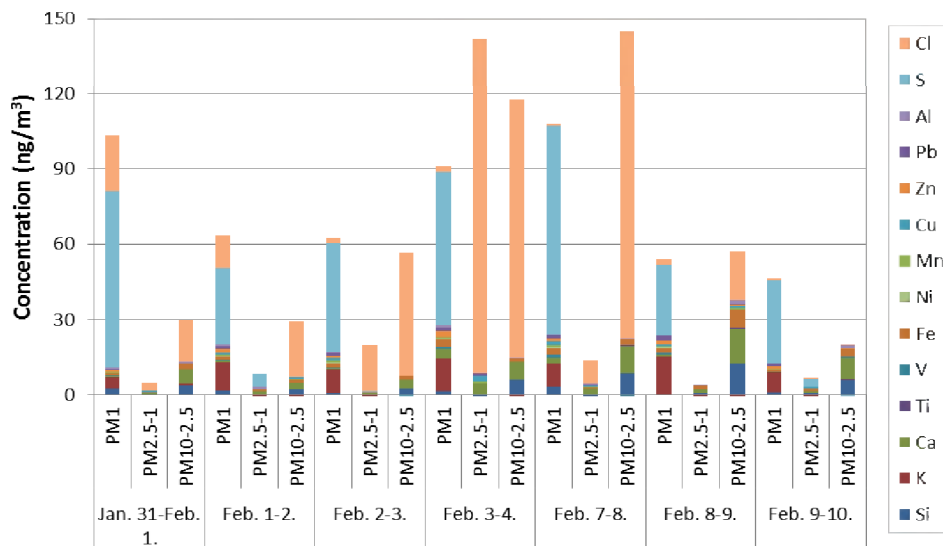
(b)

Fairly low levels of the total elemental content are found at the background site, such as the Kwinte Bank, which could also be referred to as a marine background area. Change in wind direction from marine (SW) to mixed/marine-continental (SSW) certainly increased the levels of pollutants, for instance, as experienced for samples collected near the B&W S1 marine station. For coastal samples, low total levels of pollutants were obtained as seen on Figure 13b. This was manifest in lower levels of Cl, S and ship emission related trace metals too. The elements showed similar distribution to that experienced for marine samples. For instance, increased levels of K, V,

Ni, Mn, Cu, Zn and Pb were obtained in the fine aerosol fraction, while Cl was mostly present as medium and coarse particulates.

The other trace elements, for example, V and Ni were detected at elevated levels at the marine samples too. Both elements are markers of diesel combustion, so their detection is important to make distinction between sources of pollutants in aerosols. V and Ni are present in the diesel oil of large ships, called "heavy fuel oil" (HFO). The ratio of these elements and others like Cu/V, Pb/Cu etc. might also be useful to identify these emission sources.

The relative contribution of elements (apart from S and Cl being omitted for a better visualization of the rest) to the three size fractions of atmospheric aerosols sampled in May 2010 campaign onboard Belgica and at the coastal site are indicated on Figures 14a and 14b, respectively. For marine samples (Figure 14a), high relative contribution of Si, K, Ca, and Fe can be seen in almost each fraction/area sampled. These elements contributed with an increasing percent in the coarser particulate fractions. For the shipping lanes, higher relative contribution of V, Ni, Cu, Mn and Pb appears to be obvious, especially in the fine aerosol fraction. The contribution of Al is mostly observed to be varying between the three fractions, with the lowest contribution certainly found at marine background areas (e.g., Thornton Bank/Bligh Bank). For coastal samples (Figure 14b), fairly high contributions of Si, Ca and Al (crustal elements) are mostly found in the coarse and medium particulates, while K, V, Fe, Ni, Mn, Cu, Zn and Pb contributed mostly in the fine and/or the medium fraction.

Figure 14. Relative contribution of elements (apart from S and Cl) to the three aerosol fractions of atmospheric aerosols obtained for May 2010 campaign onboard Belgica (a) and at the coastal site (b); the x-axis indicates the sampled marine area, the prevailing wind direction and the average wind speed in m/s


(a)
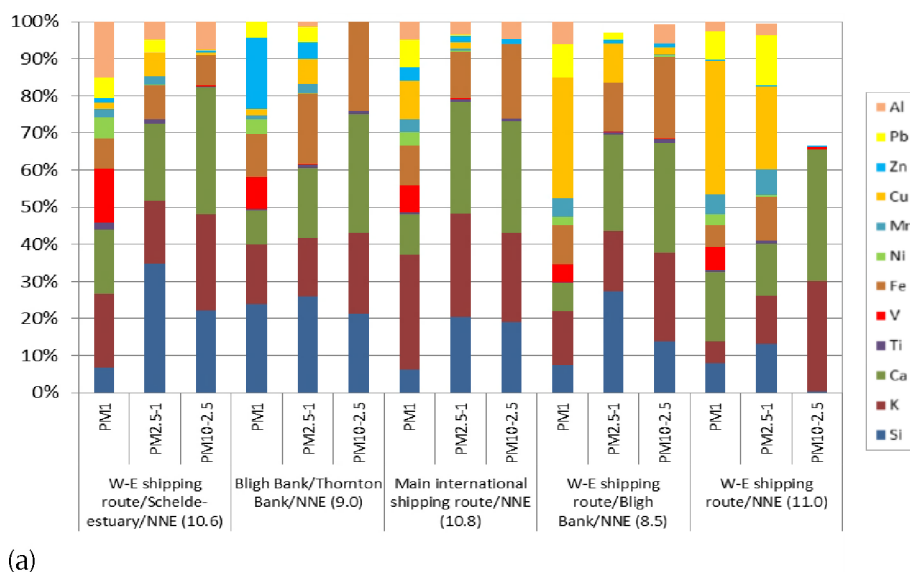
(continue Figure 14)
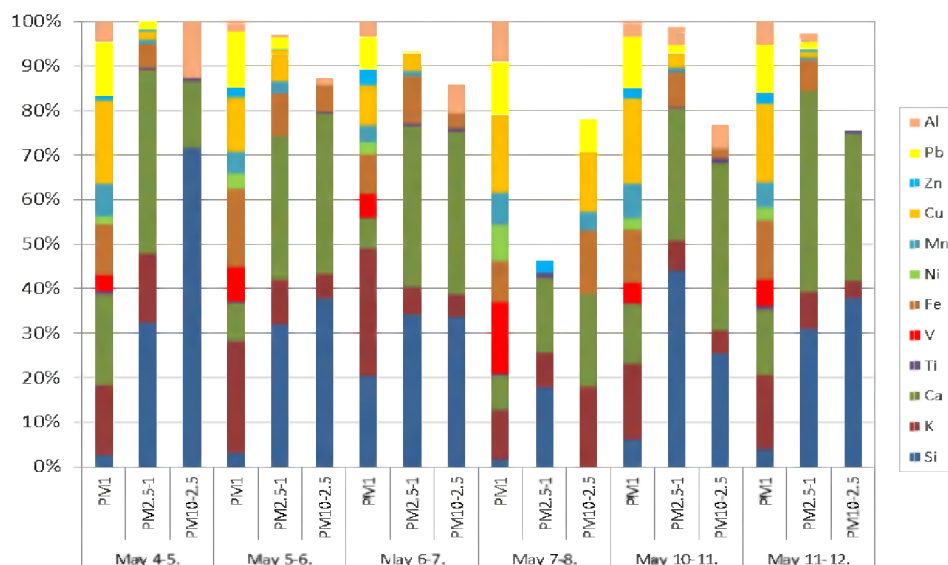
(b)

The relative contribution of elements (apart from Si and Cl) to the three size fractions of atmospheric aerosols for the first and the second weeks of the October 2010 campaign onboard Belgica are indicated on Figures 15a and 15b, respectively. As experienced during the May and September 2010 campaigns, high relative contribution of Si, K, Ca and Fe has been observed in almost each fraction/area sampled. The percentage of Al in the coarser particulate fractions was usually found to be relatively higher than in the former campaigns. The contribution of V, Ni, Cu, Mn, Zn, and Pb was more considerable in the fine particulate fractions, pointing towards the origin of elements from ship exhaust emission.

Figure 15. Relative contribution of elements (apart from Si and Cl) to the three aerosol fractions of atmospheric aerosols obtained for the first (a) and the second (b) week of the October 2010 campaign onboard Belgica; the x-axis indicates the sampled marine area, the prevailing wind direction and the average wind speed in m/s

(a)
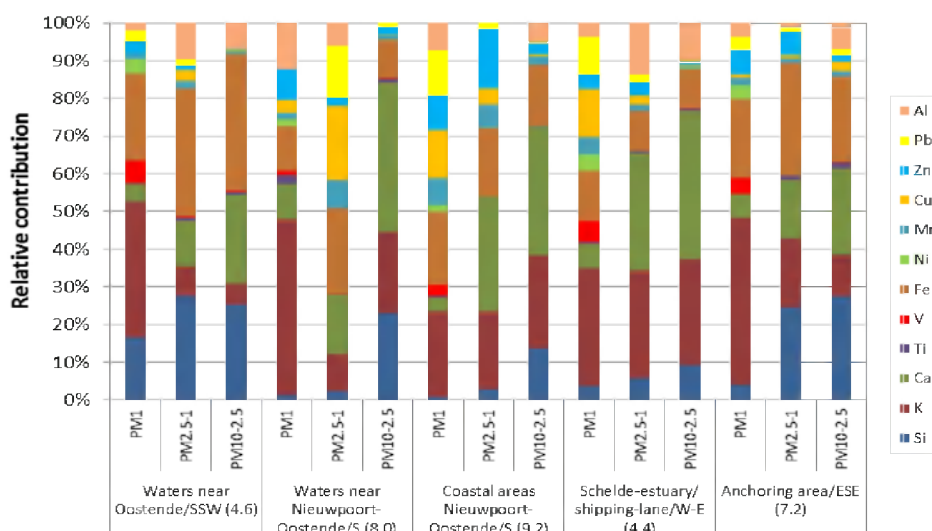
(continue Figure 15)
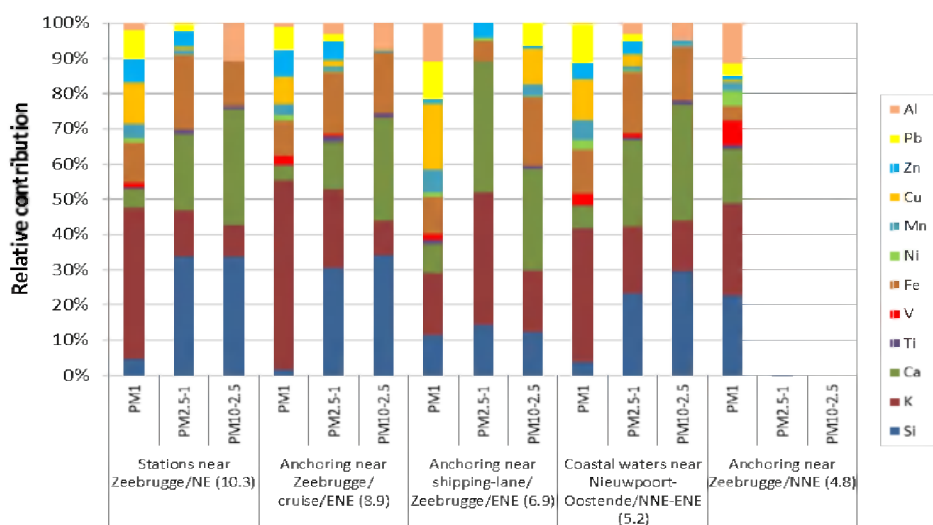
(b)

The relative contribution of elements (apart from Si and Cl) to the three size fractions of atmospheric aerosols for the first and the second week of the February 2011 campaign onboard Belgica are indicated on Figures 16a and 16b, respectively. Similar to former campaigns, high relative contribution of Si, K, Ca and Fe was generally attained in the three aerosol fractions. Ca was contributing in the coarser particulate fractions, while K was mostly contributing in the fine fraction. The contribution of Fe was found to be rather similar in the three aerosol size fractions. V and Ni were mostly observed in the fine aerosol fraction, while Mn, Cu, Zn and Pb were present in the fine and medium fractions. Interestingly, higher Al and Ti contribution was observed rather in the medium and coarse fractions.

Figure 16. Relative contribution of elements (apart from Si and Cl) to the three aerosol fractions of atmospheric aerosols obtained for the first (a) and the second (b) week of the February 2011 campaign onboard Belgica; the x-axis indicates the sampled marine area, the prevailing wind direction and the average wind speed in m/s


(a)
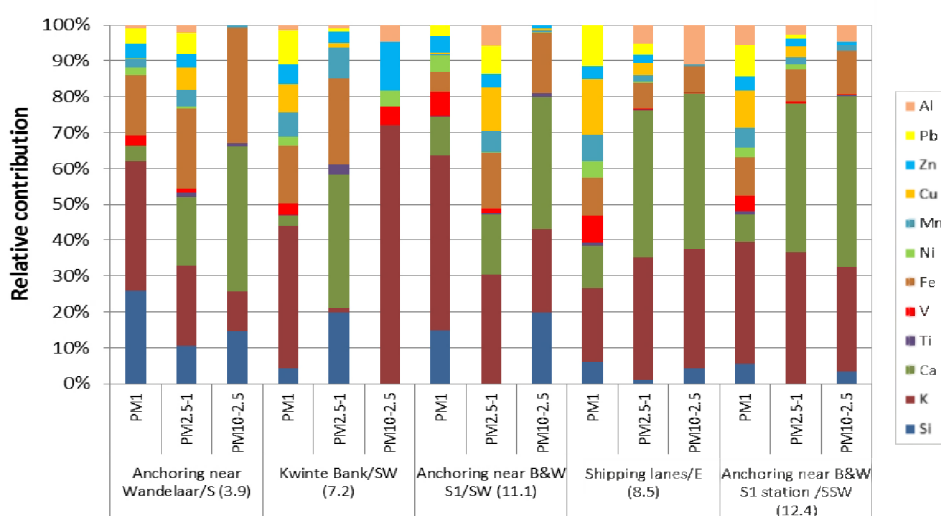
(continue Figure 16)
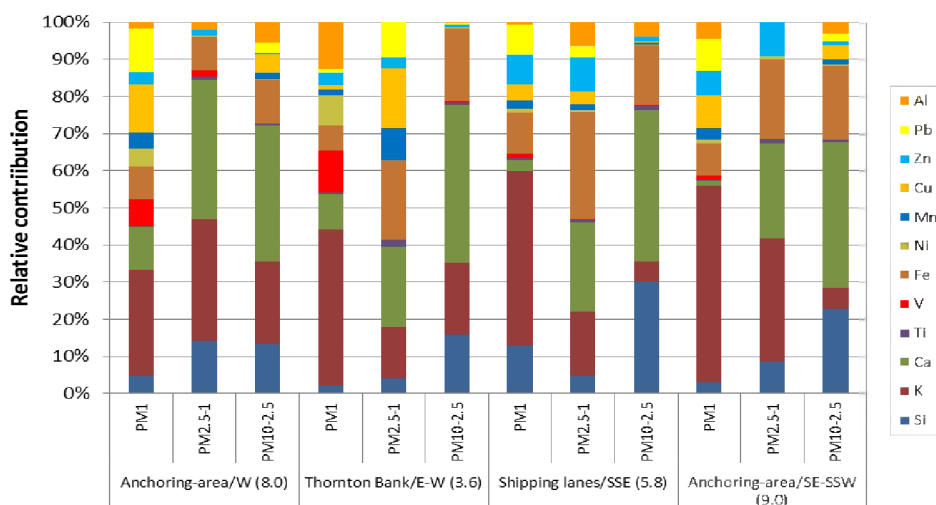
(b)

1.2.4. Atmospheric levels of ammonia and acidic gases

The results of the gaseous air sampling for HNO_2, HNO_3 and NH_3 (denuder) over various marine waters during the May 2010 campaign onboard Belgica is depicted on Figure 17. Since the prevailing strong wind (average speed: 8.5-11 m/s) was from the North Sea (NNE), it was expected that the continental anthropogenic pollution contributes to background levels only at a minimal/negligibly extent.

Figure 17. Concentrations of gaseous air components sampled during the May 2010 campaign onboard Belgica; the upper x-axis indicates the sampled marine area, the prevailing wind direction and the average wind speed in m/s
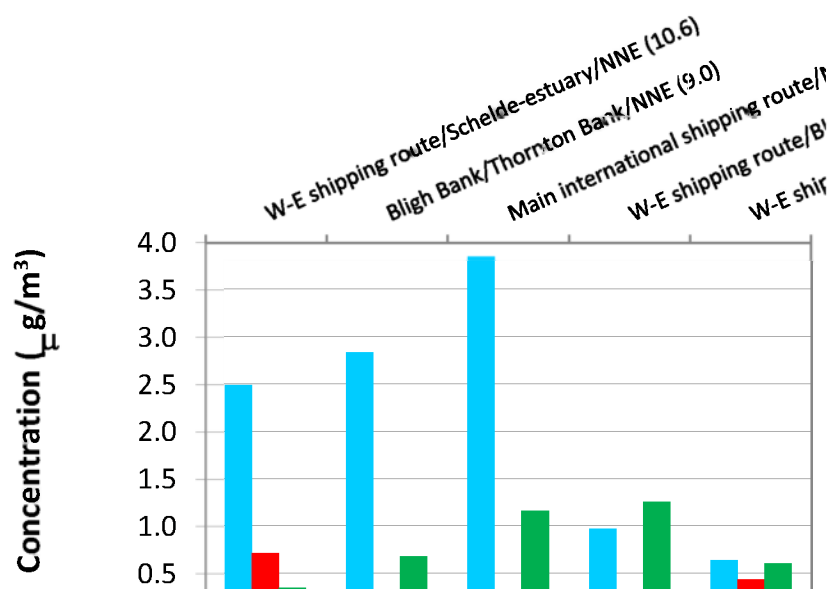
As can be seen on Figure 17, the concentration of NH_3 was generally much higher (range: 0.6-3.9 µg/m³; average: 2.2 µg/m³) than those of the acidic components (range: 0.1-0.7 and 0.4-1.3 µg/m³ with averages of 0.3 and 0.8 µg/m³ for HNO_2 and HNO_3, respectively). The highest pollutant levels are observed over the main international shipping lane, the W-E shipping lane and nearby

marine waters (e.g., Schelde estuary). These data indicate a higher gaseous pollutant content of air over the main shipping route and surrounding sites than those observed at the coastal background station in De Haan (Horemans et al., 2009).

The air concentrations of HNO_2, HNO_3 and NH_3 obtained during the September/October 2010 campaigns onboard Belgica are depicted on Figure 18. During these campaigns, the wind direction and wind speed varied considerably. Thus it was expected that some more artefacts encountered than during the May 2010 campaign. On the other hand, similarly enhanced NH_3, HNO_2 and HNO_3 levels were observed at the shipping lanes as in the May 2010 campaign. In comparison with regular marine background, the increase in their concentration is generally 2-3-fold for NH_3 and HNO_2, while the level of HNO_3 generally remains similar or even lower. The anchorage area (pilot station) also showed enhanced NH_3 and HNO_2 levels.

Figure 18. Concentrations of gaseous air components during the September/October 2010 campaigns onboard Belgica; the lower x-axis indicates the sampled marine area, the prevailing wind direction and the average wind speed in m/s
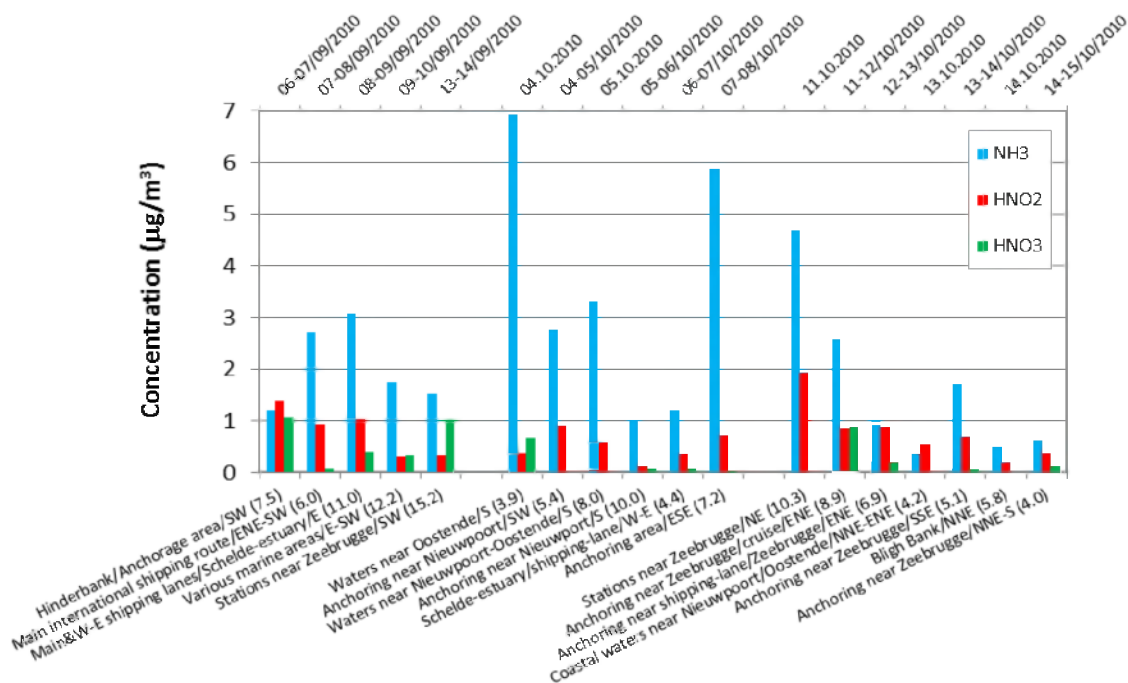

During the first week of the October campaign, near coastal waters (e.g., areas near Oostende/Nieuwpoort) showed enhanced NH_3 levels (e.g., 3-7 $\mu g/m^3$), but this was rather due to the prevailing continental winds and the impact of agricultural emission, it being characteristic for Western Belgium, including near coastal areas (see e.g., Horemans et al., 2009; Bencs et al., 2008). In the second week of the October 2010 campaign, due to the marine (NNE) winds, several sites showed fairly low concentrations, which are acceptable marine background values for NH_3, HNO_2 and HNO_3, e.g., Bligh Bank and Oostende/Nieuwpoort waters, they being in the ranges of 0.3-1.8, 0.2-0.7, n.d.-0.2 $\mu g/m^3$, respectively.

The concentrations of HNO_2, HNO_3 and NH_3 obtained during the February 2011 campaign onboard Belgica are depicted on Figure 19. In the first week of this campaign, the wind was mostly from S/SW, after then it turned to W/E/SE. The wind speed considerably varied during the whole campaign, from very low to fairly strong. It was observed during this campaign, that the low winds, especially in the mornings, gave rise to relatively long fog events, thus pollutant/particulate accumulation/coagulation, as well as temperature inversion over the sea. As can be seen on Figure 19, due to these weather conditions, generally high HNO_2 (range: 0.04-1.8 $\mu g/m^3$, average: 0.9

µg/m³) and low HNO₃ (range: 0.07-1.2 μg/m³, average: 0.2 μg/m³) air concentrations were acquired for almost each measurement cycle of this campaign. Compared to the autumn and the spring 2010 campaigns, the far marine areas (e.g., Thornton bank, being 30 km off the coast) and coastal background sites (e.g., windward side of the anchorage area) showed relatively raised gaseous NH₃ and HNO₂ levels, i.e., ranging from 0.4-5.6 and 0.5-1.8 µg/m³, respectively. However, low air concentrations were acquired near B&W S1 stations for both species, i.e., 0.4 and 0.04 µg/m³, respectively, which values are likely representing better the background level of the marine atmosphere.

Figure 19. Concentrations of gaseous air components during the February 2011 campaign onboard Belgica; the lower X-axis indicates the sampled marine area, the prevailing wind direction and the average wind speed in m/s
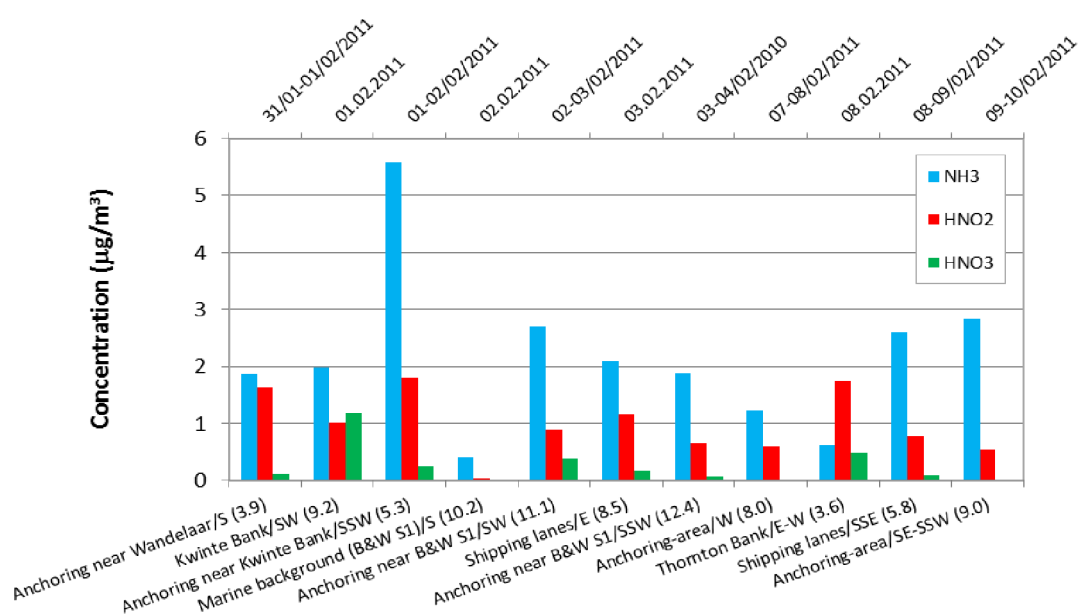

The air concentrations of HNO₂, HNO₃ and NH₃ obtained during the March 2011 campaigns onboard Belgica are depicted on Figure 20. During this sampling period, the wind direction was from NE (marine), but its speed varied to a great extent (from wind-still periods up to 5-6 B). In general, shorter fog events with similar temperature inversions were observed, like during the February 2011 campaign. Accordingly, similar to the February campaign, high HNO₂ (range: 0.3-3.1 µg/m³, average: 1.1 µg/m³) and very low HNO₃ (range: 0.03-0.2 μg/m³, average: 0.1 μg/m³) concentrations were obtained for almost each measurement cycle/area within this campaign. However, the air concentration of NH₃ was higher (range: 1.9-9.5 μg/m³, with an average of 3.1 μg/m³) than that observed for the February 2011 campaign. It is interesting to notice that the level of HNO₂ did not change considerably, not even over open sea waters (e.g. main, international shipping lanes). On the other hand, the NH₃ concentration fluctuated site-specifically, e.g., it was the highest at the shipping lanes near the Schelde estuary and the anchorage area (leeward side).

Figure 20. Concentrations of gaseous air components during the March 2011 campaign onboard Belgica; the lower x-axis indicates the sampled marine area, the prevailing wind direction and the average wind speed in m/s
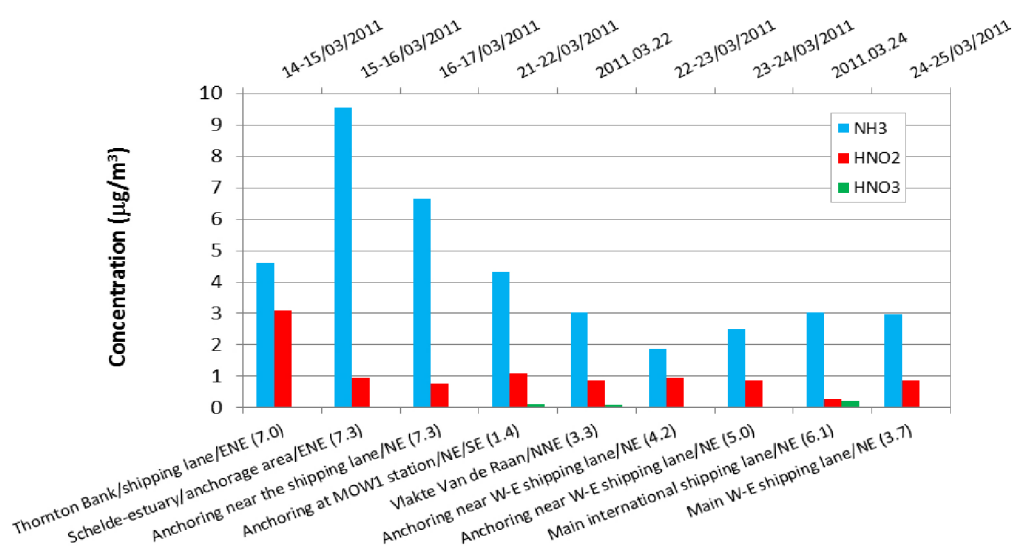

Air concentrations of HNO_2, HNO_3 and NH_3 obtained during the May 2011 campaigns onboard Belgica are depicted on Figure 21. During this sampling period, the prevailing wind direction was mostly southwestern (i.e., oceanic origin), but its speed varied to a great extent, from wind-still periods up to 5-6 B.

Figure 21. Concentrations of gaseous air components during the May 2011 campaign onboard Belgica; the upper x-axis indicates the sampled marine area, the prevailing wind direction and the average wind speed in m/s
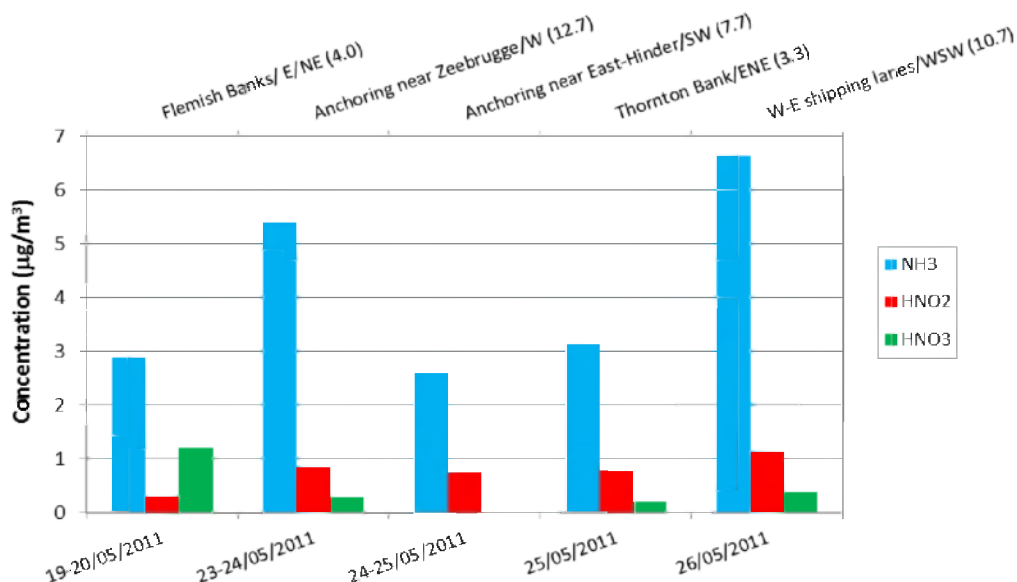
Compared to the February and March campaigns of 2011, the HNO_2 level (range: 0.7-1.1 $\mu g/m^3$, average: 0.8 $\mu g/m^3$) was generally lower, while the HNO_3 concentration (range: 0.01-2.6 $\mu g/m^3$, average: 0.3 $\mu g/m^3$) was a bit higher in this campaign. The NH_3 levels (range: 2.6-6.6 $\mu g/m^3$,

average: 5.4 $\mu g/m^3$) were higher than during the February/March campaigns. Site-specifically, high pollutant levels were attained at near coastal sampling areas (e.g., Flemish Banks) and the shipping lanes (Figure 21).

1.2.5. Water soluble components in size-segregated aerosols

The water-soluble (ionic) components in the three size-fractions of atmospheric aerosols detected during the cruises and the coastal campaigns in May 2010 are depicted in Figures 22a and 22b, respectively. In all the samples and aerosol fractions, F^- and NO_2^- were generally not detected with the present sampling/analytical method, or found at very low levels. In the marine air samples (Figure 22a), the contribution of coarse fraction is the highest (range: 4.7-17 $\mu g/m^3$, average: 6.7 $\mu g/m^3$) of the three size fractions, in the form of sea salt as Na^+, Cl^-, and Mg^{2+}, but NO_3^- and SO_4^{2-} are also present at increased levels, as compared to the lower aerosol fractions. On the other hand, the contribution of ionic species in the medium and fine fractions to the total ionic PM content is rather low (range: 1-3.5 $\mu g/m^3$, average: 1.6 $\mu g/m^3$). In the fine fraction, mostly NH_4^+ and SO_4^{2-} were found, while in the medium fraction, considerable percentages of sea salt (Na^+ and Cl^-) and anthropogenic NO_3^- is observed. These sampling cruises were mostly performed along the shipping lanes (leeward sides), besides relatively strong marine winds (mostly from NNE) were prevailing during the whole campaign. Consequently, the enhanced concentrations of aerosol nitrate and sulphate likely originate from ship emission. This is especially manifest in the 2-3-times increased levels of ionic pollutants for all three aerosol fractions observed during the cruises along the main international shipping lane (Figure 22a).

Figure 22. Concentration distribution of ionic components between three aerosol fractions during the May 2010 campaign onboard Belgica (a) and at the coastal background site (b); the extended x-axis indicates the sampling area, the prevailing wind direction(s) and the average wind speed in m/s
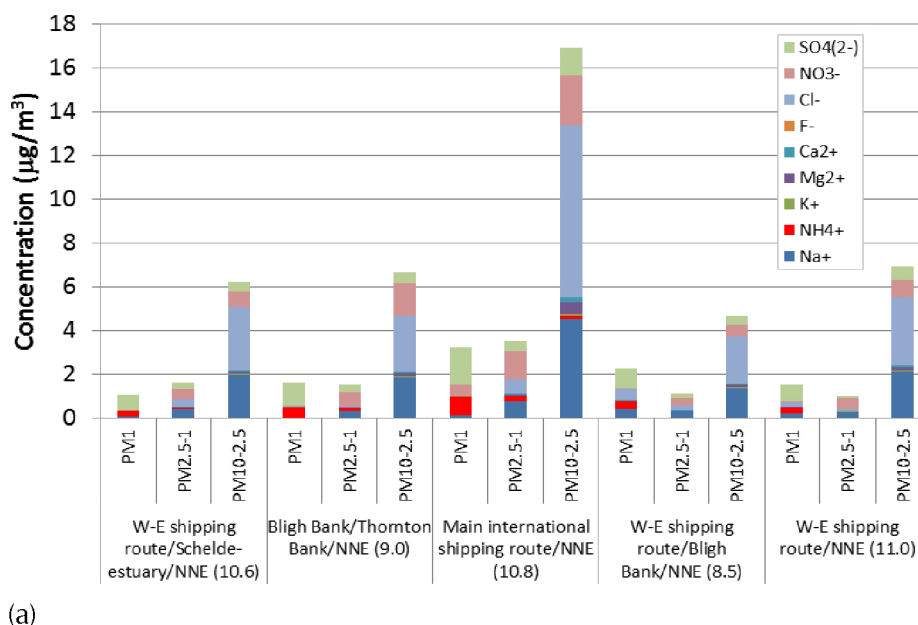
(a)

(continue Figure 22)
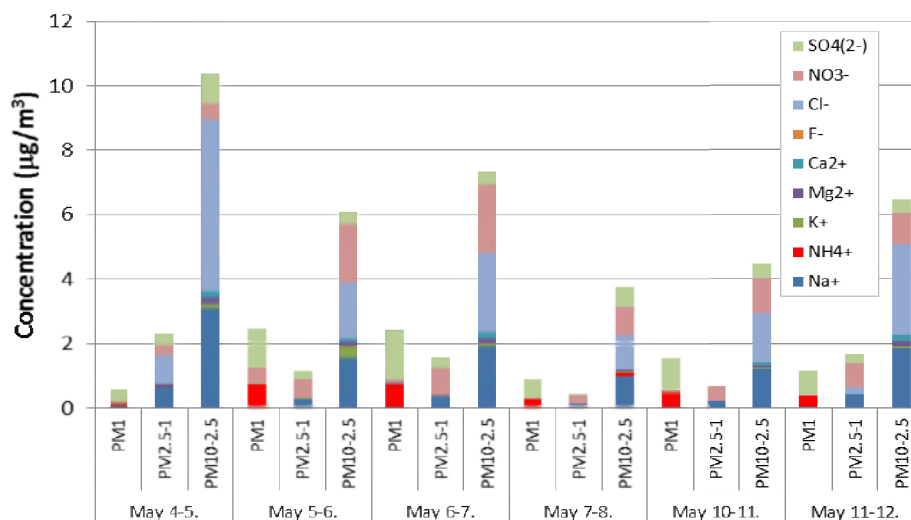
(b)

Similar ionic composition and size-distribution trend could be observed for the samples taken at the coastal site (Figure 22b). However, the concentration of anthropogenic species (e.g., nitrate, sulphate) is a bit higher than in the marine samples, while the contribution of sea salt species is of lower or similar extent.

The ionic components in the three size-fractions of atmospheric aerosols detected during the cruises in September 2010 are depicted in Figures 23a and 23b, respectively. Similar to the May 2010 campaign, in general, the level of the coarse aerosol fraction was observed to be the highest (range: 7-15 $\mu g/m^3$, average: 9.4 $\mu g/m^3$). Especially high concentrations of NO_3^-, SO_4^{2-} and NH_4^+ are observed over the main international and W-E shipping lanes and waters/marine sampling stations near Zeebrugge. However, the contribution of ionic species is different, in a sense that over the shipping lanes the anthropogenic components (NO_3^-, SO_4^{2-} and NH_4^+) dominate, while in the aerosols collected near Zeebrugge the sea salt is more abundant. Over coastal waters near Oostende/Nieuwpoort, the aerosol composition was generally found to be similar, though the total concentrations were a bit lower. It is to be noted, however, that during these samplings, the wind-speed was higher (average: 12-15 m/s) than during cruises over the shipping routes. This strong wind could dilute the air levels of the anthropogenic pollutants, as well as promoted the formation of more sea spray, as can be seen from the pattern of the observed aerosol composition (Figure 23a). As a comparison, the values observed at the coastal reference site in the first part of the September campaign (Figure 23b) represent very similar sea salt constitution, but higher NO_3^- and SO_4^{2-} content.

Figure 23. Concentration distribution of ionic components between three aerosol fractions in September 2010 campaign onboard Belgica (a) and at the coastal background site (b); the extended x-axis indicates the sampling area, the prevailing wind direction(s) and the average wind speed in m/s

(a)

(b)

The ionic components in the three size-fractions of atmospheric aerosols detected during the first and the second week's cruises in October 2010 are depicted on Figures 24a and 24b, respectively. This campaign was characterized with a mixed influence of winds from the continent and the sea. As expected on the base of former campaigns, the coarse aerosol fraction (range: 2.4-13.2 $\mu g/m^3$, average: 5.8 $\mu g/m^3$) was dominating mostly over the medium (range: 0.5-11.6 $\mu g/m^3$, average: 1.0 $\mu g/m^3$) and the fine (range: 0.6-12.7 $\mu g/m^3$, average: 1.5 $\mu g/m^3$) fractions (Figure 24a). The two exceptions were the samples collected over an anchoring area (pilot station) close to the shipping-lane to Zeebrugge, where the ionic concentration of the medium and fine aerosol fraction was higher by 1.5-2-fold than that of the coarse fraction. These lower sized-aerosol fractions mostly consisted of NH_4^+ salts of NO_3^- and SO_4^{2-}, which are products of secondary atmospheric reactions. The dense traffic intensity seems to provide an enhanced level of the precursor gases (especially, NH_3 and HNO_2, see Figure 18), and offers a possible explanation for the higher content of finer

particulates. The other samples/areas were characterized by low loadings of the medium and fine fractions, most of them consisting of NH_4^+ salts of NO_3^- and SO_4^{2-}, while the coarse fraction mostly contained aged sea spray (e.g., mixtures of NaCl, $NaNO_3$ and Na_2SO_4). However, the trend in the change of the aerosol composition is obvious, samples taken over marine areas influenced by the ship-traffic show increased concentrations of ionic pollutants (e.g., secondary nitrate and sulphate aerosols), as well as in the form of aged sea salt.

Figure 24. Concentration distribution of ionic components between three aerosol fractions in the first (a) and second (b) weeks of the October 2010 campaign onboard Belgica; the extended x-axis indicates the sampling area, the prevailing wind direction(s) and the average wind speed in m/s

(a)

(b)
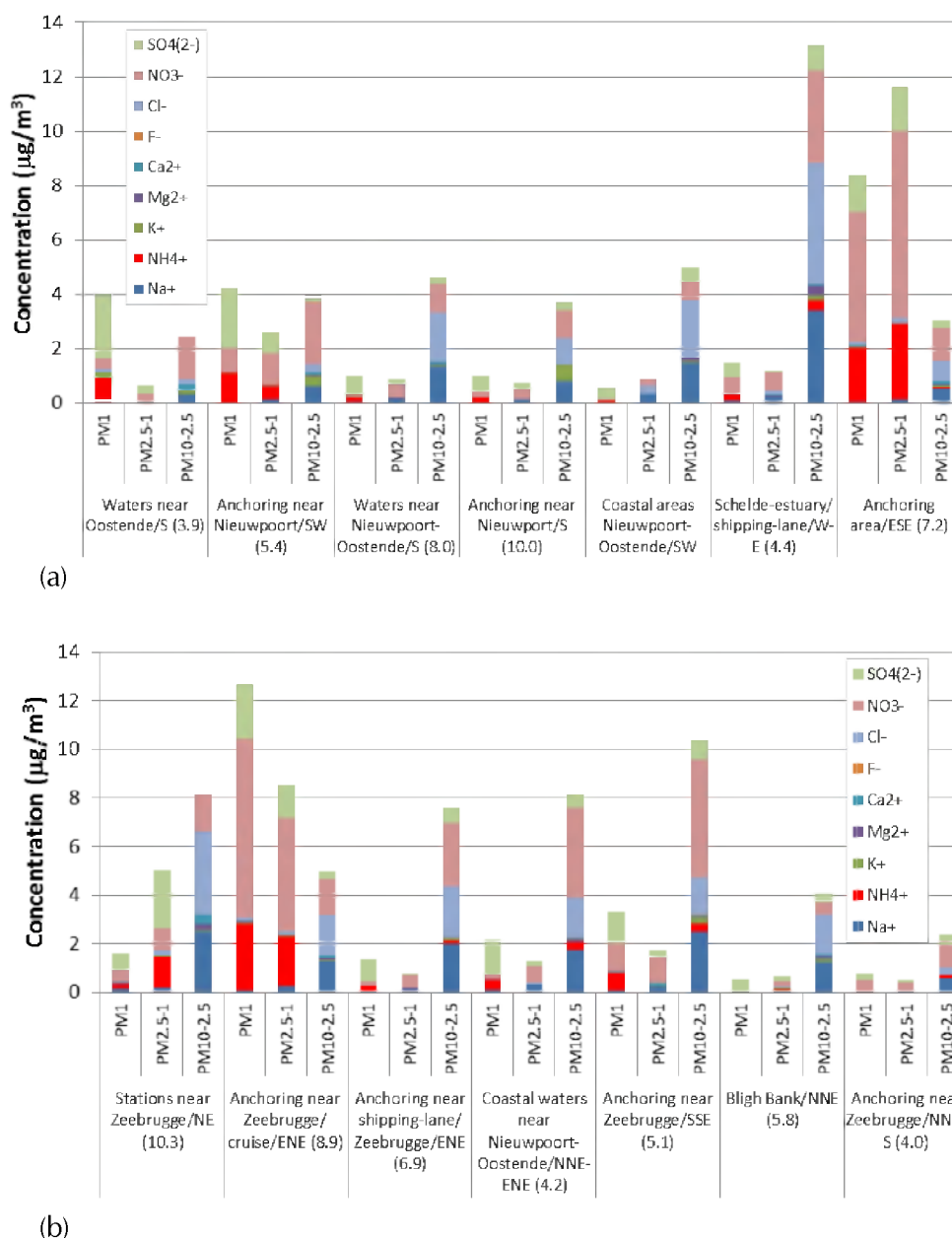
Comparing the results to those observed at the coastal site during the October campaign (Figure 25), one can see similar temporal trends in the ionic aerosol content as experienced over near coastal marine areas. On the other hand, the differences between the air concentrations of the coarse, median and fine aerosol fractions at the coastal site are generally lower (ranges: 0.02-6.0, 0.5-5.4 and 0.4-10 µg/m^3, with averages of 3.0, 2.5 and 3.1 µg/m^3, respectively) than those found over the sea. This is likely due to the terrestrial pollutant input to coastal areas supported by the weather conditions during this campaign (e.g. continental winds).

Figure 25. Concentration distribution of ionic components between the three aerosol fractions in October 2010 campaign at the coastal site of De Haan
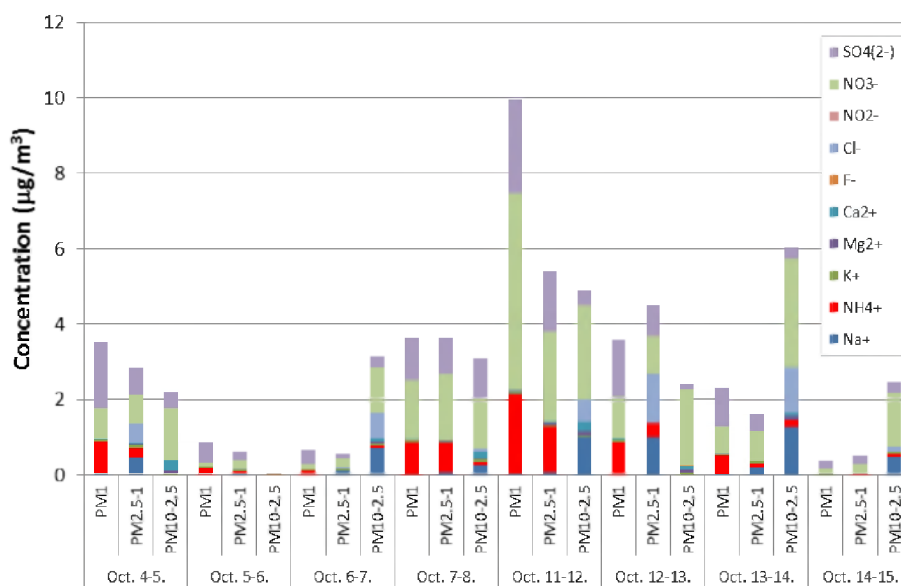
The ionic components in the three size-fractions of atmospheric aerosols detected during the first and the second weeks' cruises in March 2011 are depicted on Figures 26a and 26b, respectively. In this campaign, winds from the sea (NE/ENE) were mostly prevailing. This campaign was characterized with higher concentrations in the fine (range: 4.1-36 µg/m^3, average: 15 µg/m^3) and the medium (range: 1.2-17 µg/m^3, average: 9.2 µg/m^3) aerosol fractions than that of the coarse fraction (range: 0.4-11 µg/m^3, average: 5.6 µg/m^3). The highest concentrations of ionic species were observed in the first week of the campaign when most of the cruises were conducted on coastal waters to Schelde-estuary, the anchorage area, all being on or close to the shipping-lanes. The second week of the campaign could be characterized by much lower pollution content, but then again the fine ionic aerosol content was mostly found to be the highest. Compared to former campaigns, this reverse trend of the aerosol size distribution is mostly due to the weather, e.g., much lower average wind speed, the high relative humidity, fairly long morning fog-events, temperature inversion, etc. These weather conditions promoted the formation/coagulation of fine particulates, and resulted in enhanced atmospheric levels of ionic compounds. This is also manifest in the aerosol content, consisting mostly of NH$_4^+$, NO$_3^-$ and SO$_4^{2-}$ salts in the fine and medium fractions, while the sea salt components are generally present in the coarse particulate fraction.

Figure 26. Concentration distribution of ionic components between three aerosol fractions in the first (a) and second (b) weeks of the March 2011 campaign onboard Belgica; the extended x-axis indicates the sampling area, the prevailing wind direction(s) and the average wind speed in m/s
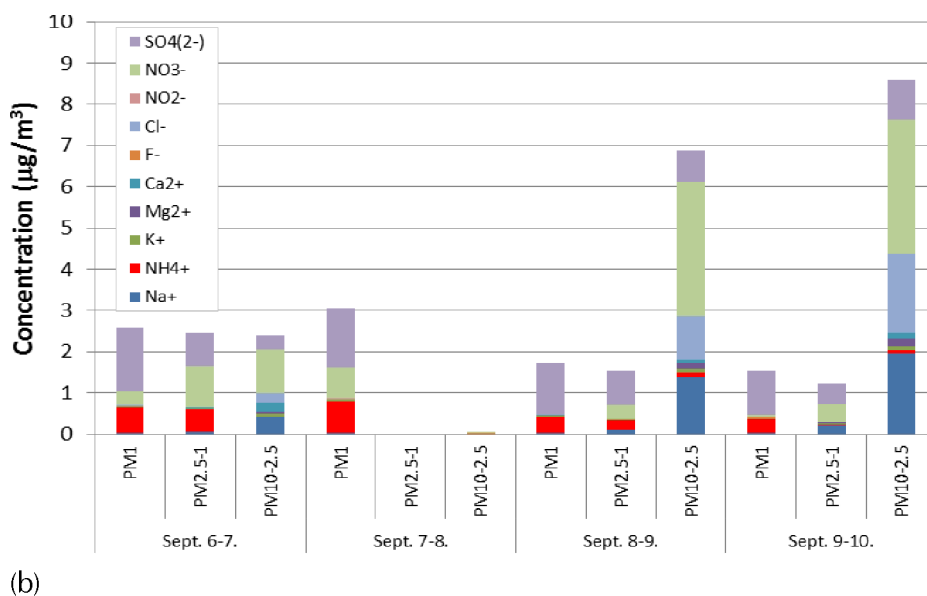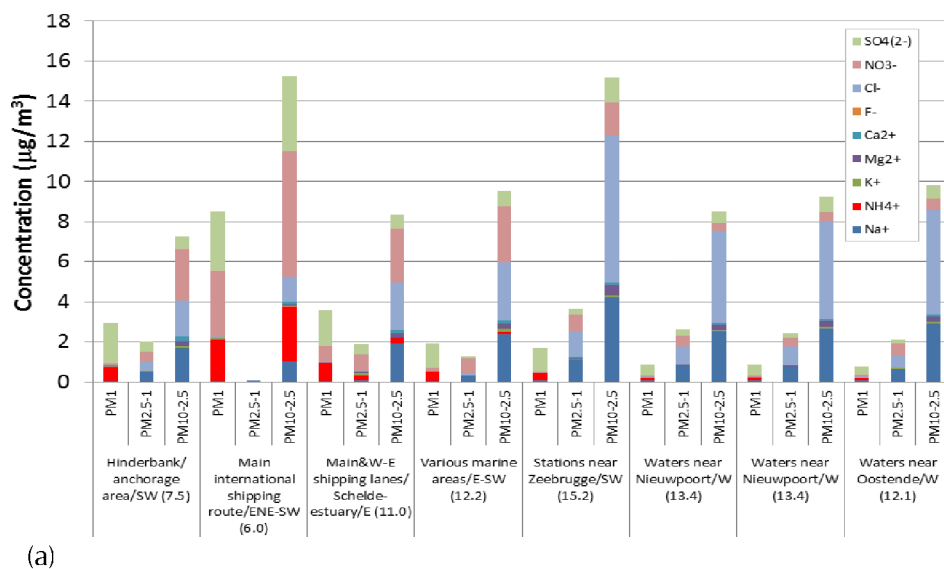

(a)

(b)
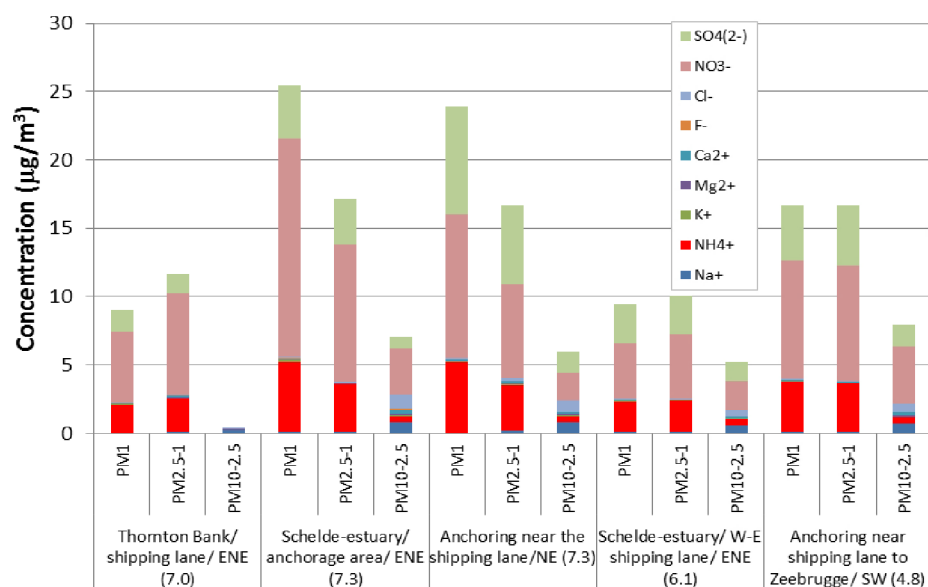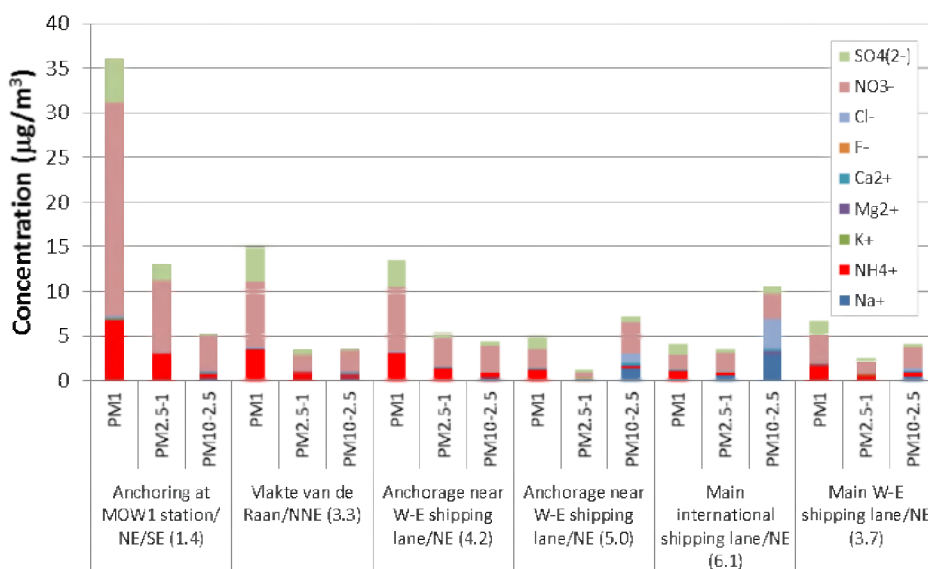
The ionic components in the three size-fractions of atmospheric aerosols detected during the first and the second weeks' cruises in May 2011 are depicted on Figures 27a and 27b, respectively. In this campaign, although the wind direction and its speed were considerably varying, it was of marine origin mostly. Similarly, as observed for the 2010 spring and autumn campaigns, the highest levels of ionic species are generally observed in the coarse fraction (range: n.d.-18.7 $\mu g/m^3$, average: 11 $\mu g/m^3$), while the fine and the medium fraction had similar concentrations, i.e., ranges: 1.2-13.2 and 1.5-4.7 $\mu g/m^3$, averages: 3.7 and 3.0 $\mu g/m^3$, respectively. Interestingly, in several areas, sea salt was prevailing in the coarse and medium sized aerosols. In general, high pollutant content was found for cruises near the shipping-lanes, close to the Schelde estuary/Vlakte van de Raan, which are all affected by high ship traffic intensity. Relatively high ionic content of

anthropogenic species are found near the area of Flemish Banks, and also the Thornton Bank, which is likely due to the low marine winds during these sampling periods, and the nearby ship-emission, maybe, the emission of Belgica too. The point measurements performed on anchor at different coastal areas has given very similar ionic composition.

Figure 27. Concentration distribution of ionic components between three aerosol fractions in the first (a) and second (b) weeks of the May 2011 campaign onboard Belgica; the extended x-axis indicates the sampling area, the prevailing wind direction(s) and the average wind speed in m/s
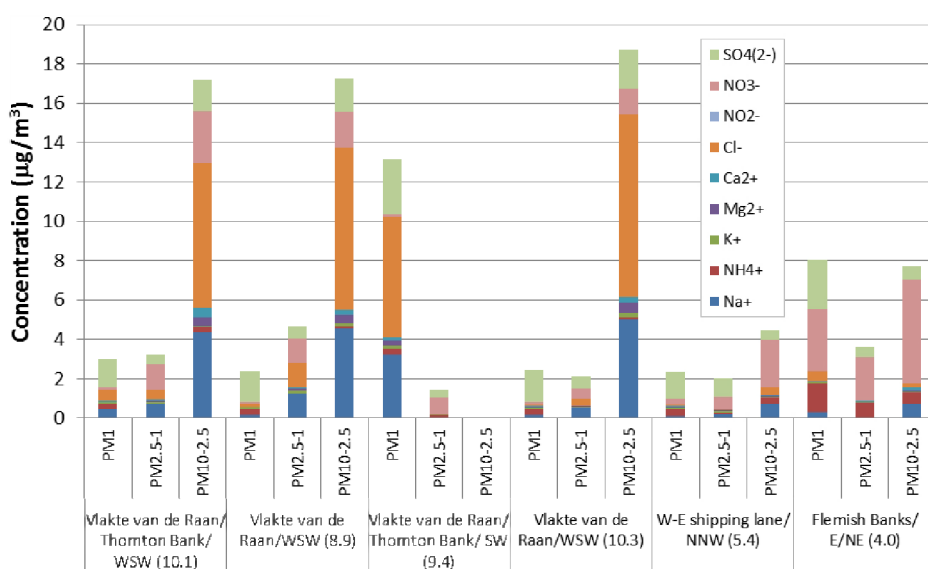
(a)
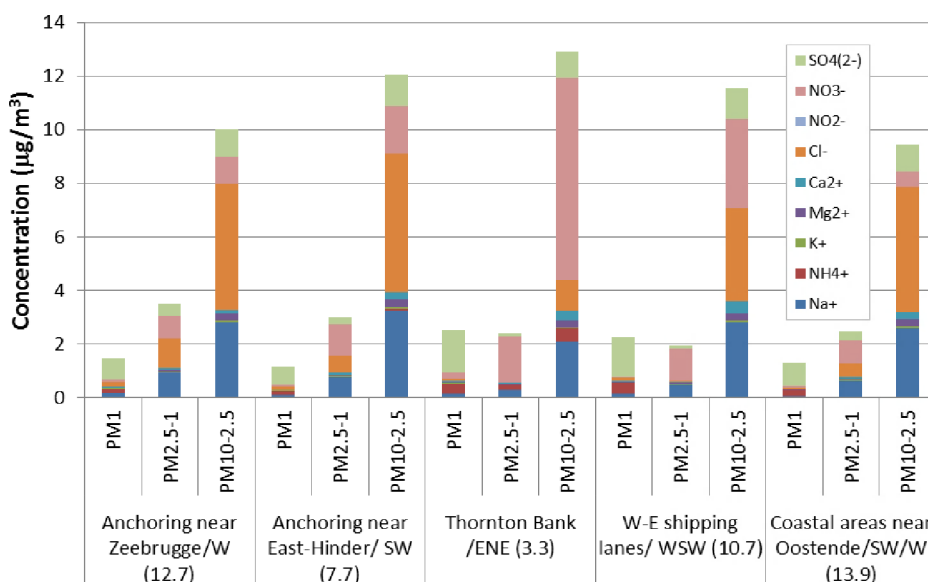
(b)

1.2.6. Monitoring and mapping of atmospheric black carbon concentration

A typical daily temporal evolution of the black carbon (BC) content of atmospheric air over the Bligh Bank (a representative of the Belgian marine areas) and over the international shipping route from the Bligh Bank to the British Channel and back is depicted on Figure 28. As can be seen, the BC level was fluctuating from 70 to 1550 ng/m^3 with an average value of 366 ng/m^3. This average BC value observed to be higher than those, obtained as the background level ($\sim$200 ng/m^3) for other marine areas out of the international shipping lane. The peak values of BC were also observed well distinguishable from the background value observed for the corresponding marine area (Figure 28). These BC peaks were attributed to the plume of the exhaust emission originating from ships passing close to the research vessel (Belgica) from windward direction. It is to be noted that the distance between these ships and the research vessel was never shorter than 200-300 m, but was proven to be close enough to distinguish the exhaust BC from the local background. This observation is in line with preliminary results on coastal monitoring of ship plumes performed at Hoek Van Holland (Balzani Lööv et al., 2010).

The concentrations of the "UV-active" air components were fluctuating from 35 to 2040 ng/m^3 with an average value of $\sim$320 ng/m^3. These data show the presence of PAH components evolved along with the EC content of ship exhaust plumes, which was further studied by the assistance of highly sensitive analytical techniques, e.g., GC-MS, as follow in the next section 1.2.7.

Figure 28. Temporal evolution of the black carbon (BC) and "UV-active" content of atmospheric air observed during the 2010 May campaign onboard Belgica; covered marine areas: Bligh Bank (00:00-7:00 a.m.) and the international shipping route from the Bligh Bank till the British Channel and back (10:00 a.m. − 12:00 p.m.)
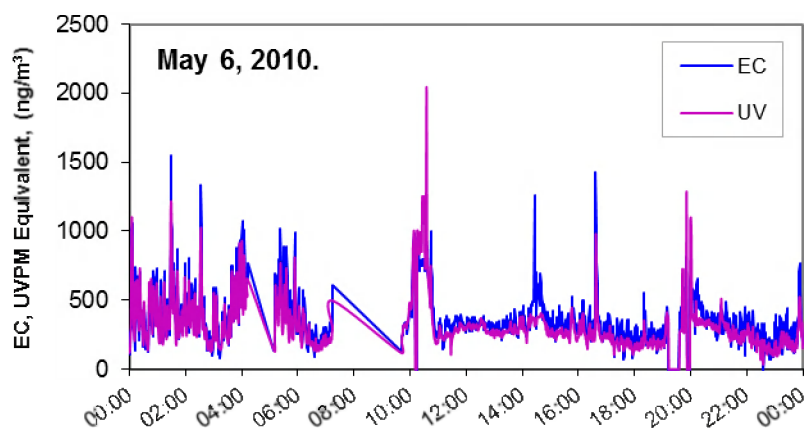
The high resolution concentration map of the BC over the studied marine areas of the North Sea for the May, September and October 2010 campaigns is depicted on Figure 29. It is to be noted that BC data was sampled in each minute over the cruise track of campaigns. As can be seen, the quite high BC levels with values of larger than 1200-1800 ng/m^3 (marked with red/amber colours) are experienced along the international shipping route and the shipping lanes towards the Schelde estuary, the anchorage areas of the cargo ships (pilot boat area). On the other hand, the BC levels show steep fall when diverting from these waters; e.g., to 100-400 ng/m^3, which one can accept as the background level of this marine area. It should also be mentioned, that the weather conditions highly influenced the observed BC values. For instance, northern/northeastern (marine) winds generally caused dilution of the air pollution, whereas the southern, southwestern, or eastern (continental) winds generally enhanced the background BC levels.

Figure 29. Concentration distribution of atmospheric black carbon (in ng/m³ unit) over the Belgian North Sea and the international shipping route observed during the Belgica cruises in 2010 (a); magnified BC map of the Belgian continental shelf (b)

(a)   (b)
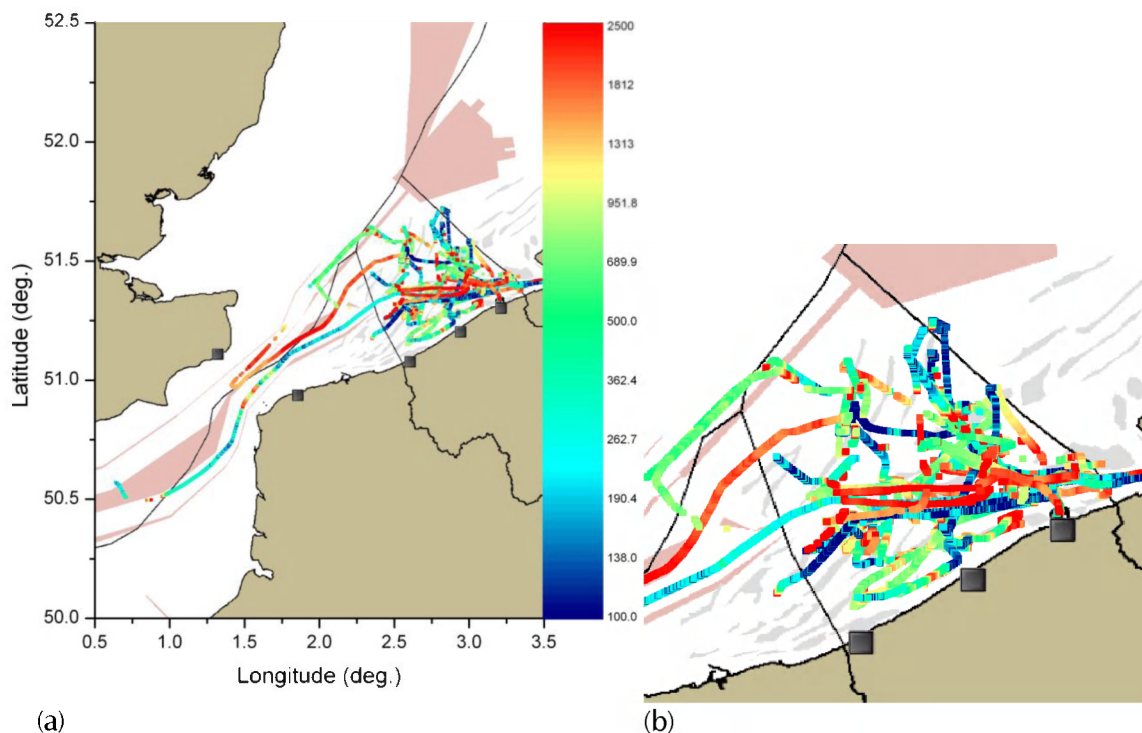
The high resolution concentration map for atmospheric black carbon of the studied marine areas over all the Belgica campaigns is depicted on Figure 30. It is to be noted that this image is made with the method of averaging the data according to a geographical grid with a size of 0.01° by 0.01°. As can be seen, the trends are as expected on the base of the 2010 campaign data. Namely, the BC concentration is the highest over and close to the main shipping lanes (e.g., 1.5-2.5 µg/m³), for instance, the W-E oriented shipping lane, which connects the large Belgian harbours to the main international shipping route. The BC concentration is also high near the anchorage area. The concentration is only slightly increased (compared to the marine background level) at sites off the shipping routes, as well as near coastal sites. But then again, the BC concentration is high near the harbour of Zeebrugge, mostly due to the high intensity of ship traffic in this region.

Figure 30. Map of the Belgian continental shelf (a) and its atmospheric black carbon concentration pattern in ng/m³ (b) with all data of the Belgica campaigns (concentrations are averaged and plotted according to geographical location using a grid of 0.01° by 0.01°)

(a)   (b)
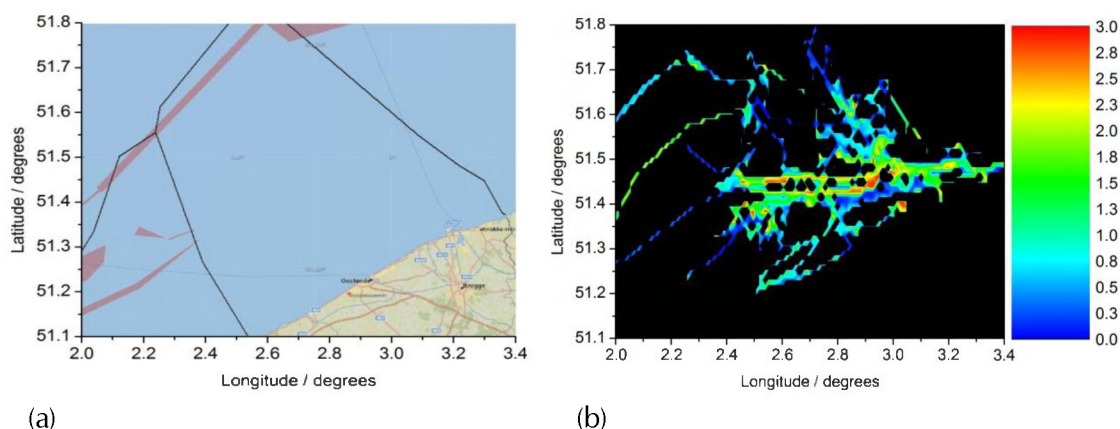
1.2.7. Air levels of polycyclic aromatic hydrocarbons

Figures 31-35 visualize the air levels of PAHs that were found during various sampling campaigns (May, October 2010 and February, March, May 2011). Eleven PAH compounds have been identified in the sampled PM, including phenenthrene (Phe), anthracene (Ant), fuoranthene (Flu), pyrene (Pyr), benzo(a)anthracene (BaA), chrysene (Chry), benzo(bjk)fluoranthenes (BbjkF), benzo(a)pyrene (B(a)P), dibenzo(a,h)anthracene (DiB(a,h)A), benzo(ghi)perylene and indeno (1,2,3-cd)pyrene (I(1,2,3-cd)P). Benzo(bjk)fluoranthene was dominant amongst all PAHs, followed by chrysene and pyrene. The total PAHs concentration was in the range of 152–4690 pg/m³, being the lowest during the cruise: the Bligh Bank/Anchoring near Zeebrugge in October 2010 and the highest during the cruise on the shipping lanes and the anchoring near the pilot station ship anchoring-area in February 2011.

In May 2010, the PAH levels were observed to be commensurable at the coastal sampling station of De Haan to those observed over the shipping routes/Bligh Bank (Figure 31). For the October 2010 campaign, the highest levels of PAHs are observed at the sampling stations near Zeebrugge, near the shipping lanes, and the anchoring area (Figure 32). Very low levels of PAHs are observed at Bligh Bank, and Anchoring near Zeebrugge, , and on waters near Oostende/Nieuwpoort under influence of NNE and SSW/SW marine winds. These air PAH levels can be accepted as a typical marine background for the Southern Bight of the North Sea. Similarly low PAH levels were observed at the Thornton Bank in February 2011 (Figure 33). Interestingly, in this sampling campaign, the PAH levels increased to a various extent over the shipping lanes, the anchoring area and Kwinte bank, which is likely due to weather conditions, most importantly, the wind direction, and speed.

During the March 2011 campaign, the lowest levels of PAHs are observed at the Vlaakte van de Raan area under marine winds, while increased PAH concentrations were observed near the shipping lanes and anchoring areas (Figure 34), as observed for other campaigns too. In the May 2011campaign, similar to the March 2011 campaign, the lowest levels of PAHs are observed at

the Vlaakte van de Raan area under marine winds with fairly high velocity. Increased concentrations of PAHs are observed at the Thornton Bank/Vlakte van de Raan, likely due to sailing over the shipping lanes, which certainly raise the pollutant levels. Increased PAH levels were also observed over the Thornton Bank and the Flemish Banks under the influence of continental (E/NE) winds.

Seasonally, in general, lower PAH concentrations were found in October and May months (with the exception of May 2010- here however only two samples were available from onboard sampling – due to technical problems/bad weather conditions), than during February and March. This is consistent with the fact that meteorological conditions (less daylight hour, reduced ambient air temperatures thus lower volatilization and photochemical activity) contribute to the higher PAHs levels in winter season.

Figure 31. Concentration distribution of PAHs in total PM sampled during May 2010 campaign onboard Belgica and in De Haan sampling station; (the extended x-axis indicates the sampling area, the prevailing wind direction(s) and the average wind speed in m/s)
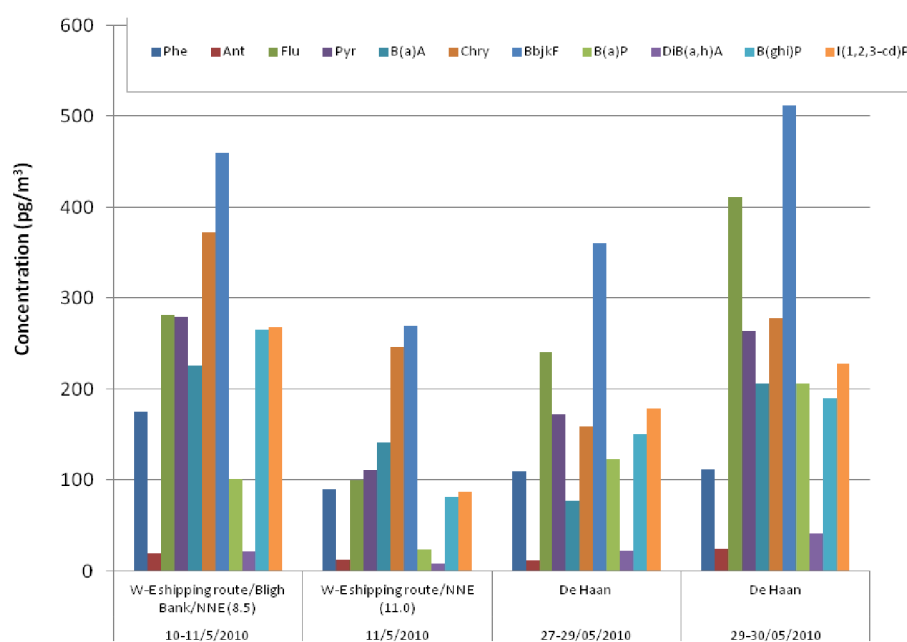
Figure 32. Concentration distribution of PAHs in total PM sampled during October 2010 campaign onboard Belgica; (the extended x-axis indicates the sampling area, the prevailing wind direction(s) and the average wind speed in m/s)
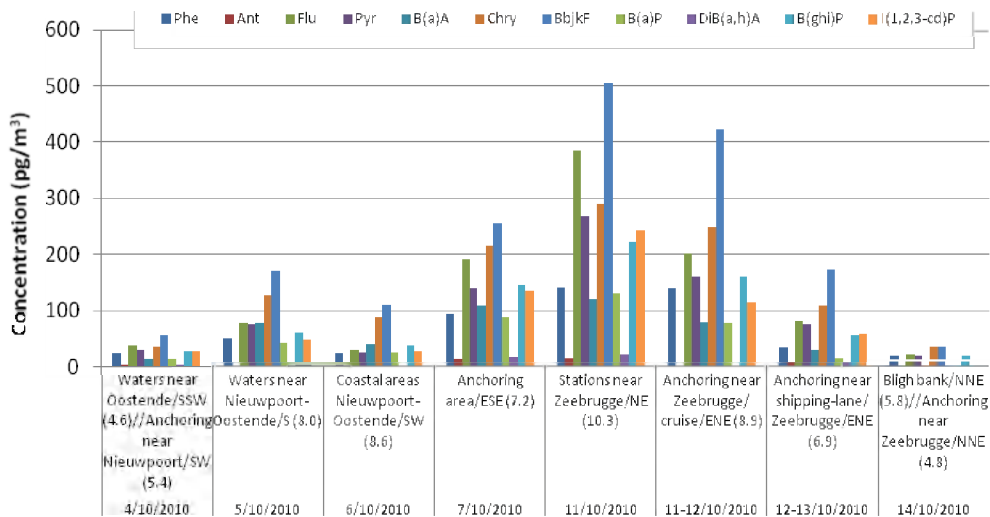
Figure 33. Concentration distribution of PAHs in total PM sampled during February 2011 campaign onboard Belgica; (the extended x-axis indicates the sampling area, the prevailing wind direction(s) and the average wind speed in m/s)
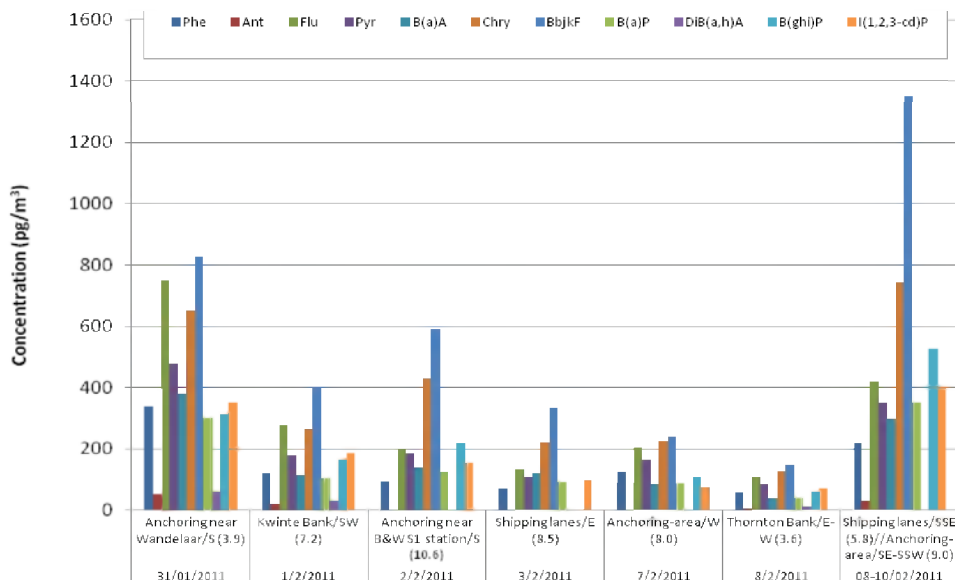
Figure 34. Concentration distribution of PAHs in total PM sampled during March 2011 campaign onboard Belgica; (the extended x-axis indicates the sampling area, the prevailing wind direction(s) and the average wind speed in m/s)
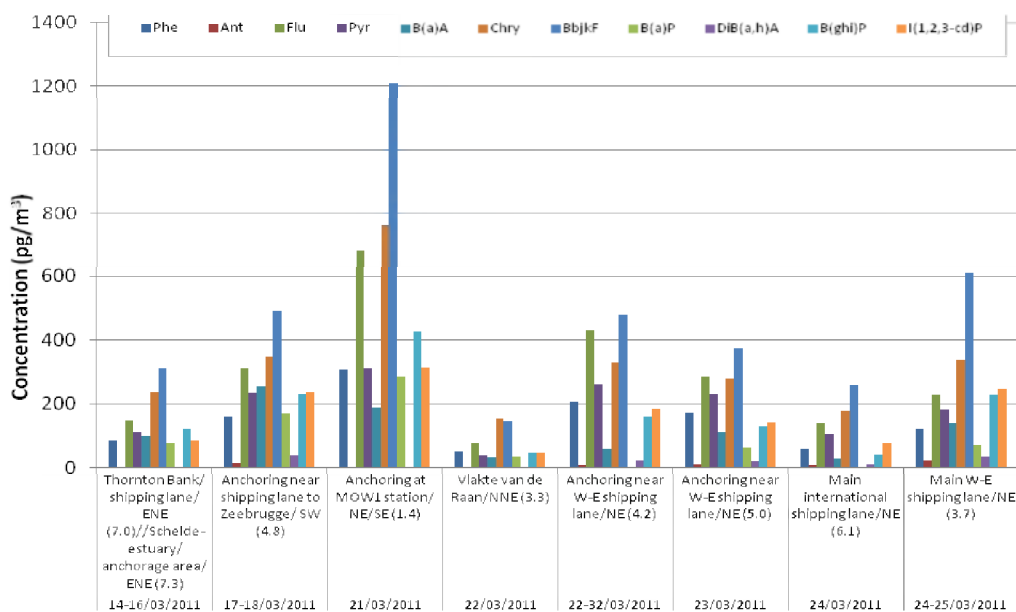
Figure 35. Concentration distribution of PAHs in total PM sampled during May 2011 campaign onboard Belgica; (the extended x-axis indicates the sampling area, the prevailing wind direction(s) and the average wind speed in m/s)
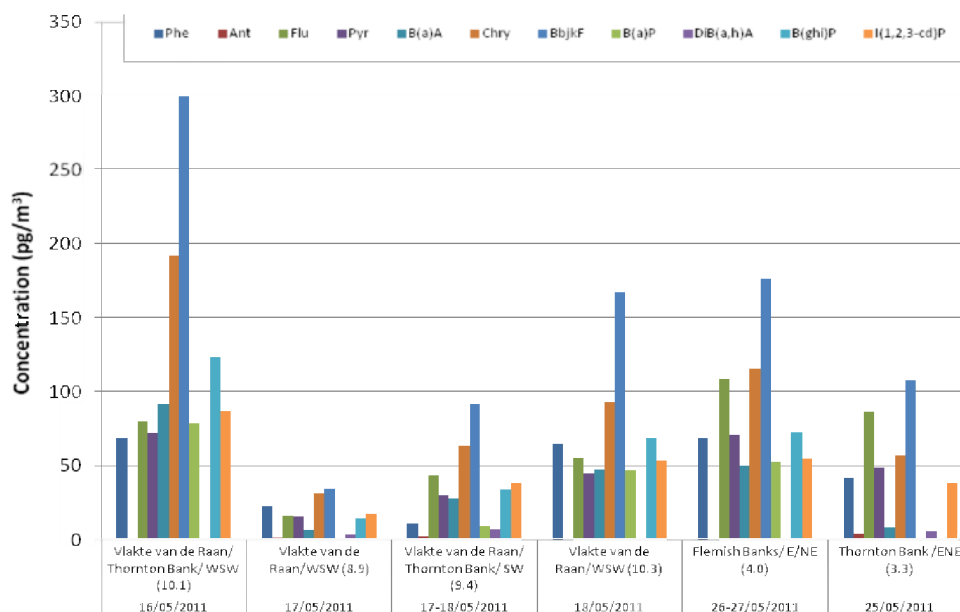
Work Package 2: Emission model for maritime transport

2.1. Introduction – Emissions as input for air quality models

Emissions of pollutants are a crucial input to any air quality modelling exercise. In general, two methods can be used to provide emission estimates for air pollutants. Emissions are inventoried using either a bottom up, or a top down approach.

Annual quantities of anthropogenic emissions to the air are mostly compiled by regional or national environmental agencies and categorized by source category for a particular geographic area and specific time interval. Hereto, a bottom up approach is used: emissions are estimated for individual sources and summed over all sources to obtain estimates at city, provincial, country, continental and global level. In this approach the following relation is valid:

$$\text{local emission} = \text{'activity'} \times \text{'activity factor'}$$

In the EU, the competence for emission inventories is fragmented over different national or regional agencies. This results in different standards, methods and source categories being used when compiling emission inventories, even within single countries. Collecting emissions from regional and national emission inventories for usage in air quality models with a transboundary model domain is therefore a challenging task.

An alternative for the bottom up compilation of emissions is the top down disaggregation of emission totals reported by supranational or global inventories. In a top down approach, emissions are estimated based on national, regional or provincial data. These emissions are given a geographic distribution by using some measure of activity data, which is directly or indirectly related to the emissions. These activity data, holding information on the geographical patterns, are called proxy data. Typical examples are population density maps, road networks, location of power plants, land cover maps. In a top down approach the local emission is defined as follows :

$$\text{local emission} = \text{'proportion'} \times \text{'total emission'}$$

The 'total emission' is an estimate from the national, regional or provincial data (note that gridded data at low resolution is also an option), the proportion is computed based on the proxy data.

In general, bottom up emissions contain the highest level of detail as they are obtained based on information that only might be available to local authorities. However, local data are often not useful for a variety of reasons: they may not be complete (missing pollutants, missing sector information, only data for a specific year, etc.), they may reveal patterns that are difficult to explain, they may not cover the whole model domain, etc. Therefore, bottom up data are often replaced by top down (downscaled) emission data, or at least completed with modelled emission data.

The emission data sets used for the modelling in SHIPFLUX were obtained by combining bottom up and top down emission estimates.

2.2. Bottom up (high-resolution) emissions for the Belgian Continental Shelf (BCS) and the river Scheldt

2.2.1. Introduction

For the Belgian Continental Shelf (BCS) and the river Scheldt, bottom up emissions were computed by VITO. To map the maritime traffic in the Belgian territorial waters and surroundings three sources of information were used: AIS (Automatic Identification System) messages, AIS vessel data and a Lloyd's database. The AIS data were delivered by VLIZ. With the AIS data the emissions on the river Scheldt and the BCS have been calculated. Only emissions of tankers, passenger ships

and cargo ships are taken into account. For the harbour emissions the results of the MOPSEA project ("Monitoring programme on air pollution from sea-going vessels", BELSPO) have been used.

2.2.2. Input data

2.2.2.1. AIS messages

AIS messages are sent more or less every mile or every half an hour. The area covered by the messages is between 2.246628333° and 4.751421667° longitude and 51.03702333° and 52.09211333° latitude.

For later analysis and validation the area was divided into different zones (see Figure 36):
- 5 harbours: Antwerp, Zeebrugge, Ghent, Ostend and Vlissingen (green),
- The North Sea: Belgian 12-mile zone (blue), Belgian Continental Shelf (BCS, blue), exit/entry zones to the BCS (red), Dutch Continental Shelf (yellow);
- The river Scheldt (blue);
- Other entry/exit zones: Scheldt-Rhine canal, Canal of Zuid-Beveland (red).
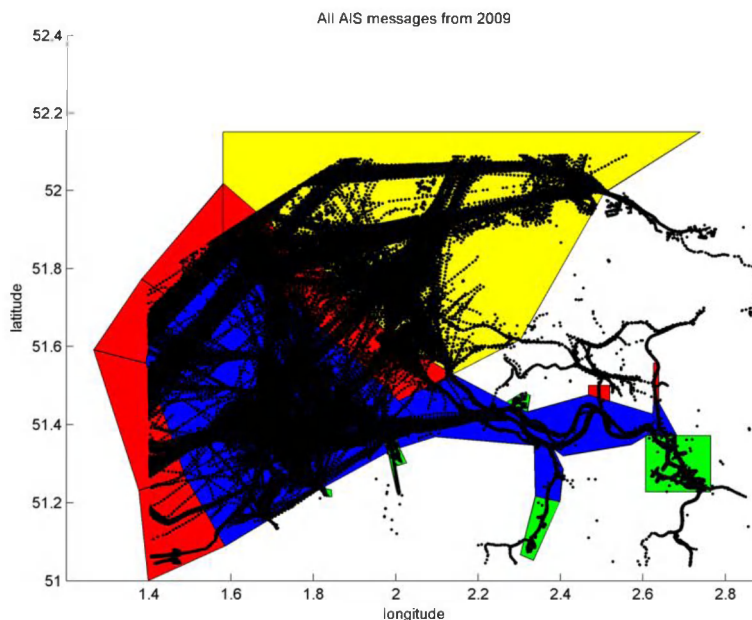
Figure 36. AIS messages received in 2009 (longitude multiplied by cos51° for correct aspect ratio) and division into different zones

In 2009, 15 939 327 messages were received in 2009. Table 5 shows the content of an AIS message.

Table 5. Information available in an AIS message

Data field	Description
VesselAISID	Does not identify a ship uniquely in vessel data table, not used
AISTrajectPositionTimestamp	time stamp containing date and hour in the format "dd-mm-yyyy HH:mm:ss.sss")
AISTrajectPositionLongitude	the WGS84 degrees longitude in decimal format
AISTrajectPositionLatitude	the WGS84 degrees latitude in decimal format
VesselAISKey	Identifies the ship uniquely in vessel data table, this one is used in this study

2.2.2.2. AIS vessel data

The AIS vessel data is a table containing 640711 records with a unique VesselAISKey (see Table 6). The VesselAISIMONumber is a unique number for each ship and corresponds to the Lloyd's register number (LRNO) in the Lloyd's database. Between the VesselAISIMONumber and the VesselAISKeys there is a one-to-many relation. Hence, the VesselAISKeys can be used to identify the ship. Between the VesselAISIMONumber and the VesselAISID there is a many-to-many relation. Some VesselAISIDs correspond to many (up to 22) different ships and each VesselAISIMONumber corresponds to many VesselAISIDs. Hence, the VesselAISIDs are not used.

Table 6. Information available in table AIS vessel data

Data field	Description
VesselAISKey	Identifies the ship in an AIS message, this one is used
VesselAISID	Not a unique ship identifier, this one is not used
VesselAISLength	Length of the ship
VesselAISIMONumber	IMO number, link with Lloyd's database
VesselAISName	Name of the ship
VesselTypeAISDescription	Type of the ship (Cargo, Tanker, Passenger, etc.
...	Other data not of interest

The VesselTypeAISDescription gives general information about the type of the ship. For emissions calculation only Cargo, Tanker and Passenger ships were taken into account. Smaller ships like pilot vessels, tugs, dredgers and fishing vessels are not taken into account. For emissions calculation the classification into Cargo, Tanker or Passenger ship is not sufficient. A more detailed classification is obtained from the Lloyd's database.

2.2.2.3. Lloyd's database

The Lloyd's database contains the necessary information to calculate the emissions of a given ship. We have a database of the year 2004 that contains information about 9481 ships (see Table 7).

Table 7. Relevant information available in Lloyd's database.

Data field	Description
LRNO	Lloyd's Register Number = VesselAISIMONumber
Scheepstype	10 ship types
Lengte	Length of the ship
Catlengte	Ship length category (< 100, 100 – 150, 150 – 200, 200 – 250, > 250)
Type brandstof	Fuel type (Diesel oil, Heavy fuel oil, Gas boil off)
DateBuild	Build year
CatBouwjaar	Build year category (5-year intervals)
Main Stroke Type	Main engine type (2-stroke, 4-stroke or steam turbine)
PowerKWPrime	Main engine nominal power
PowerHulpmotor	Auxiliary engine nominal power
RPM	Nominal main engine speed
…	

The correspondence between the Lloyd's ship type and the AIS ship type is given in Table 8.

Table 8. Correspondence between the Lloyd's ship type (Scheepstype) and the AIS ship type (VesselTypeAISDescription)

Lloyd's ship type	VesselTypeAISDescription
Containers	Cargo
Dry bulk carrier	Cargo
General Cargo	Cargo
Reefers	Cargo
RoRo	Cargo
Passenger ship	Passenger
Chemical tanker	Tanker
Gas tanker	Tanker
LNG tanker	Tanker
Oil bulk (crude)	Tanker
NVT	-

To summarize the methodology for the identification of a ship, every AIS message contains the time, the latitude, the longitude and a VesselAISKey. This VesselAISKey refers to another table: the AIS vessel data. This table contains the IMO number and the AIS ship type. Only ships of AIS type 'tanker', 'passenger' or 'cargo' were taken into account. The IMO number appears in the Lloyd's database. This database contains the necessary information to calculate the emissions of a ship.

2.2.3. Emissions calculation

2.2.3.1. Introduction

In the marine area of this study (Belgian Continental Shelf and river Scheldt) emissions are calculated using the AIS data. Harbour emissions are obtained from the MOPSEA model.

In a first step, the ship that sent an AIS message has to be identified, i.e., its IMO number has to be determined. With this number the characteristics of the ship that determine the emissions can be obtained. Next, the time interval and speed corresponding to each message are calculated. Then, the emissions corresponding to each message result from the combination of emission

functions and ship characteristics. Finally, the results were validated with results from the MOPSEA project.

2.2.3.2. Ship identification

To get the IMO number of a ship, the VesselAISKey of the AIS message table was linked with the VesselAISKey in the vessel data table (see above). For 85.1 % of the messages (13 570 777 messages) the IMO number is known. 73.3 % of the messages come from a tanker, a passenger or a cargo ship. Because a Lloyd's database dating from 2004 has been used, only for 36.1 % of the messages the Lloyd's ship type could be determined (5 760 221 messages). If the Lloyd's ship type is not known the VesselTypeAISDescription is used. In this way 37.2 % of the messages could be identified as coming from a cargo, tanker or passenger ship.

2.2.3.3. Time interval and speed

The data were ordered per ship and per time. Then the time increment was calculated as the difference between the following and the previous time divided by 2. The speed was calculated as the central derivate of position to time. The speed determines the maximum continuous rate (MCR) or engine load. Speeds below 2 knots were considered as anchoring and have MCR zero. On the North Sea, higher speeds are considered as cruising with an MCR of 85%. On the river Scheldt higher speeds are considered as reduced speed with a MCR of 65%. These assumptions are the same as used in the MOPSEA project and are confirmed with the speed distribution shown in Figure 37.
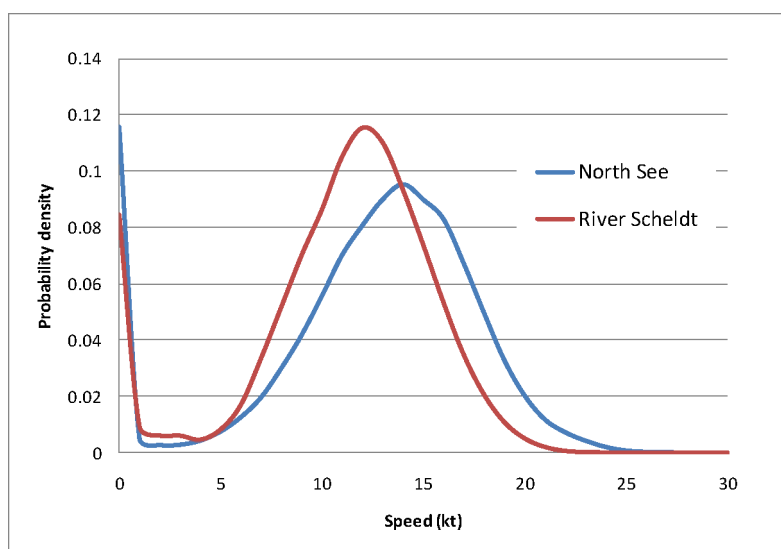
Figure 37. Speed distribution of the AIS messages on the North Sea and on the river Scheldt

Some data cleaning was necessary. Points with times increments higher than 3600 seconds were eliminated. Normally ships send a message every 1800 seconds or every mile. Abnormally high speeds, i.e., speeds higher than 35 knots were eliminated, too. These anomalies represented only 1.2% and 0.26% of the data, respectively.

2.2.3.4. Emissions

Finally, emissions of the ships in the Lloyd's database were calculated. The emissions are a function of the ship type, the fuel, the technology class (build year), the engine load (MCR) and the main engine type (MET). The MCR is determined by the calculated speed, the other data are found in the Lloyd's database.

Because not all ships are present in the Lloyd's database emission factors are calculated with the known ships. A differentiation between zones (North Sea or river Scheldt) and AIS ship type (tanker, cargo and passenger) is necessary because of the speed difference. The emission factors are applied to the partially known ships, i.e., ships in the scope of this study, but not present in the Lloyd's database.

2.2.3.5. Validation with MOPSEA results

The results were validated with the outcome of the MOPSEA project. In the framework of the MOPSEA project, predictions were made for the emissions in the Belgian 12-mile zone and on the river Scheldt in the year 2010. In this project, emission calculations were based on ship movements and average travel times. In Table 9, these predictions are compared with the emission calculations based on AIS data of 2009. There is a good agreement between both results. However, CO_2 and PM_{10} emissions are closer to the lower MOPSEA predictions while NOx and SO_2 emissions are closer to the higher predictions.

Table 9. Validation of top down emission estimates based on AIS Data for 2009 with the outcome of the MOPSEA project in which predictions for 2010 were made

Pollutant	AIS data 2009	MOPSEA prediction 2010	
	Main + Auxiliary Engines in kton	Main + Auxiliary Engines in kton	
		Low	High
NO_x	18.7	17.1	18.1
NMVOC	0.501	n/a	n/a
NH_3	2.37E-03	n/a	n/a
PM_{10}	1.106	1.25	1.34
$PM_{2.5}$	0.678	n/a	n/a
SO_2	5.81	5.16	5.48

2.2.3.6. Emissions for the Belgian harbours from MOPSEA

Table 10 shows the emissions in the Belgian harbours.

Table 10. Harbour emissions from the MOPSEA model.

Year	Region	Pollutant	Emissions_kton
2009	Antwerp	CO_2	43.38
2009	Antwerp	NO_x	1.203
2009	Antwerp	PM_{10}	0.06900
2009	Antwerp	SO_2	0.4105
2009	Ghent	CO_2	6.609
2009	Ghent	NO_x	0.1733
2009	Ghent	PM_{10}	0.01034
2009	Ghent	SO_2	0.06194
2009	Ostend	CO_2	1.002
2009	Ostend	NO_x	0.02315
2009	Ostend	PM_{10}	0.00153
2009	Ostend	SO_2	0.00944
2009	Zeebrugge	CO_2	9.036
2009	Zeebrugge	NO_x	0.22446
2009	Zeebrugge	PM_{10}	0.01314
2009	Zeebrugge	SO_2	0.07931

Query in E-motion_Maritime_emissies.accdb
SELECT tbl_Mari_O_ME_Emissions_Geo.Year, tbl_Mari_O_ME_Emissions_Geo.Region, tbl_Mari_O_ME_Emissions_Geo.Pollutant, Sum([Emission]/1000) AS Emissions_kton FROM tbl_Mari_O_ME_Emissions_Geo GROUP BY tbl_Mari_O_ME_Emissions_Geo.Year, tbl_Mari_O_ME_Emissions_Geo.Region, tbl_Mari_O_ME_Emissions_Geo.Pollutant HAVING ((((tbl_Mari_O_ME_Emissions_Geo.Year)=2009) AND ((tbl_Mari_O_ME_Emissions_Geo.Pollutant)="NOx" Or (tbl_Mari_O_ME_Emissions_Geo.Pollutant)="SO2" Or (tbl_Mari_O_ME_Emissions_Geo.Pollutant)="CO2" Or (tbl_Mari_O_ME_Emissions_Geo.Pollutant)="PM10"));

2.2.4. Possible improvements of the applied methodology

The speed could be used to make a more accurate estimate of the MCR. Also, the AIS data could be coupled to a more recent version of the Lloyd's database. Finally, the age distribution of the unknown ships is supposed to be equal to the one of the known ships in this study. Hence, the fleet in the simulations is (somewhat) too old.

2.2.5. Results

Figure 38 shows as an example, the annual mean NOx emissions as derived from the 2009 AIS data. The main shipping routes are clearly visible on this map, especially the route going to/from Antwerp via the Scheldt. Apart from this, the two areas where the ships have to wait for the assistance of a pilot to be allowed to enter the Scheldt are also characterized by significantly enhanced emissions.

As the AIS data cover a somewhat larger area than only the Belgian marine waters, emission maps have been produced for an area including also parts of the neighbouring Dutch, French and UK marine areas. The advantage of having emissions for a larger area at our disposal is to have a common emission dataset for the AURORA-model, in which the domain has to be larger than the Belgian marine areas under study.

However, due to the long-range transport of air pollutants, shipping emissions from a still larger area had to be taken into account. This step is described in the following sections.
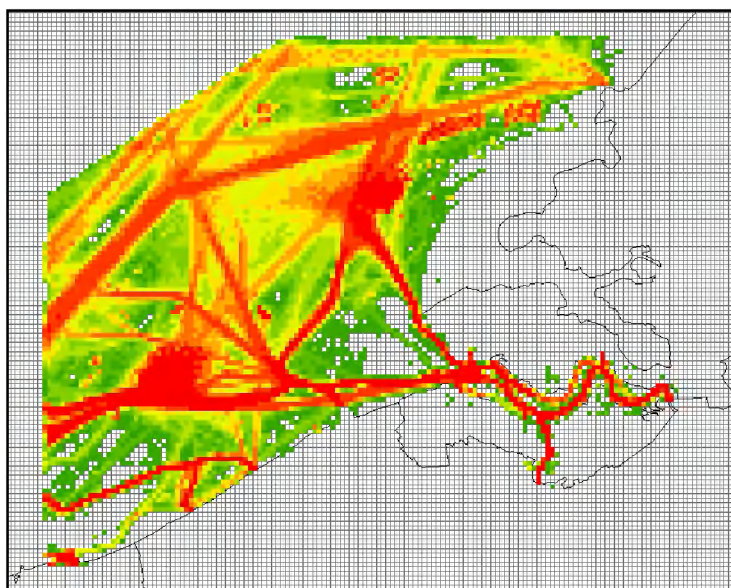
Figure 38. Annual mean NO_x-emissions for 2009 on a 1 km x 1 km grid for the Belgian marine waters and parts of the neighbouring Dutch, French and UK marine waters

2.3. Shipping emissions in the North Sea harbour areas

In the framework of PASODOBLE, a collaborative project under THEME FP7-SPACE-2009-1 of the EC's Seventh Framework Programme, DCMR Milieudienst Rijnmond (The Netherlands) provided bottom up emissions for the North Sea harbour areas. These emissions were used to validate the VITO shipping emissions on the BCP. Indeed, the DCMR data allowed to compare spatial patterns and absolute numbers for regions that were covered by both data sets.

The bottom up marine emissions provided by the DCMR yield emissions totals for 2008 for CO, CO_2, NMVOC, NOx, PM and SO_2 per port area in the Netherlands: Amsterdam, Rotterdam, Western Scheldt, Eems (see Figure 39). The grid size that is used is 500 m x 500 m (DCMR, 2008).
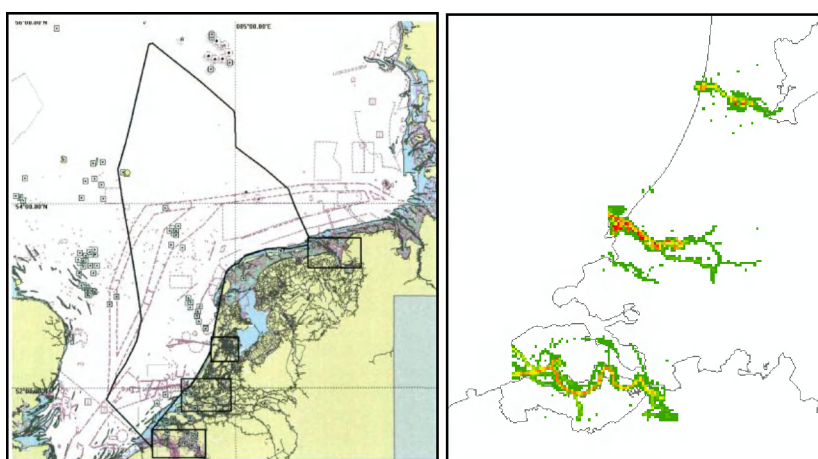
Figure 39. Left: Extent of the domains covering the 4 different port areas: Western Scheldt, Amsterdam, Rotterdam, and Eems. Right: Spatial patterns of the emissions in the North Sea harbour areas

The geographical allocation of the marine DCMR emissions to the 1 km x 1 km air quality modelling grid occurred by summing the emissions of all emission sources contained within a particular cell. The quantitative analysis is for all ports and all pollutants summarized in Table 11.

Table 11. Quantitative analysis of bottom up shipping emissions in the North Sea harbour areas, as computed by DCMR.

2008 in ton	NMVOC	SO_2	NOx	CO	CO_2	PM
Amsterdam	109.7	992.6	2465	571.6	183300	130.8
Eems	38.39	347.2	997.0	201.8	51940	47.33
Rotterdam	433.2	4565	10180	2327	799300	590.0
Western Scheldt	320.1	3454	9430	1905	4164	518.2

As revealed by Figure 38 and Figure 39 comparison of DCMR and VITO bottom up absolute numbers can only be made for the Western Scheldt, as this is the only overlapping region. The comparison for the Western Scheldt was made by only retaining the VITO output on grid cells, which have a non-zero output in the DCMR data (for the Scheldt). Results are summarized in Table 12. It should be noted that the DCMR emission data set holds values for 2008, whereas VITO computed emissions for 2009. For these years, the influence of the economic crisis might be quite significant!

Table 12. Comparison of VITO and DCMR bottom up shipping emission data in the Western Scheldt

Western Scheldt in ton	NMVOC	SO_2	NOx	CO	CO_2	PM_{10} and $PM_{2.5}$
DCMR data (2008)	320	3454	9430	1905	416400	518
VITO data (2009)	343	4121	12600	-	483300	724 (PM_{10}) + 464 ($PM_{2.5}$)

2.4. Shipping emissions in the Greater North Sea (OSPAR region II)

In the framework of PASODOBLE, DCMR Milieudienst Rijnmond also provided bottom up emissions for the Greater North Sea, i.e. the OSPAR region II. In Figure 40 the extent of the OSPAR region II and the spatial patterns of the shipping emissions are shown. The DCMR emission data on the OSPAR region II were provided after the shipping emission database had been finalized within the SHIPFLUX project and hence could only be used to obtain a rough idea on the uncertainties on the VITO bottom up emission estimates for shipping.
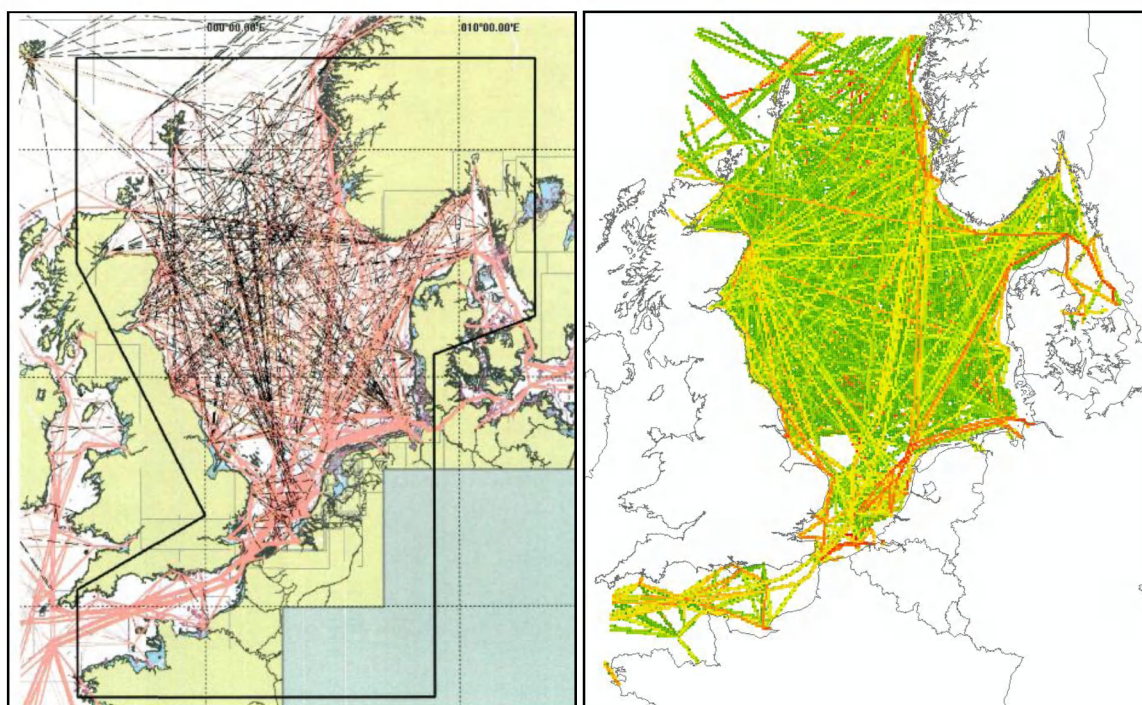
Figure 40. Left: Extent of the OSPAR region II. Right: Spatial pattern of shipping emissions in the OSPAR region II, as determined by DCMR.

The quantitative analysis for all ports and pollutants is summarized in Table 13.

Table 13. Quantitative analysis of bottom up shipping emissions in the OSPAR region II, as computed by DCMR.

2008 in kton	NMVOC	SO_2	NOx	CO	CO_2	PM
OSPAR II	12.69	162.5	447.5	73.10	17790	24.78

As revealed by Figure 38 and Figure 40 comparison of DCMR and VITO bottom up absolute numbers can only be made for the BCP, as this is the only overlapping region. The comparison was done by only retaining the bottom up DCMR output of grid cells which have a non-zero output in the VITO data for the BCP. Emissions in the Western Scheldt were not taken into account. Results are summarized in Table 114.

Table 14. Comparison of VITO and DCMR bottom up shipping emission data on the BCS

Belgian Continental Plate in kton	NMVOC	SO_2	NOx	CO	CO_2	PM_{10} and $PM_{2.5}$
DCMR data (2008)	0.966	12.54	34.39	5.610	1360	1.917
VITO data (2009)	0.680	8.064	25.88		1079	1.605 (PM_{10}) + 0.972 ($PM_{2.5}$)

2.5. Conclusions on bottom-up emission estimates

Comparison between VITO and DCMR data resulting from a bottom up approach reveals confidence in the acquired data. In general very similar spatial disaggregation patterns are obtained. Furthermore, the absolute numbers computed are within the same order of magnitude. Comparison of data on the Western Scheldt reveals lower emissions computed by DCMR, as

compared to the VITO results. However, it should be taken into account that different years, 2008 and 2009, respectively, are compared. Within this time interval, the economic crisis might have induced a significant impact on the shipping traffic and consequently on the resulting emissions. Comparison of bottom up approaches on the BCP reveals similar results: absolute numbers in the same order of magnitude. For this region, the DCMR results appear to be somewhat higher. However, one needs to take into account that a detailed quantitative analysis was difficult to make, as the emissions were computed on different grids, with different resolutions and for different years.

2.6. Top-down disaggregation of shipping emission totals

2.6.1. The E-MAP tool

Maps of the spatial distribution of atmospheric emissions are key input to any air quality assessment. Many spatially resolved emission data have been produced in Europe, but often they cover single states, or regions, target single pollutants, or focus on single source categories. In order to overcome these limitations, VITO has developed the emission mapping GIS tool, E-MAP, which is based on spatial surrogates for the disaggregation of atmospheric emission inventories (Maes et al., 2009).

E-MAP is based on a top down approach. The methodology of the E-MAP disaggregation tool is presented in Figure 41. Emissions known at country level are disaggregated based on proxy data and weights. The weights are calculated based on land use and land cover areas, statistical data, and transportation routes and volumes.

Concrete, the spatial disaggregation of the emission data is done with the so-called spatial surrogates, which are used to assign a statistical weight to the emission data. The simplest way to convert the total emission into a local emission is

$$E_L = E_T * \frac{V_L}{V_T}$$

where E_L stands for the local emission, E_T for the total emission, V_L for the local value of the surrogate variable and, V_T for the total value of the surrogate variable.

The challenge in the disaggregation of the emission totals is to obtain as much geo information at attribute level.
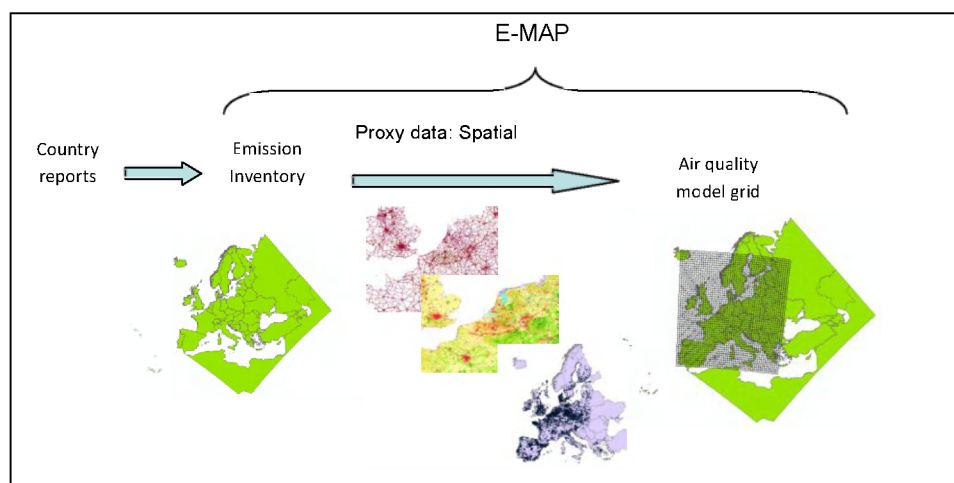
Figure 41. Conceptual presentation of the E-MAP disaggregation tool methodology

2.6.2. Top-down shipping emission estimates

The spatial proxy data that are used in the E-MAP tool developed for SHIPFLUX are stemming from Dienst Hydrografie, The Netherlands. They provided a shipping traffic density map, shown in Figure 42 (http://www.noordzeeloket.nl/Images/ VesselTraffic_tcm14-2878.pdf).

Based on this map the E-MAP spatial surrogates were computed. The spatial surrogates are then used to spatially disaggregate the North Sea emission totals as reported in European emission inventories.
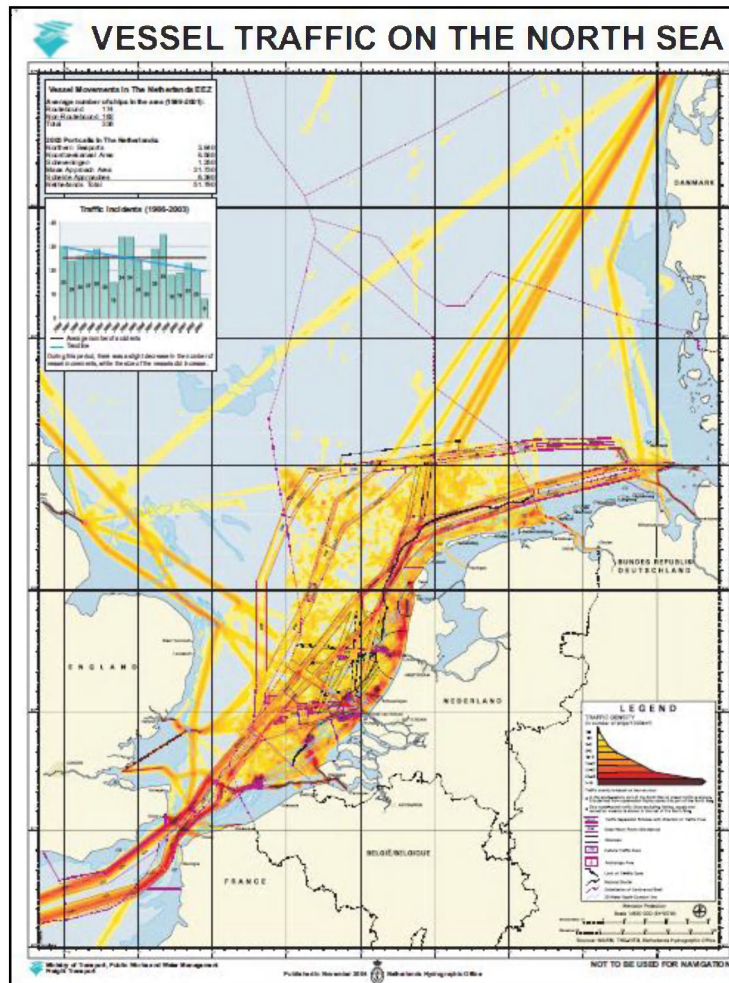
Figure 42. Vessel Traffic Densities on the North Sea, as computed by Dienst Hydrografie, the Netherlands.

Spatial patterns of shipping emissions as computed with the VITO E-MAP tool developed for SHIPFLUX are shown in Figure 43. Comparison of the spatial patterns as obtained with the bottom up approach (see Figure 38) with the patterns as obtained with the top down approach (see Figure 43) reveals that the bottom up approach contains much more details. Unfortunately, the bottom up emissions do not cover the whole SHIPFLUX modelling domain and therefore, they cannot be used as such. Instead of solely using the top down emissions, which do cover the whole SHIPFLUX modelling domain, it was decided to combine bottom up and top down emissions, as to obtain emissions on the whole domain, but to keep the high level of details from the bottom up emissions. The integration of emission data sets resulting from two different approaches as to obtain a single data set is discussed below.
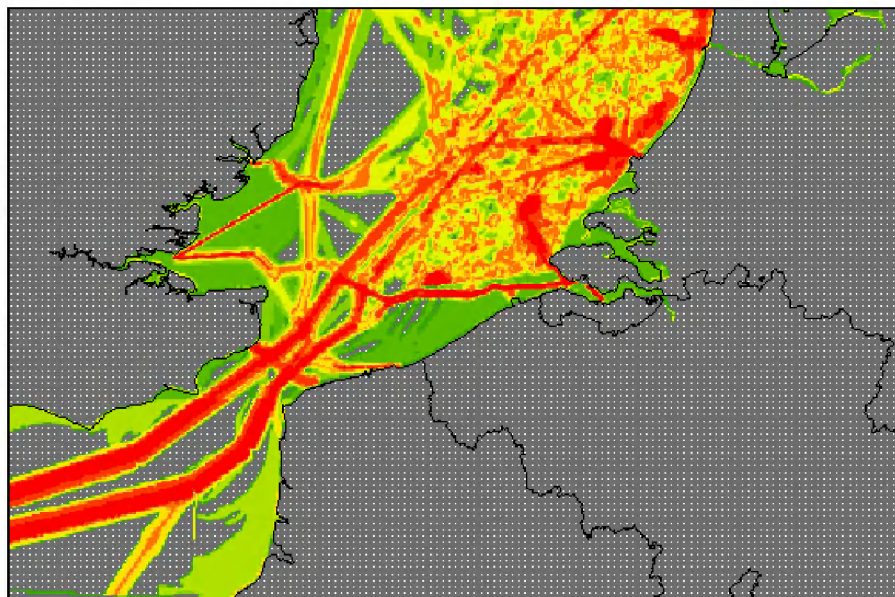
Figure 43. Spatial pattern of shipping emissions in the North Sea, as determined with the VITO top down methodology applied in E-MAP.

2.7. Integration of Bottom Up and Top Down Emission Estimates

2.7.1. Compatibility between bottom up and top down estimates

In order to obtain emission data sets that could be used for the SHIPFLUX air quality modelling, bottom up and top down marine emissions computed by VITO were combined.

First, the compatibility of both data sets was checked, both on spatial patterns and on absolute numbers. The compatibility based on the spatial patterns is shown in Figure 44. It can be observed that the main shipping lanes are revealed from both approaches. In general the compatibility is relatively good.
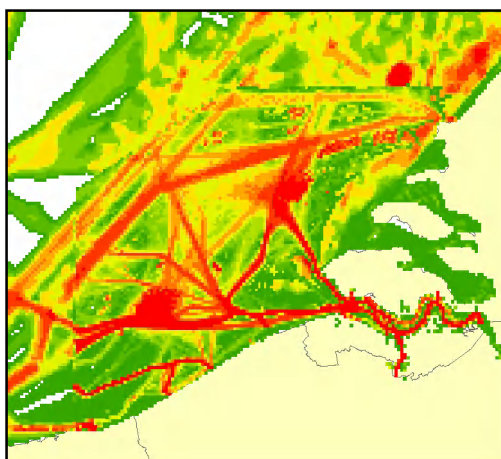
Figure 44. Bottom up disaggregation pattern for shipping emissions, plotted on top of top down pattern. Both patterns are plotted with a different colour scale as to better illustrate the compatibility of the geographical location of the shipping lanes

In order to check the compatibility of absolute numbers, the top down output was 'clipped' with the bottom up domain. In Figure 45, the bottom up result (NOx 2009 in kton/km²) and the 'clipped' top down result (NOx 2010 in kton/km² - IIASA scenario NEC2007 baseline current legislation) are shown. Both maps were plotted with a different scale (quantile plots), so as to clearly reveal the spatial patterns.
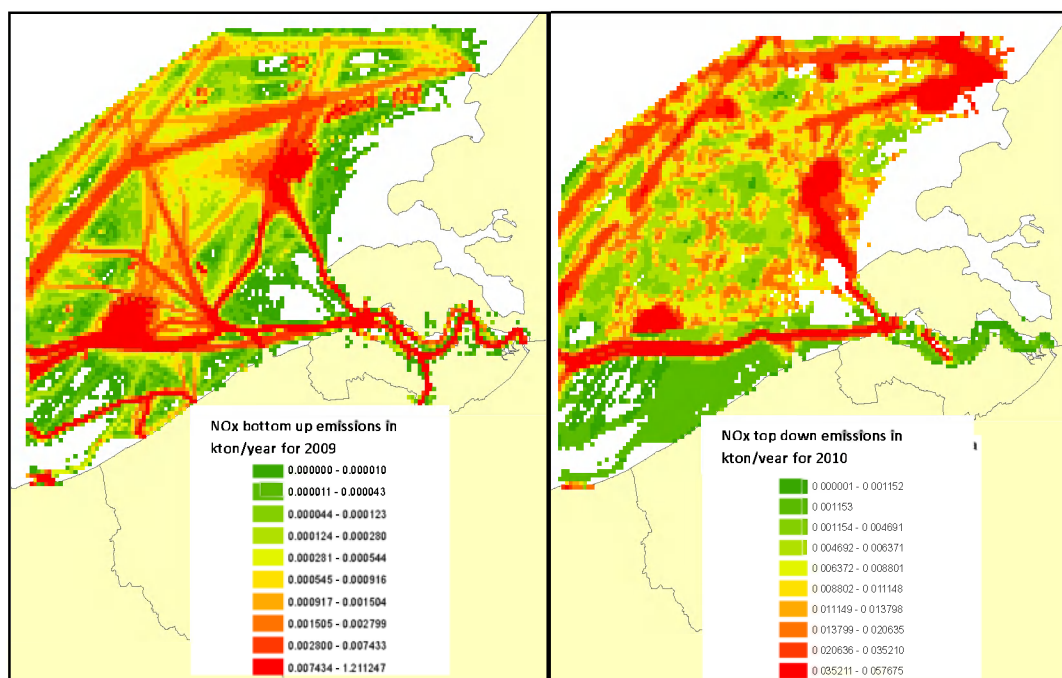
Figure 45. Left: Bottom up NOx emissions stemming from shipping in kton/km². Emissions were computed based on AIS data for 2009. Right: Top down NOx emissions stemming from shipping in kton/km². Emissions were disaggregated starting from the GAINS scenario 'NEC 2007 baseline current legislation for 2010', provided by IIASA.

When comparing absolute numbers in both data sets for the same domain, i.e. the BCS, large differences are obtained. A summary is given in Table 15.

Table 15. Comparison of absolute numbers for shipping emissions on the BCP obtained with a top down and a bottom up approach

ton/year	EMAP 2010 (top down)	AIS 2009 (bottom up)
NH_3	0	5
NMVOC	5805	1020
NOx	105700	38310
PM_{10}	7561	2321
$PM_{2.5}$	7156	1431
$PM_{10-2.5}$	405	890
SO_2	42660	121403

In order to clarify the huge differences in absolute numbers resulting from the different approaches (bottom up versus top down), a comparison between different data sets was made.

2.7.2. Comparison between European emission inventories

The top down results are obtained by taking IIASA emission totals for the North Sea as a starting point. Hereto the scenario 'NEC2007 baseline current legislation' for 2010 was chosen. Another European emission inventory could have been chosen as well. In Table 16, the used IIASA numbers (North Sea) are listed and compared with available numbers for the North Sea in the EMEP emission inventory. This table reveals that the shipping emissions for the North Sea, contained in the IIASA and the EMEP inventories are within the same order of magnitude. Therefore, downscaling emissions taking EMEP numbers as a starting point would result in

similar disaggregated emissions, i.e., emissions that are significantly higher than what is obtained by a bottom up approach.

Table 16. Shipping emissions for the North Sea in the IIASA and the EMEP emission inventory for several years

North Sea kton/year	IIASA – 2010 (projection)	EMEP - 2007	EMEP - 2008	EMEP – 2010 (projection)
NH_3	0			
NMVOS	43	27	28	1
NOx	783	754	761	647
PM_{10}	56			
$PM_{2.5}$	53	54	54	25
$PM_{10-2.5}$	3			
SO_2	316	441	399	454

2.7.3. Comparison of VITO data with DCMR data

2.7.3.1. Emissions on the NCS (Netherlands Continental Shelf)

- Numbers extracted from 'Emissions 2008: Netherlands Continental Shelf, Port Areas and Ospar Region II', Final Report, Marin, §6.5':

Table 6-11 Emissions of ships in ton in NCS for 2008 and 2007

Nr	Substance	EMS NCS 2007	Emission in ton in 2008 Main Engine	Emission in ton in 2008 Auxiliary Engine	Emission in ton in 2008 Total	2008 as % of 2007	at anchor 2008
1237	NMVOC	3,347	2,199	236	2,434	72.7%	66
4001	SO_2	58,600	28,298	2,935	31,233	53.3%	830
4013	NO_x	117,000	79,352	6,838	86,190	73.7%	1,950
4031	CO	17,860	12,874	1,292	14,165	79.3%	371
4032	CO_2	4,600,000	3,055,508	357,384	3,412,891	74.2%	103,447
6598	PM10 and PM2.5	7,109	4,407	375	4,782	67.3%	105
	Ships		172	172	172		70

- 3rd column (NCS 2007): numbers for 2007; EMS refers to a specific method which has been used until 2007, when no AIS data were available yet. 6th column (Total 2008): numbers for 2008, based on the AIS method. When interpreting the computation in the 7th column, it should be noted that 2 different methods were used.
- In Total 2008 no emissions for stationary vessels are taken into account. According to the author, these vessels would cause an additional fraction of only 3%. They were not taken into account as they were not taken into account for 2007 either.
- The huge reduction from 2007 to 2008 (NOx: 30%, SO_2: 50%) would be the result of the economic crisis (reduction of the number of shipping movements and lowering of speed to save fuel costs - 80% of max speed instead of 90%). The even larger reduction for SO_2 is due to the reduction of the percentage sulphur in the fuel.
- Comparison with bottom up emissions computed by VITO is not possible, as the VITO domain for bottom up emissions is chosen, so as to cover only the BCS. A very rough estimate for the top down methodology (E-MAP) would lead to **387000 ton NOx** (computed as number of ships in NCS/number of ships in North Sea * EMEP emissions North Sea). This number should be compared with the **86190 ton NOx** form the above table. When scaling the top down North Sea emissions so that they would equal the bottom up emissions in the VITO bottom up domain (BCS), the rough estimate would lead to **136000 ton NOx**.

- From this, it can be decided that the marine DCMR numbers are even smaller than the VITO bottom up marine data. This is in agreement with what we found for the Western Scheldt (however, data for 2008 and 2009 were compared, the economic crisis might influence the result).

2.7.3.2. Emissions in the Greater North Sea (OSPAR region II)

- The OSPAR region II covers the North Sea and a small part of the Atlantic Ocean.
- Numbers extracted from 'Emissions 2008: Netherlands Continental Shelf, Port Areas and OSPAR region II', Final Report, Marin, §7):

Table 7-1   Emissions at sea in ton in the OSPAR region II

Nr	Substance	SAMSON emissions in 2008		
		Main Engine	Auxiliary Engine	Total
1237	NMVOC	9,329	1,017	10,346
4001	SO_2	119,418	12,615	132,033
4013	NO_x	334,056	29,469	363,524
4031	CO	53,866	5,563	59,429
4032	CO_2	12,932,130	1,539,223	14,471,353
6598	PM10 and PM2.5	18,519	1,609	20,128
	Ships	767.2	767.2	767.2

- These numbers were computed with SAMSON, and as such not based on AIS data (as AIS data are not available for the whole OSPAR region II). The comparison between numbers computed with SAMSON and based on AIS is, however, made on the NCS. Both methodologies resulted in similar values. However, these methods are not fully independent, which induces evidence for good agreement.
- Comparison with numbers provided by IIASA (GAINS NEC2007 baseline current legislation 2010) reveals that IIASA numbers are significantly larger than DCMR numbers! For example: NOx North Sea = 783 kton as stated by IIASA, whereas 363 kton is computed by DCMR. Moreover, the OSPAR region II is larger than only the North Sea.

2.7.4. Conclusions on integration of bottom up and top down emission estimates

Comparison of different data sets in different regions reveals that bottom up approaches based on AIS data (DCMR and VITO) result in significantly lower emission totals as compared to top down approaches based on proxy data, starting from EMEP or IIASA totals.

As in general local bottom up approaches result in more reliable data and as the VITO data show good agreement with bottom up results in the Netherlands, it was decided to take the bottom up results as the reference within the SHIPFLUX project.

In order to obtain emission data sets that cover the whole air quality modelling domain, the VITO bottom up emission data sets on the BCP were completed with 'scaled' top down results. Hereto, the top down results were first computed for the whole air quality model grid. In a next step, the top down emission totals on the BCP were compared with the bottom up results. From this comparison a scaling factor was deduced, which then was applied on the top down results for the shipping emissions on the whole air quality model grid. More details are given in the following chapters.

The comparison of the results of the air quality modelling with observations is described later in this report. This comparison provides not only information on the performance of the applied air quality models, but also on the quality of the used input data, especially the used emission

data. In advance of the results of this comparison we can already mention in this chapter that the choice for the bottom-up emissions as the reference and scaling the top-down emissions for the remaining sea areas to the level of the bottom-up emissions in this project seems to be confirmed by the measurements.

2.8. Emission scenarios in SHIPFLUX

2.8.1. Emission standards according to MARPOL Annex VI

Figure 46 shows the emission standards for NOx and SOx according to MARPOL Annex VI. The MARPOL Annex VI convention came into force on 19th May 2005. This annex includes, among other things, that the sulphur content of heavy fuel oil may not exceed 1.5 mass % in the "Sulphur Emission Control Areas" (SECA's) after 19th May 2006, among which also the North Sea. After the 1st of January 2010 the sulphur content should not exceed 1% mass, and after the 1st of January 2015 the maximum content is lowered to 0.1% mass sulphur. This sulphur restriction is also prescribed by the 2005/33/EC directive. This directive also imposes the use of 0.1 mass% sulphur from the 1st January 2010 for inland navigation and sea-going vessels at berth with a 2-hour minimum duration. In Belgium a restriction on sulphur content for ships at berth of 0.2% was already in force before 2010.

In the non-SECA's (e.g., the North Atlantic Ocean), the maximum allowed sulphur content of fuel oil is 4.5 % mass. From 2012 on, this value is reduced to 3.5 % mass and from 2020 (or 2025, still to be decided) the maximum S-content in non-SECA's will be 0.5 % mass.

Concerning NOx emissions, from 15th May 2005, main engines built after the year 1999 have to comply with restrictions for the NOx emissions. The following standards are valid or planned. Up to 2011, the Tier I NOx emission standard applies for all sea areas. From 2011 on, the Tier II standard applies for all sea areas (emission controlled and non-emission controlled sea areas). Finally, from 2016 on, the Tier III standard will be valid in NOx emission controlled areas (ECA's). Tier II prescribes roughly a NOx emission reduction by 20% in comparison to Tier I. Tier III even prescribes a NOx emission reduction by roughly 80% in comparison to Tier I. However, at the time of compiling this report (February 2012), it seems unlikely that the North Sea will become a NOx emission control area by 2020. Hence, we did not include a shift to Tier III in the emission projections for the scenario 2020.
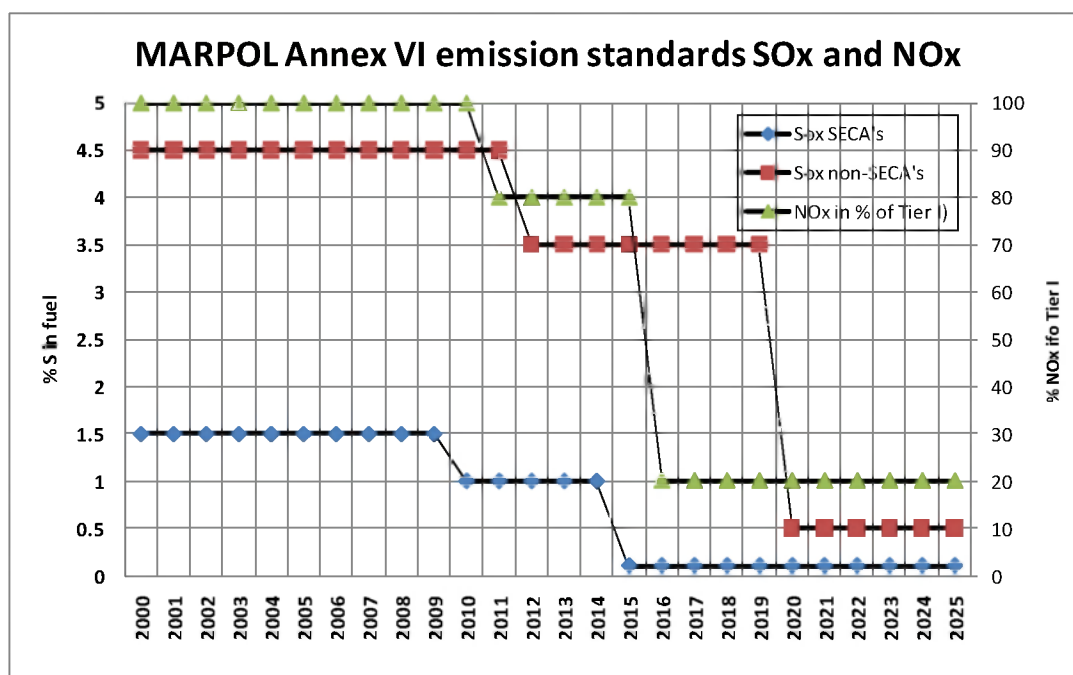
Figure 46. Emission standards for NOx and SOx according to MARPOL Annex VI

2.8.2. Shipping emissions for the scenarios 2012 and 2020

We used the E-motion MARI module to calculate the emissions under the sulphur and NOx restrictions for the years 2012 and 2020. The shipping activity data was kept constant at the level of the year 2009. The fleet composition as well as the used fuels were taken as for the future years 2012 and 2020. A change in all emission factors was taken into account. As pointed out earlier, the Tier III standard has not been applied to the North Sea shipping emissions in the Scenario 2020 as it seems to be unlikely that this standard will be introduced for the North Sea until then. However, due to the renewal of the fleet a higher percentage of Tier II engines will be present in 2020 than this is the case in 2012, leading to lower NOx emissions for the 2020 scenario compared to the 2012 scenario. Table17 shows an overview of the relevant parameters for the shipping emissions for the base year and for the two future scenario years.

Table17. Sulphur content of fuels and NOx emissions used in the baseline and in the 2012 and 2020 scenarios

Parameter	Baseline	Scenario 2012	Scenario 2020
(m/m % S) Diesel oil (at berth)	0.2	0.1	0.1
(m/m % S) Heavy Fuel Oil, North Sea	1.5	1	0.1
(m/m % S) Heavy Fuel Oil, North Atlantic	4.5	3.5	0.5
NOx emissions in % of Tier I	100	80	80

2.9. Emission data sets created in SHIPFLUX for the classical pollutants

2.9.1. Overview of the model calculations and emission data sets by model run

Within the SHIPFLUX project, a base year, a scenario for 2012 and a scenario for 2020 have been modelled. Each of these model runs required a specific emission data set. Below we give an overview of the different model runs. In the next paragraph, the procedures to obtain the according emission data sets by year/scenario are discussed in more detail.

- Base Case
- Base Case – Influence of Shipping
- Scenario 2012
- Scenario 2012 – Influence of Shipping
- Scenario 2020
- Scenario 2020 – Influence of Shipping
- Base Case heavy metals
- Base Case heavy metals – Influence of Shipping
- Base Case PAH's
- Base Case PAH's – Influence of Shipping

Air quality modelling within SHIPFLUX occurred with the AURORA model. This model uses the method of nested simulations. In the framework of SHIPFLUX, the nesting occurred in concentration fields obtained with the BelEUROS model on a grid covering Europe. More details are given in the next chapter. Consequently, for each run, both emissions for AURORA and for BelEUROS were prepared. Moreover, within the SHIPFLUX project, the focus lies on shipping. Therefore, marine based emissions were dealt with separately.

In the following, for each scenario, three different steps in creating emission data sets are discussed:

- Land based emission data set for AURORA

- Marine based emission data set for AURORA
- Emission data set for BelEUROS

2.9.2. Base year

2.9.2.1. Land based emission data set for AURORA

Land based emissions for AURORA were computed with the E-MAP tool. The IIASA scenario 'NEC2007 baseline current legislation' was taken as a starting point. The year 2010 was chosen as reference year. In the 'NEC2007 baseline current legislation' inventory, the emissions listed for the European seas were ignored. An example of the resulting spatially disaggregated land based emissions on the air quality modelling grid is given in Figure 47, showing non-point source NOx emissions (kTon) aggregated over all SNAP sectors.
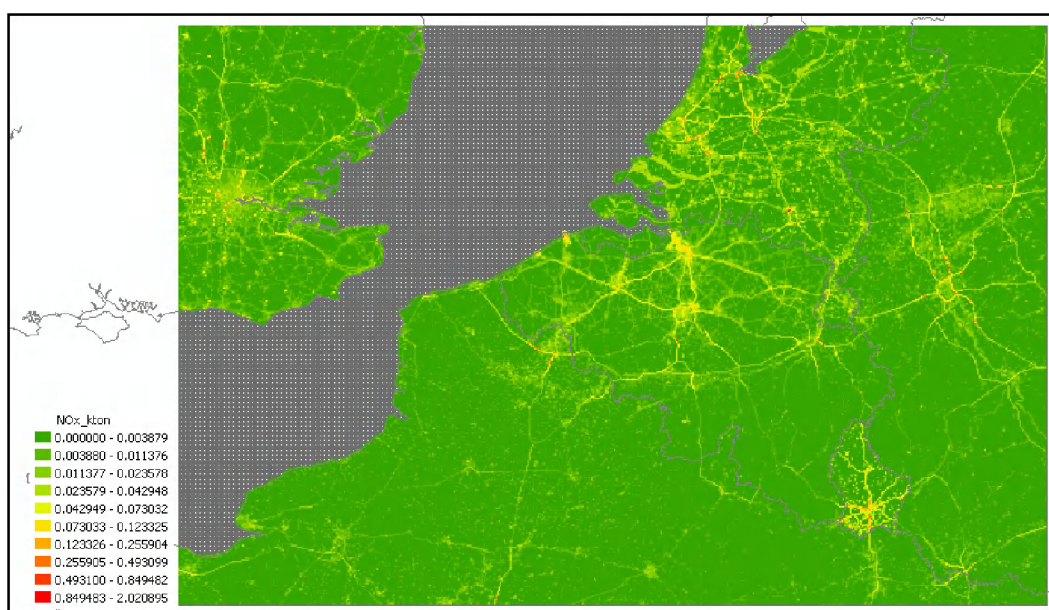
Figure 47. Land based emissions for AURORA resulting from E-MAP, taking IIASAs 'NEC2007 baseline current legislation' scenario for 2010 as a starting point - Non-point source NOx emissions (kTon) aggregated over all SNAP sectors.

2.9.2.2. Marine based emission data set for AURORA

Marine based emissions for AURORA were obtained by combining the VITO bottom up emissions on the BCP for 2009 with the scaled top down shipping emissions obtained with E-MAP by taking the IIASA scenario 'NEC2007 baseline current legislation' for 2010 as a starting point.

An example of the resulting spatially disaggregated marine based emissions on the air quality modelling grid is given in Figure 48, showing both, the different steps in the process and the final result. NOx emissions were chosen as to illustrate the process. In Table 18, the scaling factors that were applied to the top down results are listed.
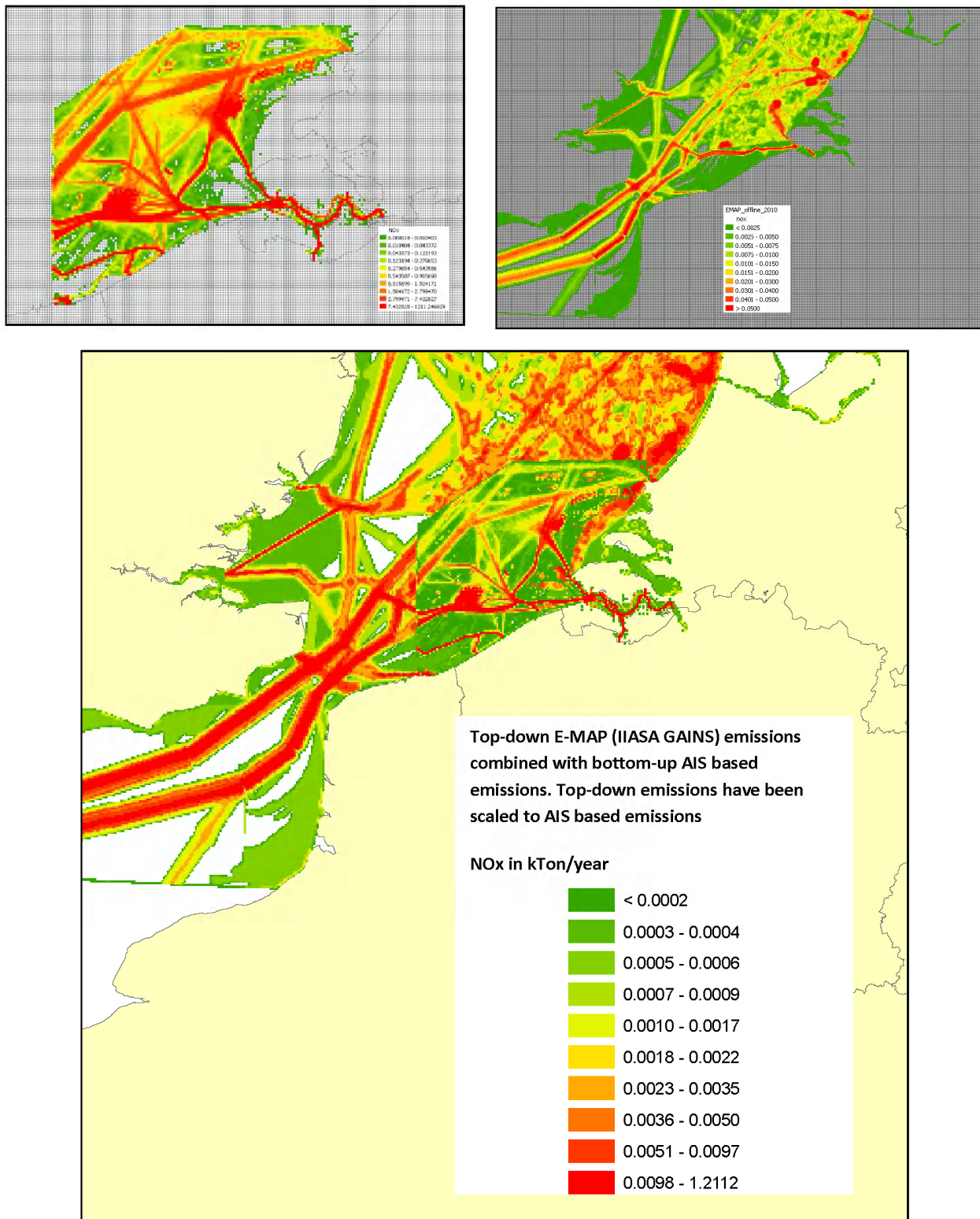
Figure 48. Top Left: Bottom up marine NOx emissions for 2009 on the BCP in ton; Top Right: Top down marine NOx emissions for 2010 on the model grid; Bottom: marine based emissions for AURORA resulting from the integration of bottom up and scaled top down NOx emissions in kTon.

Table 18. Comparison of top down (2010) and bottom up (2009) absolute numbers on the BCP and the resulting scaling factors

BCP kton/year	Top down 2010	Bottom up 2009	Scaling factor
NH_3	0.000	0.005	1 (div. by 0)
NMVOC	5.805	1.020	0.17565286
NOx	105.7	38.31	0.36235378
PM_{10}	7.561	2.321	0.30692009
$PM_{2.5}$	7.156	1.431	0.19992174
$PM_{10-2.5}$	0.405	0.890	2.19891277
SO_2	42.67	12.14	0.28460064

The computed scaling factor was applied on the whole domain (North Sea + Atlantic Ocean), the E-MAP output on the BCP was replaced by the bottom up emission data.

2.9.2.3. Emission data set for BelEUROS

Emissions for BelEUROS were computed with the E-MAP tool. The IIASA scenario 'NEC2007 baseline current legislation' was again taken as the starting point and the year 2010 was chosen as reference year. As the absolute emissions in BelEUROS and AURORA should be comparable, the BelEUROS shipping emissions were scaled. To perform the scaling, top down emissions were compared with the combined bottom up-top down AURORA emissions.

2.9.3. Base case – Influence of shipping

The land based emission data set for AURORA is identical to the land based emission data set for AURORA in the base case. The marine based emission data set for AURORA is obtained by applying a reduction of 25 % on the marine based emission data set for AURORA in the base case. The emission data set for BelEUROS is obtained by applying a reduction of 25 % on the marine emissions of the emission data set for BelEUROS in the base case.

2.9.4. Scenario 2012

2.9.4.1 Land based emission data set for AURORA

Land based emissions for AURORA were computed with the E-MAP tool. The IIASA scenario 'NEC2007 baseline current legislation' was taken as the starting point. As this scenario does not contain a projection for 2012, it was computed from the 2010 and the 2015 projections with the formula:

emissions 2012 = emissions 2010 + (emissions 2015 - emissions 2010)*2/5

In the created 'NEC2007 baseline current legislation' for 2012, the emissions listed for the European seas were ignored. The resulting spatially disaggregated land based emissions on the air quality modelling grid are very similar to the ones shown in Figure 47 for the base case.

2.9.4.2. Marine based emission data set for AURORA

Marine based emissions for AURORA were obtained by combining the VITO bottom up emissions on the BCP for 2012 with the scaled top down shipping emissions obtained with E-MAP by taking the created IIASA scenario 'NEC2007 baseline current legislation' for 2012 as starting point.

The process and the resulting spatially disaggregated marine based emissions on the air quality modelling grid are very similar to the ones described for the base year. In Table 19, the scaling factors that were applied on the top down results (for 2015) are listed.

Table 19. Comparison of top down (2015) and bottom up (2012) absolute numbers on the BCP and the resulting scaling factors (applied on 2015 emissions to obtain 2012 results)

BCP kton/year	Top down 2015	Bottom up 2012	Scaling factor
NH_3	0.000	0.005	1 (div. by 0)
NMVOC	5.265	0.842	0.160
NOx	116.2	35.99	0.310
PM_{10}	8.506	2.165	0.254
$PM_{2.5}$	8.101	1.209	0.149
$PM_{10-2.5}$	0.459	0.956	2.082
SO_2	48.33	7.960	0.165

2.9.4.3. Emission data set for BelEUROS

Emissions for BelEUROS were computed with the E-MAP tool. The created IIASA scenario 'NEC2007 baseline current legislation for 2012' was taken as the starting point. As the absolute emissions in BelEUROS and AURORA should be comparable, the BelEUROS shipping emissions were scaled. To perform the scaling, top down emissions were compared with the combined bottom up-top down AURORA emissions.

2.9.5. Scenario 2012 – Influence of shipping

The land based emission data set for AURORA is identical to the land based emission data set for AURORA in the scenario 2012. The marine based emission data set for AURORA is obtained by applying a reduction of 25% on the marine based emission data set for AURORA in the scenario 2012. The emission data set for BelEUROS is obtained by applying a reduction of 25% on the marine emissions of the emission data set for BelEUROS in the scenario 2012.

2.9.6. Scenario 2020

2.9.6.1. Land based emission data set for AURORA

Land based emissions for AURORA were computed with the E-MAP tool. The IIASA scenario 'NEC2007 baseline current legislation' for 2020 was taken as starting point. In the 'NEC2007 baseline current legislation' inventory, the emissions listed for the European seas were ignored. The resulting spatially disaggregated land based emissions on the air quality modelling grid are very similar to the ones shown in Figure 47 for the base case.

2.9.6.2. Marine based emission data set for AURORA

Marine based emissions for AURORA were obtained by combining the VITO bottom up emissions on the BCP for 2020 with the scaled top down shipping emissions obtained with E-

MAP by taking the IIASA scenario 'NEC2007 baseline current legislation' for 2020 as the starting point. The process and the resulting spatially disaggregated marine based emissions on the air quality modelling grid are very similar to the ones described for the base case. In Table 20, the scaling factors that were applied on the top down results (for 2015) are listed.

Table 20. Comparison of top down (2020) and bottom up (2020) absolute numbers on the BCP and the resulting scaling factors.

BCP kton/year	Top down 2020	Bottom up 2020	Scaling factor
NH_3	0.000	0.005	1 (div. by 0)
NMVOC	4.996	0.726	0.145
NOx	127.7	33.74	0.264
PM_{10}	9.721	1.960	0.202
$PM_{2.5}$	9.181	0.863	0.094
$PM_{10-2.5}$	0.513	1.096	2.136
SO_2	54.82	0.980	0.018

2.9.6.3. Emission data set for BelEUROS

Emissions for BelEUROS were computed with the E-MAP tool. The IIASA scenario 'NEC2007 baseline current legislation' for 2020 was taken as the starting point. As the absolute emissions in BelEUROS and AURORA should be comparable, the BelEUROS shipping emissions were scaled. To perform the scaling, the top down emissions for 2020 were compared with the combined bottom up-top down AURORA emissions.

2.9.7. Scenario 2020 – Influence of shipping

The land based emission data set for AURORA is identical to the land based emission data set for AURORA in the scenario 2020. The marine based emission data set for AURORA is obtained by applying a reduction of 25% on the marine based emission data set for AURORA in the scenario 2020. The emission data set for BelEUROS is obtained by applying a reduction of 25% on the marine emissions of the emission data set for BelEUROS in the scenario 2020.

2.10. Emission data sets created in SHIPFLUX for heavy metals

2.10.1. Base Year heavy metals (Cd and Pb)

2.10.1.1. Introduction

Table 21 shows an overview of available emission data for heavy metals. The availability is shown with respect to shipping emissions for the BCS and other sea areas and for land-based emissions in Flanders and in the remaining parts of Europe. It becomes clear that the availability of emission data for heavy metals is very limited. The necessary emission data is only available for cadmium (Cd) and for lead (Pb). For all other heavy metals, European emissions are missing. Hence, because of the importance of long-range transport on heavy metal concentrations, we decided to restrict the modelling of heavy metals to Cd and Pb.

Table 21. Overview of available emission data for heavy metals

HM	Shipping emissions BCS	Shipping emissions other sea areas	Land-based emissions Flanders	Land-based emissions Europe
As	X	X	✓	X
Cd	✓	X	✓	✓
Cr	X	X	✓	X
Cu	X	X	✓	X
Ni	✓	X	✓	X
Pb	✓	X	✓	✓
Zn	X	X	✓	X

No heavy metal emissions were created on the European continental scale as input to the BelEUROS model, due to poor emission data for most European countries. Instead, nesting of the AURORA model has been carried out assuming constant heavy metal concentrations at the domain boundaries.

2.10.1.2. Land based emission data set for AURORA

- Land based emissions for Flanders

Flemish land based emissions for AURORA were computed starting from disaggregated heavy metal emissions for 2005, which were developed in a project for the Flemish Environment Agency (VMM) in 2009 (Viaene et al., 2010). Emission totals, provided by the VMM in the framework of SHIPFLUX, revealed that heavy metal emissions in Flanders dropped significantly between 2005 and 2009. Therefore, the spatially disaggregated Flemish emissions for 2005 were scaled as to obtain 2009 emissions. This was done based on the emission totals provided by the VMM. An example of spatially disaggregated heavy metal emissions in Flanders for the year 2009 is shown in Figure 49 for Cd.
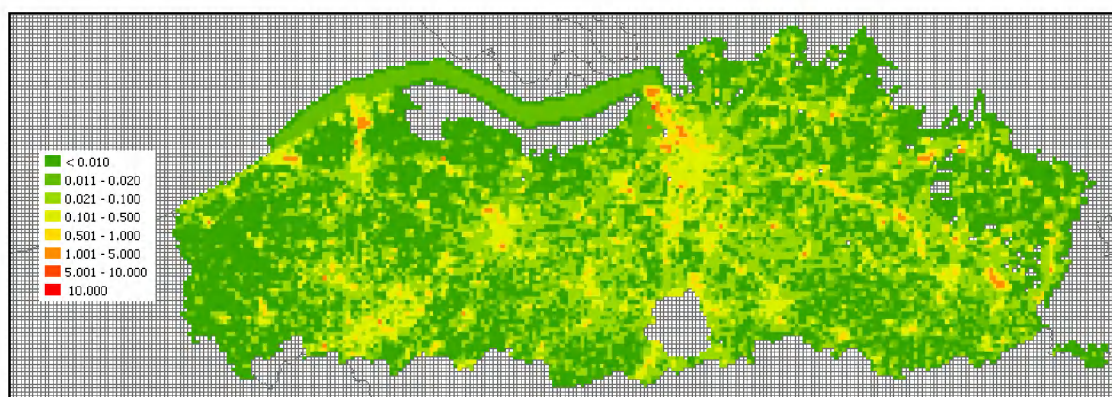
Figure 49. Spatially disaggregated Cd emissions for 2009 in kg/km².

- Non-Flemish Land based emissions

Non Flemish land based emissions for AURORA were computed with an E-MAP tool, which was specifically developed to spatially disaggregate heavy metal emissions. European national emission totals for 2005 were taken as the starting point. Update towards 2009 did not occur, as not all required data were available. Spatial patterns were taken from the E-MAP tool to disaggregate the main pollutants, CO, NMVOC, NOx, PM and SOx. The heavy metal E-MAP database generates emissions for the whole AURORA domain, including Flanders. An example of spatially disaggregated heavy metal emissions obtained with the E-MAP tool for Pb is shown in Figure 50.
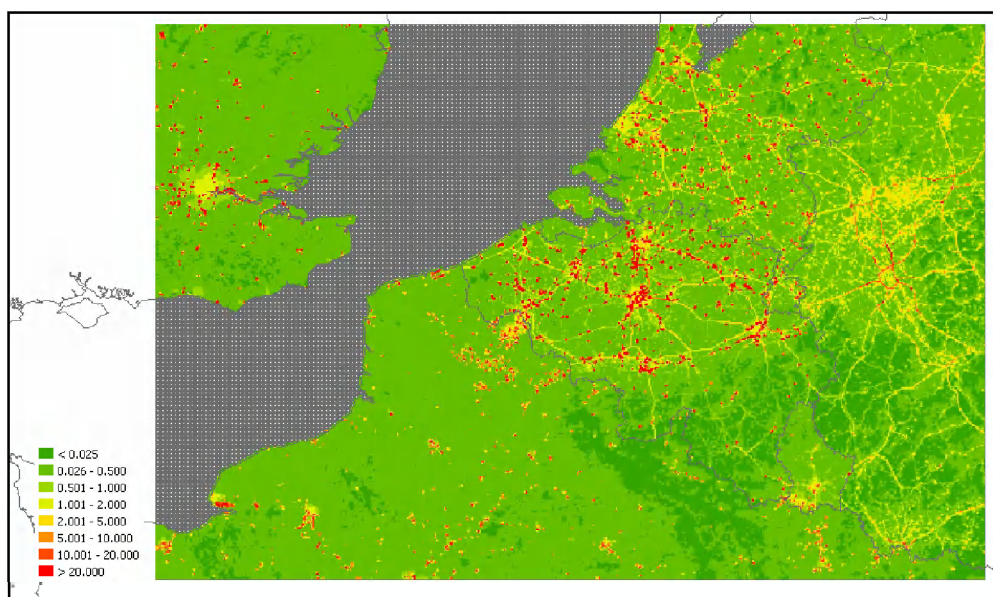
Figure 50. Spatially disaggregated Pb emissions for 2005 in kg/km²

- Combination of Flemish and non-Flemish land based emissions

Flemish emissions in the E-MAP output were replaced by the bottom up Flemish emissions. This is illustrated for Pb in Figure 51. It should be noted that quite some inconsistencies in between different data sets were discovered. A summary is given in Table 22.

Table 22. Heavy metal emission totals for different regions in different data sets

Emissions in kg	Flanders [1]		Belgium [2]		Belgium [3]	
	Cd	Pb	Cd	Pb	Cd	Pb
2005	1954	59580	1679	77180	1700	76000
2009	1523	29220	-	-	2175	45290

(1) Emissions reported in VMM's annual report
(2) Emissions obtained in the framework of the project 'Depositie PAKs – ZM' for VMM in 2009
(3) Emissions reported on the EMEP website
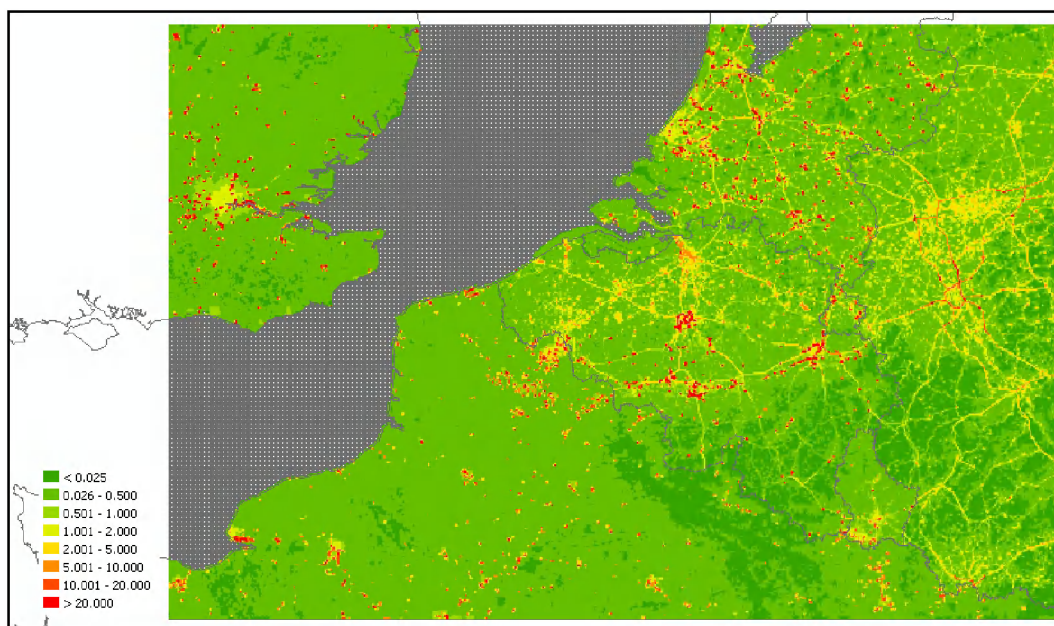
Figure 51. Spatially disaggregated Pb emissions in kg/km² after integration of bottom up Flemish emissions in the top down results

2.10.1.3. Marine based emission data set for AURORA

Marine based emissions for AURORA were obtained by combining the VITO bottom up emissions on the BCP for 2009 with top down shipping emissions obtained with E-MAP. E-MAP could, however, not be used as such, as no international shipping emissions exist for heavy metals. Therefore, the following approach was followed:

- the NOx shipping emissions as computed by the combination of bottom up and E-MAP were taken as the starting point
- per heavy metal (HM), the bottom up emissions on the BCP for NOx and for the HM were compared and a scaling factor = HM/NOx was computed
- the computed scaling factor was applied on the NOx top down emissions on the whole sea, so as to obtain HM emissions
- on the BCP top down emissions were replaced by bottom up emissions.

In this way, emissions for the whole sea, including the bottom up results, were obtained.

2.10.2. Base case heavy metals – Influence of shipping

The land based emission data set for AURORA is identical to the land based emission data set for AURORA in the base case heavy metals. The marine based emission data set for AURORA is obtained by applying a reduction of 25% on the marine based emission data set for AURORA in the in the base case heavy metals. For heavy metals, no emissions for the BelEUROS model were computed. Nesting of the AURORA model occurred by assuming continuous concentrations at the boundaries.

2.11. Emission data sets created in SHIPFLUX for the PAHs

Table 23 shows an overview of available emission data for the polycyclic aromatic hydrocarbons (PAHs). The availability is shown with respect to shipping emissions for the BCS and other sea areas and for land-based emissions in Flanders and in the remaining parts of Europe. It becomes clear that also the availability of emission data for the PAHs is very limited. The necessary emission data is only available for B[a]P, B[b]F and B[k]F. Shipping emission factors for I[1,2,3-cd]P were observed to be zero.

Table 23. Overview of available emission data for PAHs

PAH	Shipping emissions BCS	Shipping emissions other sea areas	Land-based emissions Flanders	Land-based emissions Europe
naphthalene	✓	X	✓	X
anthracene	✓	X	✓	X
phenanthrene	✓	X	✓	X
fluoranthene	✓	X	✓	X
pyrene	✓	X	✓	X
benzo(a)anthracene	✓	X	✓	X
chrysene	✓	X	✓	X
benzo(b)fluoranthene	✓	X	✓	✓
benzo(k)fluoranthene	✓	X	✓	✓
benzo(a)pyrene	✓	X	✓	✓
indeno(1,2,3-cd)-pyrene	X	X	✓	✓
benzo(ghi)perylene	✓	X	✓	X
acenaphthene	✓	X	✓	X
acenaphthylene	✓	X	✓	X
fluorene	✓	X	✓	X
di-benzo(a,h)anthracene	✓	X	✓	X

For PAHs, no emissions for BelEUROS were computed, due to poor emission data for most European countries. Instead, nesting of the AURORA model occurred by assuming continuous concentrations at the domain boundaries.

2.11.1. Base case PAHs (benzo[a]pyrene, benzo[b]fluoranthene, benzo[k]fluoranthene)

2.11.1.1. Land based emission data set for AURORA

Land based emissions for AURORA were computed starting from disaggregated PAHs' emissions for 2005, which were developed in a project for the VMM in 2009 (Viaene et al., 2010).

2.11.1.2. Marine based emission data set for AURORA

Marine based emissions for AURORA were obtained by combining the VITO bottom up emissions on the BCP for 2009 with top down shipping emissions obtained with E-MAP. The same approach as for the heavy metals was followed.

2.11.2. Base case PAHs – Influence of shipping

The land based emission data set for AURORA is identical to the land based emission data set for AURORA in the base case of PAHs. The marine based emission data set for AURORA is obtained by applying a reduction of 25% on the marine based emission data set for AURORA in the in the base case PAH's.

Work Package 3: Deposition calculations with air quality models

3.1. Introduction

3.1.1. Model domain

Two different 3-dimensional Eulerian grid models have been used to calculate concentrations and dry and wet deposition of air pollutants in the study area. Because of the high contribution of long-range transport to the concentrations and deposition of air pollutants, emission sources located in a large domain (e.g., the European continent) have to be taken into consideration. On the other hand, model calculations with a high resolution, such as the resolution of 3 km x 3 km in this study, cannot be carried out for a large region, due to computational limitations. Hence, a nesting approach has been followed in this study, in which the European domain is calculated using a grid resolution of 60 km x 60 km, followed by a smaller grid covering Belgium, the Netherlands, the Grand Duchy of Luxembourg and parts of Germany, France and the UK using a 15 km x 15 km resolution. The boundary conditions for the 15 km x 15 km grid are taken from the calculation for the 60 km x 60 km grid. Subsequently, applying the same nesting approach of using concentrations of the calculation for the larger domain as boundary conditions for the smaller domain, calculations were done for a 7 km x 7 km grid and finally a 3 km x 3 km grid. The complete Belgian Continental Shelf (BCS) is located within this 3 km x 3 km grid, resulting in high resolution concentration and deposition maps for the entire area of interest.

Figure 52 shows the four different model domains and grid resolutions used in this study: The 60 km x 60 km domain and the 15 km x 15 km domain are calculated with the BelEUROS model, the 7 km x 7 km and the 3 km x 3 km domain are calculated with the AURORA model.
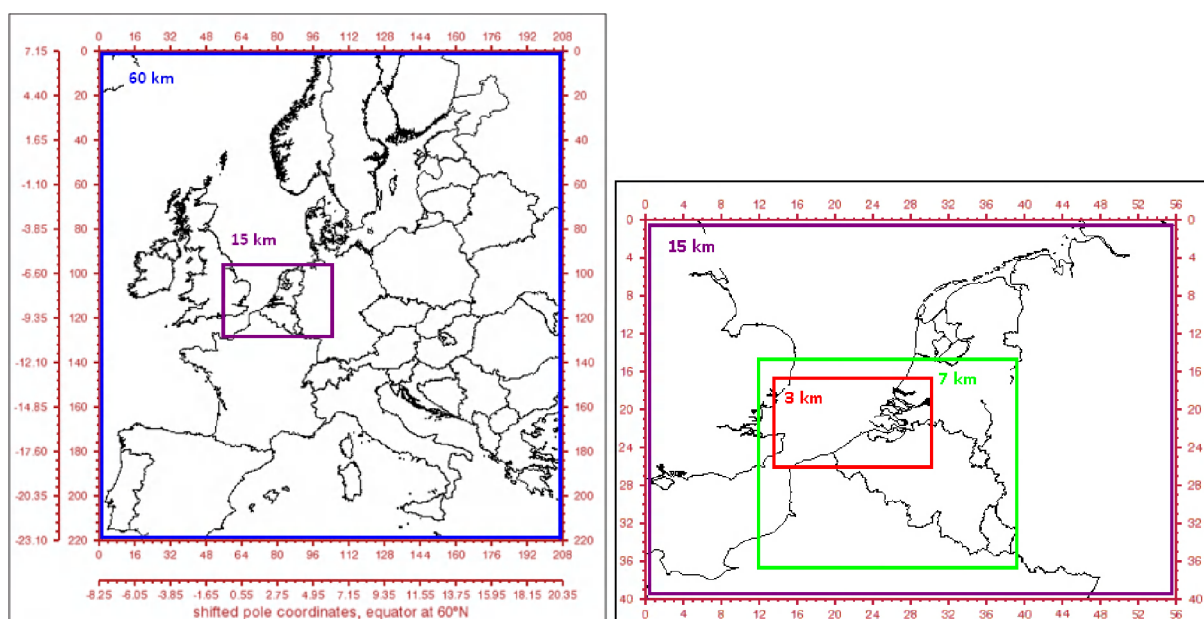
Figure 52. The four different model domains and grid resolutions used in the nesting approach of this study to realize high resolution concentration and deposition maps for the BCS

3.1.2. Main input data used for the BelEUROS and AURORA models

BelEUROS and AURORA are both 3-dimensional Eulerian chemical transport models. They use emissions, meteorological data and land use information as their main input parameters. Emission data have to cover the complete model domain of the respective calculations, meaning e.g. that for the 60 km x 60 km grid emission data for almost the whole of Europe have to be used. They

originate from European emission databases such as the one of the EMEP Centre on Emission Inventories and Projections (EMEP – CEIP, www.ceip.at) and the emission databases of IIASA (International Institute for Applied Systems Analysis, Laxenburg, Austria; www.iiasa.ac.at). Emission data for international shipping were used not only for the North Sea, but also for the Baltic Sea, the Mediterranean Sea and the European part of the Atlantic Ocean.

Meteorological data for both models are derived from the European Centre for Medium-Range Weather Forecasts (ECMWF, Reading, UK; www.ecmwf.int) and includes parameters such as temperature, relative humidity, wind velocity, wind direction, cloud cover, mixing layer height and precipitation.

Gas phase chemistry (e.g., ozone formation) and aerosol chemistry (e.g., formation of sulphates and nitrates from gaseous precursors) are treated by the chemical mechanisms of the models. The main modules used for the chemical mechanisms are the Carbon Bond chemical gas phase mechanisms (Gery et al., 1989) in their most recent versions (i.e. CB-IV-99 and CB-V) and the ISORROPIA chemical equilibrium module (Nenes et al., 1998). The main output parameters are the concentrations and dry and wet deposition data for approximately 70 chemical species. Aerosols are calculated in two size fractions, i.e., $PM_{2.5}$ and $PM_{10-2.5}$.

A description of the BelEUROS model, its applications to air quality in Belgium and a validation exercise can be found in Deutsch et al. (2008a, 2008b, 2008c, 2008d, 2011). Model development, applications and validation examples for the AURORA model can be found in Mensink et al. (2001), De Ridder et al. (2008), Van de Vel et al. (2008) and Lefebvre et al. (2011).

3.2. Update of the deposition routines in the AURORA model

The main topic of this task was to improve the current deposition scheme used in the AURORA air quality model especially with regard to deposition above the sea.

3.2.1. The original deposition scheme in the model

The deposition velocity, V_d is expressed as follows for water, using a typical resistance-based approach:

$V_d = 1/(R_a + R_b + R_c)$ with

$\quad R_a = u_a/u_*^2$

$\quad\quad\quad u_a$ = wind speed [m/s]
$\quad\quad\quad u_*$ = friction velocity [m/s]

$\quad R_b = 1/(ku_*)*\ln(z_0/z_{0h})*(Sc/Pr)^{2/3}$ for gaseous components; $(\ln(z_0/z_{0h}) = 2)$
$\quad\quad\quad k$ = von Karman constant (0.4)
$\quad\quad\quad z_0$ = roughness length [m]
$\quad\quad\quad Sc$ = Schmidt number [-]
$\quad\quad\quad Pr$ = Prandl number [-]

$\quad R_b = 1/(u_**(Sc^{-2/3} + 10^{-3/st}))$ for particles
$\quad\quad\quad st = vs*u_*^2/(g*vis\_kin)$
$\quad\quad\quad vs = d^2 * \rho* g * CunCor)/(18*vis\_dyn)$
$\quad\quad\quad d$ = particle diameter [m]
$\quad\quad\quad \rho$ = density [kg/m^3]

g = gravitational acceleration (=9.81 m^2/s)

CunCor = Cunningham slip correction factor [-]

vis_dyn = dynamic viscosity [kg/m s]

vis_kin = kinematic viscosity [m^2/s]

$R_c = 2.54*10^4/(H_{i*}*T*u_*)$

H_{i*} = Henry coefficient

T = temperature [K]

3.2.2 Improvement of ln(z0/z0h)

Instead of a constant value of 2, ln(z0/z0h), becomes a function of Re_*

$Re_* = z_0*u_*/v$

$v = 1.46*10^{-5}$ m^2 s^{-1}

z_0:

Above sea: $z_0 = 0.011*u_*^2/g$ (Charnock, 1955)

Above land: value for each of the land use types (e.g., 1.1 m in urban areas)

The formula for ln(z_0/z_0h) then becomes:

- Sea: ln(z_0/z_{0h}) = -0.8 when $Re_* < 0.1$ (Zilitinkevich et al., 2001);

  ln(z_0/z_{0h}) = $1.6*Re_*^{1/2}-1.28$ when $Re^* > 0.1$;

- Land: ln(z_0/z_{0h}) = $0.04*Re_*^{1/2}$ (Zilitinkevich and Mironov, 1996, and Chen et al., 1997);

- Urban: ln(z_0/z_{0h}) = $1.29*Re_*^{1/4}-2.0$ (Kanda et al., 2007)

3.2.3. Improvement of the surface resistance for sea areas (Rc)

Following an extensive literature overview, it became evident that there is still significant uncertainty with respect to the dry deposition of gases above sea water. A recently published review paper by Fowler et al. (2009) suggests that much research still has to be carried out in this domain. Pryor and Barthelmie (2002) came up with the same conclusion, but specifically for the interaction between gaseous N-compounds and sea water. Research has already been carried out on the dry deposition of nitrogen to the oceans, both using measurements and model studies. However, the results are often unclear and certainly not applicable for the AURORA model (Rojas and Venegas, 2009, Evans et al. (2004), de Leeuw et al. (2003)).

The most complete investigation that comes up with useful results for our purposes has been carried out around the deposition of ozone on ocean water (Gallagher et al., 2001). Using measurements the authors show clearly that the surface resistance of sea water is significantly smaller for ozone (1000 s/m) than the surface resistance of fresh water for ozone (9000 s/m). This value will be adjusted in the AURORA model. Furthermore, we compared the dry deposition module of AURORA with other dry deposition models described in literature. Most of the described models parameterize the surface resistance for gaseous components above sea water (Schlunzen and Meyer, 2007, Klein et al., 2002). In Table 24, an overview is given of the surface resistances above sea found for the main components in the model compared to the value that is used in the original formulation, $2.54*10^4/(H_{i*}*T*u_*)$. The comparison shows that the surface resistance above sea water for NO_2 and NO currently used in AURORA is somewhat too high and this is therefore adjusted accordingly in the model.

Table 24. Improvement of the surface resistance above marine areas

Gas	H_{i*}	R_c (T = 280K, $u* = 0.5$ m/s)	R_c (literature)	Source
O_3	0.01	18000	1000	Gallagher et al., 2001 (observation)
NO_2	0.01	18000	7000,10000	Schlunzen et al., 2007, Klein et al., 2002 (model)
NO	0.002	90000	7000	Schlunzen et al., 2002 (model)
HNO_3	1.1014	0	0.10	Schlunzen et al., 2007, Klein et al., 2002 (model)
HNO_4	2.104	0.009		
NH_3	2.104	0.009	0,10	Schlunzen et al., 2007, Klein et al., 2002 (model)
SO_2	1.105	0.018	0,10	Schlunzen et al., 2007, Klein et al., 2002 (model)
H_2O_2	1.105	0.018		
$HCHO$	6.103	0.03		

3.3. High-resolution calculation of concentration and deposition maps for the Belgian Continental Shelf with AURORA

3.3.1. Introduction and short model description

AURORA is nested in the concentration fields calculated with BelEUROS. To reach a sufficiently high resolution with AURORA (i.e., 3 km x 3 km) high-resolution emission data is used. For shipping emissions, the results of the shipping emission model developed in Work Package 2 are used. Land-based emissions are set up using the Emission mapping tool E-MAP developed by VITO (Maes et al., 2009). This tool downscales national emission inventories (e.g., by IIASA of EMEP-CEIP, see above) using a set of proxy data, such as the CORINE land use information.

The air quality modelling system AURORA was designed to simulate the transport, chemical transformations and depositions of atmospheric constituents, at the urban to regional scale. It can be applied both in hindcasting and forecasting mode and can evaluate the effects of emission reduction scenarios, scenarios related to spatial urban structure, mobility etc., on air quality. The AURORA model consists of several modules. The emission generator calculates hourly pollutant emissions at the desired resolution, based on available emission data and proxy data to allow for proper downscaling of coarse data. The actual Chemistry Transport Model (CTM) then uses the hourly meteorological input data and emission data to predict the dynamic behaviour of air pollutants in the model region. This results in hourly three-dimensional concentration and two-dimensional deposition fields for all species of interest. The AURORA model can be driven by meteorological output provided by the ARPS (University of Oklahoma), ECMWF and MM5 models. To calculate down to the resolution of the urban scale the model has nesting capacities, i.e., it allows the user to specify lateral boundary conditions based on output from coarser resolution model runs.

For solving the advection, the AURORA model uses the Walcek (2000) scheme, which ensures monotonous advection in x, y and z directions. The model only accounts for vertical diffusion through turbulence using a solution based on the semi-implicit Crank-Nicholson diffusion scheme with damping of oscillations in the vertical direction. The dry deposition which is solved together

with the diffusion is parameterized as a downward flux as described in the previous chapter. Wet deposition is modelled using species-dependent washout coefficients and allows for accumulation to saturation in the rain drops during the washout process.

AURORA has a choice of three different chemical mechanisms for the gas phase: (1) the CB-IV-99 mechanism, which is an extension of the CB-IV (Gerry et al., 1989) mechanism with isoprene chemistry, (2) CB5 (Yarwood et al., 2005), which compared to the CB-IV-99 mechanism incorporates terpene oxidation and an improved description of the nitrate radical chemistry at night and (3) CB5 extended with oxidation reactions that result in the formation of semi-volatile organic compounds, which can condense to form secondary organic aerosols. Finally, for the formation of secondary inorganic aerosols the model uses the ISORROPIA model (Nenes et al., 1998) for calculating the equilibrium between the gas and aerosol phase for the inorganic compounds and a kinetic description of the desorption/adsorption process for the semi-volatile organic compounds.

3.3.2. Overview of input parameters for the model calculations

Generally, the influence of the meteorological conditions on air quality is considerable. Hence, inter-annual variations in air pollutant concentrations for several consecutive years are usually (much) more driven by inter-annual changes in meteorology than by the inter-annual changes of the emissions. From that perspective, it is not unusual in air quality modelling to combine meteorological conditions and emission data from different years, or emission data for different regions, or sectors from different years in one calculation. Sometimes, the limited availability of input data even makes these kinds of combinations difficult to avoid. However, they are also especially useful if more general conclusions have to be drawn with respect to the contribution of certain emission sources to air pollutant concentrations, or deposition, as in this study. In these cases, it is important to use a "representative" or "normal" meteorological year in order to get results that are not biased, due to possibly exceptional meteorological conditions. In Belgium, the year 2007 was characterized by conditions that can be referred to as rather "normal". Hence, we used meteorological data for the year 2007 for all model calculations in this study.

For the calculation of the base year (reference year) of this study, meteorological data for 2007 has been combined with shipping emission data for 2009 for the North Sea, both in the BelEUROS and the AURORA model. For the scenarios 2012 and 2020, the same meteorological data for 2007 have been used together with shipping emission projections for 2012 and 2020. By doing all simulations with the same meteorological input the changes observed can be attributed to the emissions. Also land-based emission projections for 2012 and 2020 were used for the scenarios. Table 25 gives an overview of the used input data.

Table 25. Overview of the used meteorological and emission input data for the base year and the two scenario years

Parameter	Base year	Scenario 2012	Scenario 2020
Meteorology	2007	2007	2007
Shipping emissions on BCS	2009	2012	2020
Shipping emissions on other sea areas	2010	2012	2020
Land-based emissions	2010	2012	2020

3.3.3. Modelling of heavy metals and PAHs with AURORA

For the modelling PAHs and heavy metals (Cd and Pb), we incorporated an approach developed in a previous study using the OPS model (Viaene et al., 2010). The particle phase in OPS is modelled using 5 size sections (Table 26).

Table 26. Lower and upper diameter of the five size sections considered for the particle size distribution in the model and the geometric average of these two limits

Section	Lower (µm)	Upper (µm)	Average diameter (m)
1	(0.0215)	0.95	1.43E-07
2	0.95	4	1.95E-06
3	4	10	6.32E-06
4	10	20	1.41E-05
5	20	(40)	2.83E-05

In general, PAHs are found both in the gas phase and bound on particles. The partitioning between these two phases depends on the saturated vapour pressure. This implies that in principle PAHs can migrate between the gas and the aerosol phase, depending on the ambient temperature and pressure, where with increasing temperature and lower pressure the gas phase is favoured. In this modelling exercise, we neglected this dynamic distribution and assumed that the initial distribution between the two phases is kept after emission. Taking the overall uncertainty of the PAH emissions into account, this approach seems to be justified. The distribution of the total emitted PAHs' mass over the two phases is presented in Table 27 together with the distribution over the 5 aerosol size fractions considered. The heavy metals (Pb and Cd) are only modelled as aerosols.

Table 27. Particle distribution over the gas phase and the 5 aerosol size fractions considered for the aerosol phase

Pollutant	Formula	Gas phase %	Particle mass % in each fraction				
			< 0.95 µm	0.95-4 µm	4-10 µm	10-20 µm	>20 µm
Cadmium	Cd	0.0	57.4	21.3	14.1	3.6	3.6
Lead	Pb	0.0	62.1	17.8	14.1	3.0	3.0
benzo[a]pyrene	B[a]P	9.0	46.5	25.1	17.4	5.5	5.5
benzo[b]fluoranthene	B[b]F	8.0	39.9	23.7	18.9	8.8	8.8
benzo[k]fluoranthene	B[k]F	6.0	41.5	35.5	15.2	3.9	3.9

Measurements have shown that the land surface is generally saturated with B[a]P and B[b]F, so that these two PAHs do not deposit, but they are rather emitted from the surface. The model code was, therefore, extended to allow for different surface resistance (rc) values over land and water. In order to avoid deposition above land, the rc for B[a]P and B[b]F was set to a high value (99999), which results in negligible deposition of these two pollutants (Table 28).

The initial and boundary concentrations of all pollutants were assumed to be constant. As the domain boundary in the model having the largest influence on the results, due to the predominant wind direction is the western domain boundary above the United Kingdom (UK) in the 7 km resolution calculations, the boundary concentrations were based on information from the UK. For the PAHs, concentrations for the rural site 'Hazelrigg' were used based on information found in Prevoudoros et al. (2004) and the annual report for 2010 on the UK PAH monitoring and analysis (Brown et al., 2011). For Cd and Pb values were based on maps (Figure 53) for the average concentration over UK in 2008 as published online by the Department of Environment, Food and Rural Affairs (DEFRA). The final values used for the fixed boundary concentrations of Cd, Pb and the PAHs are listed in Table 29.

Table 28. Input parameters for the molecular weight (MW), diameter, density, washout coefficient and surface resistance over land (rc_land) and water(rc_water).

| Pollutant	MW (g/mol)	Phase	Diameter (μm)	Density (kg/m³)	Washout (-)	rc_land (s/m)	rc_water (s/m)
B[a]P	252	gas	-	-	120000	99999	182
B[a]P_A1	252	aerosol	0.14	1200	30000	-	-
B[a]P_A2	252	aerosol	1.95	1400	30000	-	-
B[a]P_A3	252	aerosol	6.32	1600	70000	-	-
B[a]P_A4	252	aerosol	14.14	2000	70000	-	-
B[a]P_A5	252	aerosol	28.28	2400	70000	-	-
B[b]F	252	gas	-	-	100000	99999	182
B[b]F_A1	252	aerosol	0.14	1200	30000	-	-
B[b]F_A2	252	aerosol	1.95	1400	30000	-	-
B[b]F_A3	252	aerosol	6.32	1600	70000	-	-
B[b]F_A4	252	aerosol	14.14	2000	70000	-	-
B[b]F_A5	252	aerosol	28.28	2400	70000	-	-
B[k]F	252	gas	-	-	340000	223	182
B[k]F_A1	252	aerosol	0.14	1200	30000	-	-
B[k]F_A2	252	aerosol	1.95	1400	30000	-	-
B[k]F_A3	252	aerosol	6.32	1600	70000	-	-
B[k]F_A4	252	aerosol	14.14	2000	70000	-	-
B[k]F_A5	252	aerosol	28.28	2400	70000	-	-
Cd_1	112	aerosol	0.14	1200	30000	-	-
Cd_2	112	aerosol	1.95	1400	30000	-	-
Cd_3	112	aerosol	6.32	1600	70000	-	-
Cd_4	112	aerosol	14.14	2000	70000	-	-
Cd_5	112	aerosol	28.28	2400	70000	-	-
Pb_1	207	aerosol	0.14	1200	30000	-	-
Pb_2	207	aerosol	1.95	1400	30000	-	-
Pb_3	207	aerosol	6.32	1600	70000	-	-
Pb_4	207	aerosol	14.14	2000	70000	-	-
Pb_5	207	aerosol	28.28	2400	70000	-	-
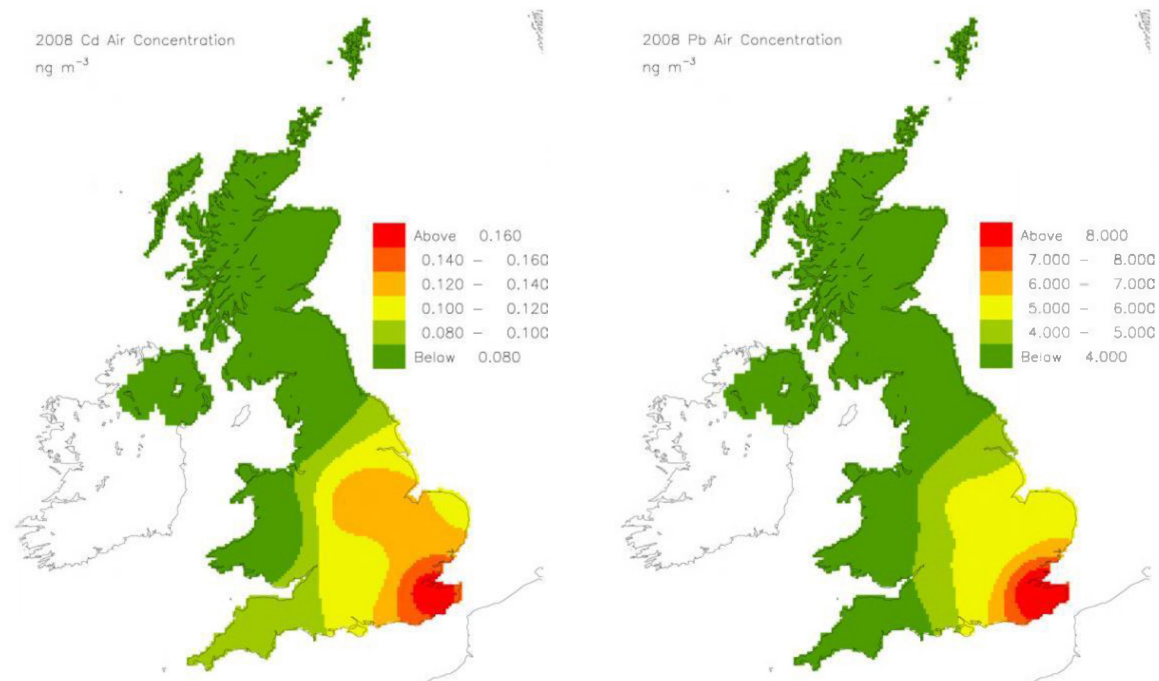
Figure 53. Average Cd and Pb concentrations for the United Kingdom in 2008 (from DEFRA website)

Table 29. Concentrations (ng/m³) used for the initial and boundary conditions in the 7 km resolution calculations

Pollutant	Initial/boundary concentration (ng/m³)
Pb	0.5
Cd	0.017
B[a]P	0.001
B[b]F	0.002
B[k]F	0.001

3.4. Validation of the model results

3.4.1. Model validation using the results from the high-resolution NO_x and SO_2 measurements during the onboard campaigns in SHIPFLUX

In a first step, the measurements were filtered for excessive values and negative values and for both NO_2 and SO_2 all values above 80 $\mu g/m^3$ were removed. During both measurement campaigns the position of the Zeeleeuw (March 2010) or Belgica (October 2010) had been tracked in time. Using this tracking information, the model results for each of the positions in time and space for which a measurement is available were extracted. As the model results are only stored on an hourly basis and for a spatial resolution of 3 km, in a next step the observed data were then averaged according to the coarser modelling resolution. In this way, a time series was obtained containing unique modelling results and their corresponding averaged observed values. In Figure 54 and Figure 55, results are shown for nitrogen dioxide (NO_2) and sulphur dioxide (SO_2) for the two campaigns of March and October 2010.
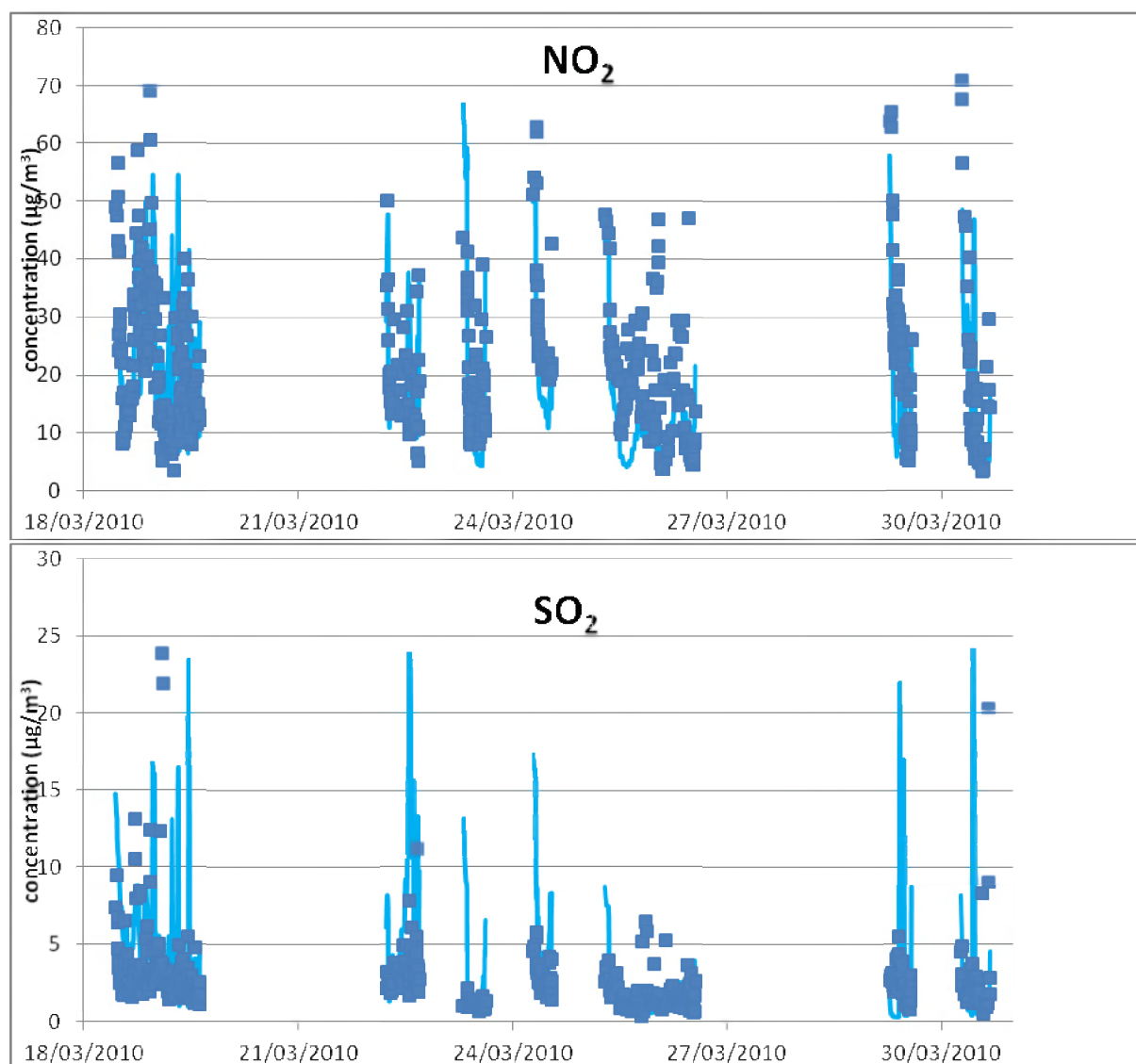

Figure 54. NO_2 and SO_2 concentrations observed (blue dots) and modeled (blue line) for the sampling campaign from March 18th 2010 to March 30th 2010 onboard the Zeeleeuw
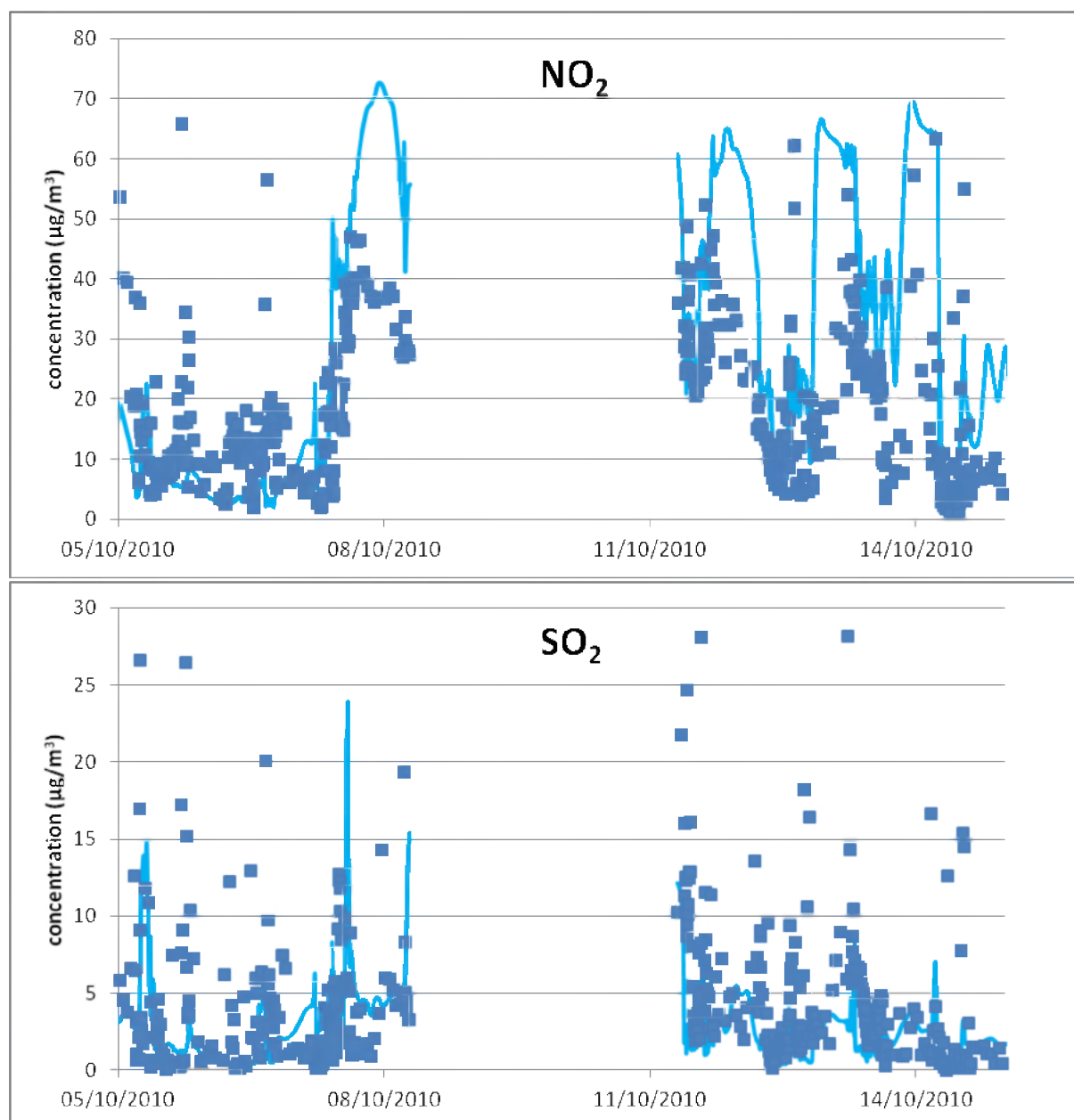
Figure 55. NO₂ and SO₂ concentrations observed (blue dots) and modeled (blue line) for the sampling campaign from October 5ᵗʰ 2010 to October 16ᵗʰ 2010 onboard the Belgica

Details for parts of these time series are shown in Figure 56. The best model results were obtained for the March 2010 sampling campaign. For this campaign, the correlation between modelled and observed values for NO₂ attains 46 % with an average underestimation of -14 % by the model. For the October 2010 campaign, the correlation for NO₂ was somewhat better (54 %), but the bias increased to 33 %. For SO₂, the modelled results show only a weak correlation with the measurements at sea. This contrasts with the results obtained for the fixed station in De Haan on land where the correlation is better between the model and the measurements (57 %) than between both the land and sea observations (25 %) and the land and sea model results (42 %). Both on sea and on the land a large positive bias is observed between modelled and observed SO₂ concentrations.
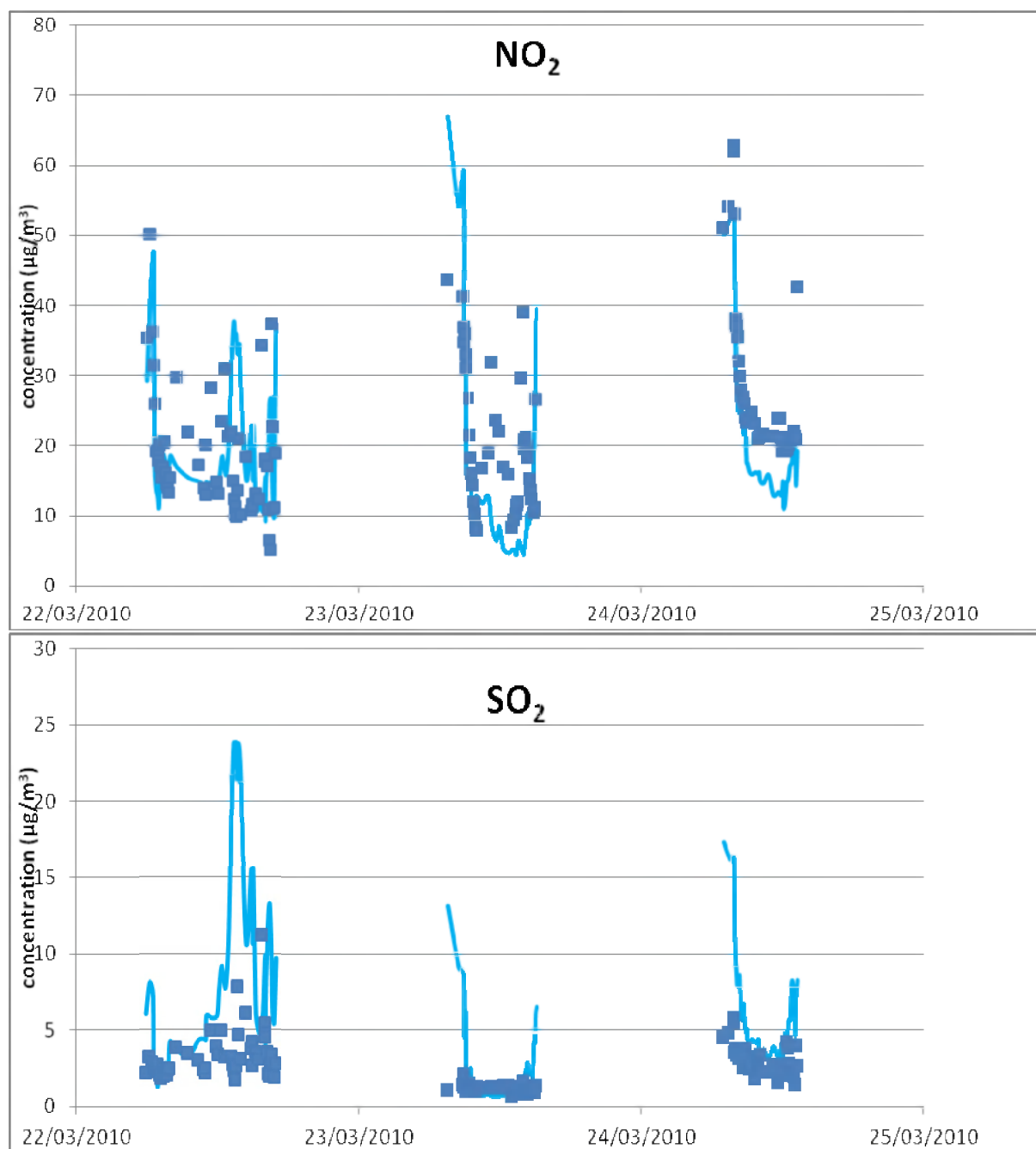
Figure 56. NO₂ and SO₂ concentrations observed (blue dots) and modeled (blue line) for the sampling campaign from March 22nd 2010 to March 25th 2010 onboard the Zeeleeuw

The differences between modelled and observed values are at least partially due to the way the emissions are conceptualized in the model. In the model, the spatial pattern of the emissions is assumed to be constant over the year, represented as line sources, while in reality ships are point sources that are moving around.

More specifically, annual total emissions have been set up using a high level of detail. However, we do not have any information regarding the temporal emission pattern by month of the year, by day of the week, or by hour of the day. Hence, as a best estimate, we suppose constant emissions throughout the whole year, meaning that 1/8760 of the annual emission value (by grid cell) is released every hour of the year in the model. In contrast, the measurements carried out on the Zeeleeuw/Belgica are highly influenced by the emissions of the ships travelling at that

moment in the vicinity of the research vessel. Those emissions may, of course, differ significantly from the mean emissions and can hence be rather unrepresentative for the annual emissions at that location.

The strong fluctuations in the observed values are probably due to either other ships passing by in the neighbourhood, or due to measurement of the plume of the research vessel itself. To compensate for the latter, some observed concentrations had been discarded, as described above.

A comparison between the observed values, the emission pattern used in the model and the average modelled concentrations for NO_2 for the period of the March 2010 measurement campaign can be found in Figure 57. It can be seen that high concentrations do not necessarily coincide with high emissions. The concentration pattern, on the other hand, shows a clear gradient of lower concentrations with increasing distance from the coast. Only for the highest shipping emission hot spots in the sea higher concentrations can be observed. This implies that concentrations above the sea are affected not only by shipping emissions, but also by land-based sources to a significant extent.
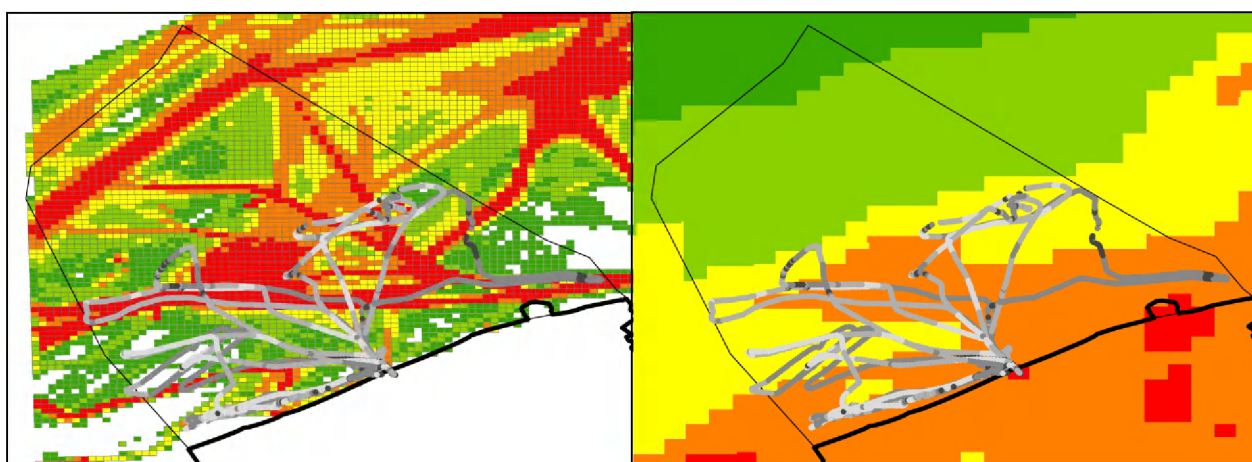

Figure 57. Maps of the BCS showing the annual mean NOx emission pattern (left) and the modelled average NO$_2$ concentration (right) during the measurement campaign of March 2010 with the observations from the March 2010 campaign superimposed. Legend for the maps: low values (green) to high values (red); legend for the observations: low values (light grey) to high values (dark grey)

For SO_2 the contribution of shipping emissions to the concentrations above sea is larger. This can explain the larger deviation between observations and model results for SO_2.

The main conclusion that can however be drawn from the presented validation is that the choice for the "low emissions" was the correct one. Otherwise the observed good agreement between observed and modelled values could not have been reached.

3.4.2. Model validation using the results for the chemical composition of PM$_{10}$ obtained during the onboard campaigns in SHIPFLUX

The second type of model validation uses the measurements of the inorganic chemical composition of PM$_{10}$ samples collected during the March 2010 and October 2010 sampling campaigns onboard the Zeeleeuw and the Belgica, as described above in this report (Work Package 1). To validate the model using the sulphate, nitrate and ammonium measurements, the model results along the parts of the ship trajectories that correspond to each of the single measurements were averaged. The results for sulphate, nitrate and ammonium are presented in Figure 58. We notice a very good correlation for sulphate for the March 2010 campaign and a fairly good correlation for the October 2010 campaign, however, with a positive bias for the October campaign which can be linked to the positive bias for the SO$_2$ concentrations. Also for ammonium, the agreement between observations and model results is good, for the March 2010 campaign even very good. For nitrate, we can observe a relatively large scattering of the values.
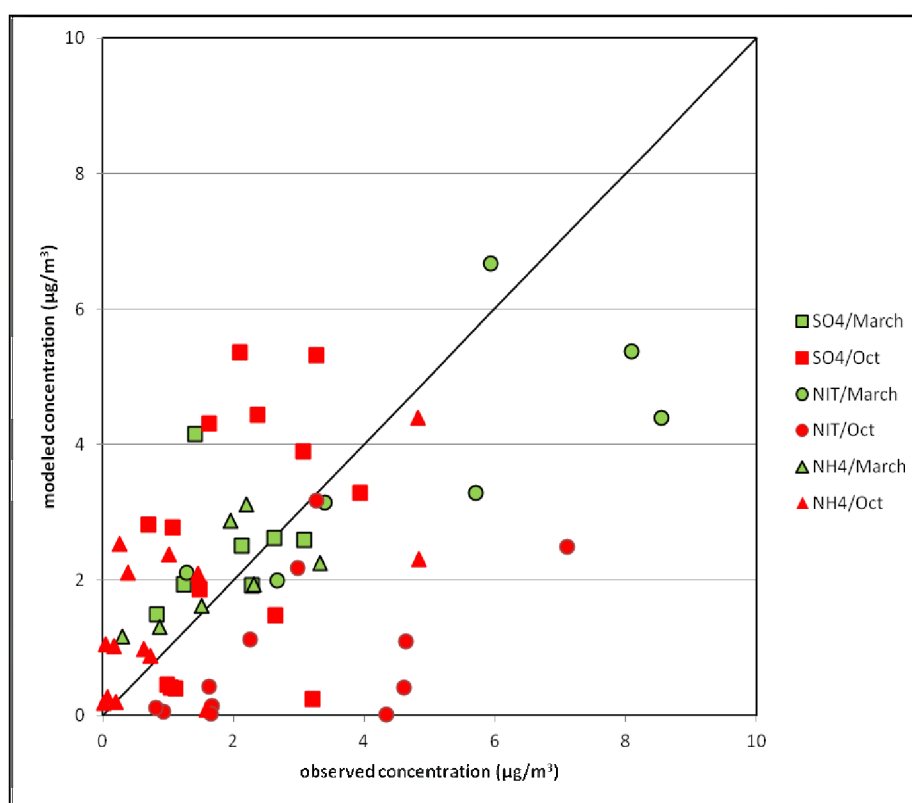

Figure 58. Scatter plot with the observed and modelled sulphate (SO4, square), nitrate (NIT, circle) and ammonium (NH4, triangle) for the March 2010 campaign onboard the Zeeleeuw (green) and the October 2010 campaign onboard the Belgica (red)

3.4.3. Model validation using deposition data from VMM

Figure 59 shows the validation of the modelled annual wet deposition for the reference calculation with observations from the acidification measurement network of the VMM.

For nitrate and especially for sulphate, the modelled wet deposition results correspond well with the observed values. For ammonium, the model calculates too high wet deposition values. As ammonium is the only cation available in the model, its concentration is calculated by applying the equilibrium constants for all relevant compounds, supposed there is enough ammonia present in the system to reach equilibrium. This may result in an overestimation of the formation of

ammonium compounds. When considering these results, one should also keep in mind that the emission used in the calculation is not those of 2007.
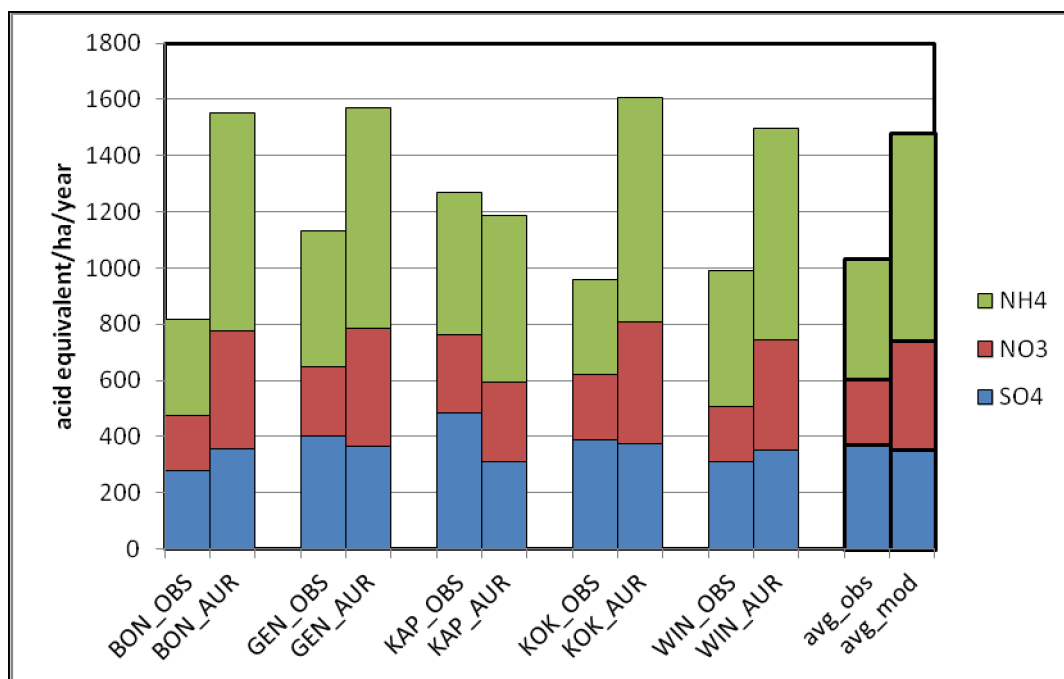

Figure 59. Observed (OBS) and modelled (AUR) wet deposition for the VMM measurement stations at Bonheiden (BON), Ghent (GEN), Kapellen (KAP), Koksijde (KOK) and Wingene (WIN) and the average observed (obs) and modelled (mod) values over these stations for 2007

3.5. Results for the base year "2009" for the classical pollutants

3.5.1. Concentrations of air pollutants

The following figures show the annual mean concentrations for the base year for several relevant pollutants. The maps have a resolution of 3 km x 3 km and show the domain of the last nesting step of the AURORA model. The Belgian Continental Shelf is shown on the maps as the main region of interest in this study. Besides a part of the Southern Bight of the North Sea, also the Belgian coast and parts of Dutch, French and UK coastal areas are parts of the 3 km x 3 km domain. As the main interest in this study is directed towards the deposition of pollutants to the Belgian Continental Shelf, the concentrations maps are shown here rather for illustrative purposes.

Figure 60 shows the annual mean concentration of nitrogen dioxide and sulphur dioxide for the base year. The concentrations of both pollutants are higher above land than above sea, but for SO_2 the influence of shipping emissions is also clearly visible.
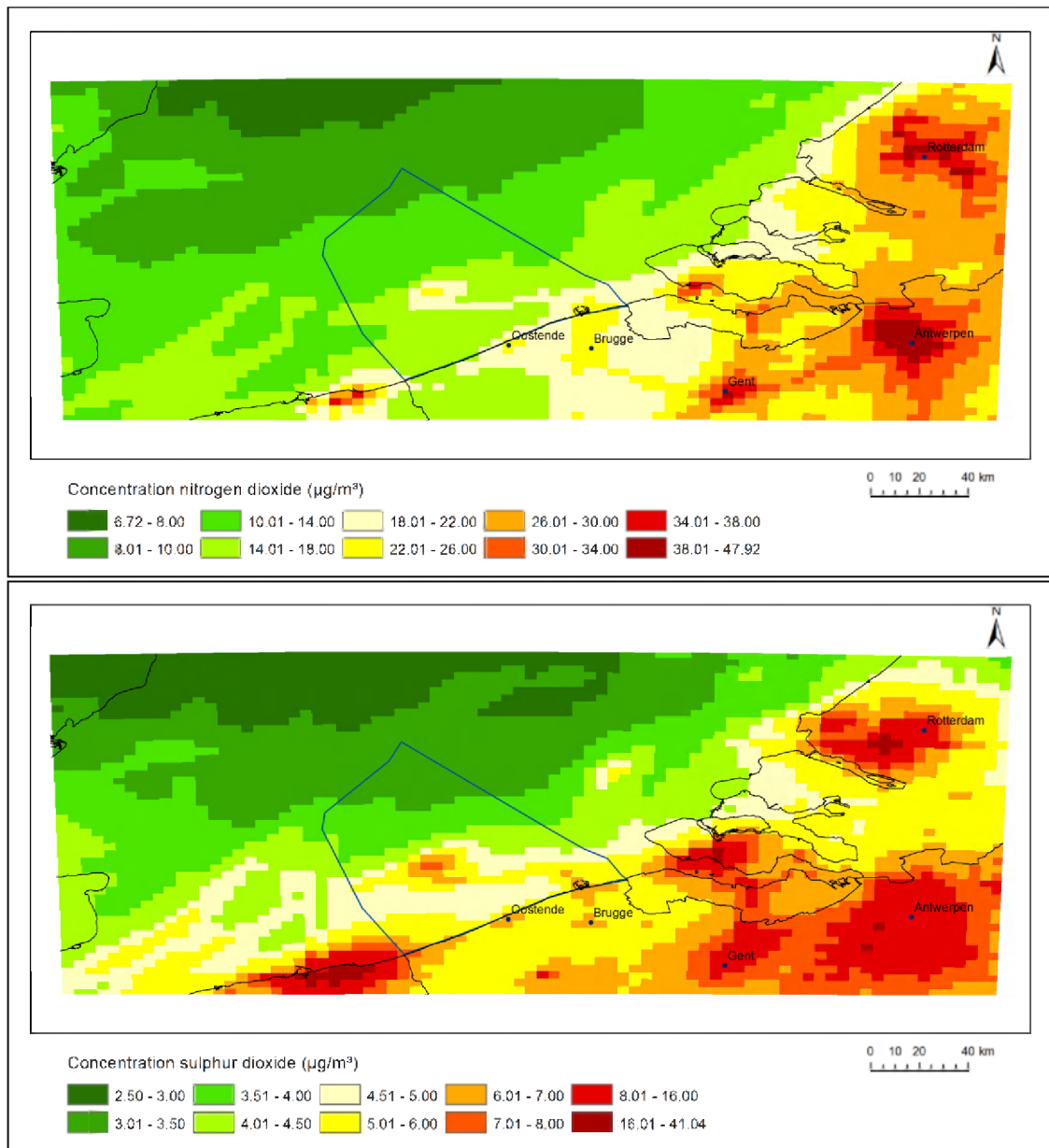
Figure 60. Concentration maps of NO₂ (above) and SO₂ (below) in the 3 km x 3 km domains for the base year

Figure 61 shows the annual mean concentrations of ammonia (NH_3) and $PM_{2.5}$. Especially the first of these pollutants is clearly linked rather to land-based emissions than to shipping emissions. However, as ammonia plays an important role in the deposition of nutrients the ammonia concentration map is also of importance in this study.
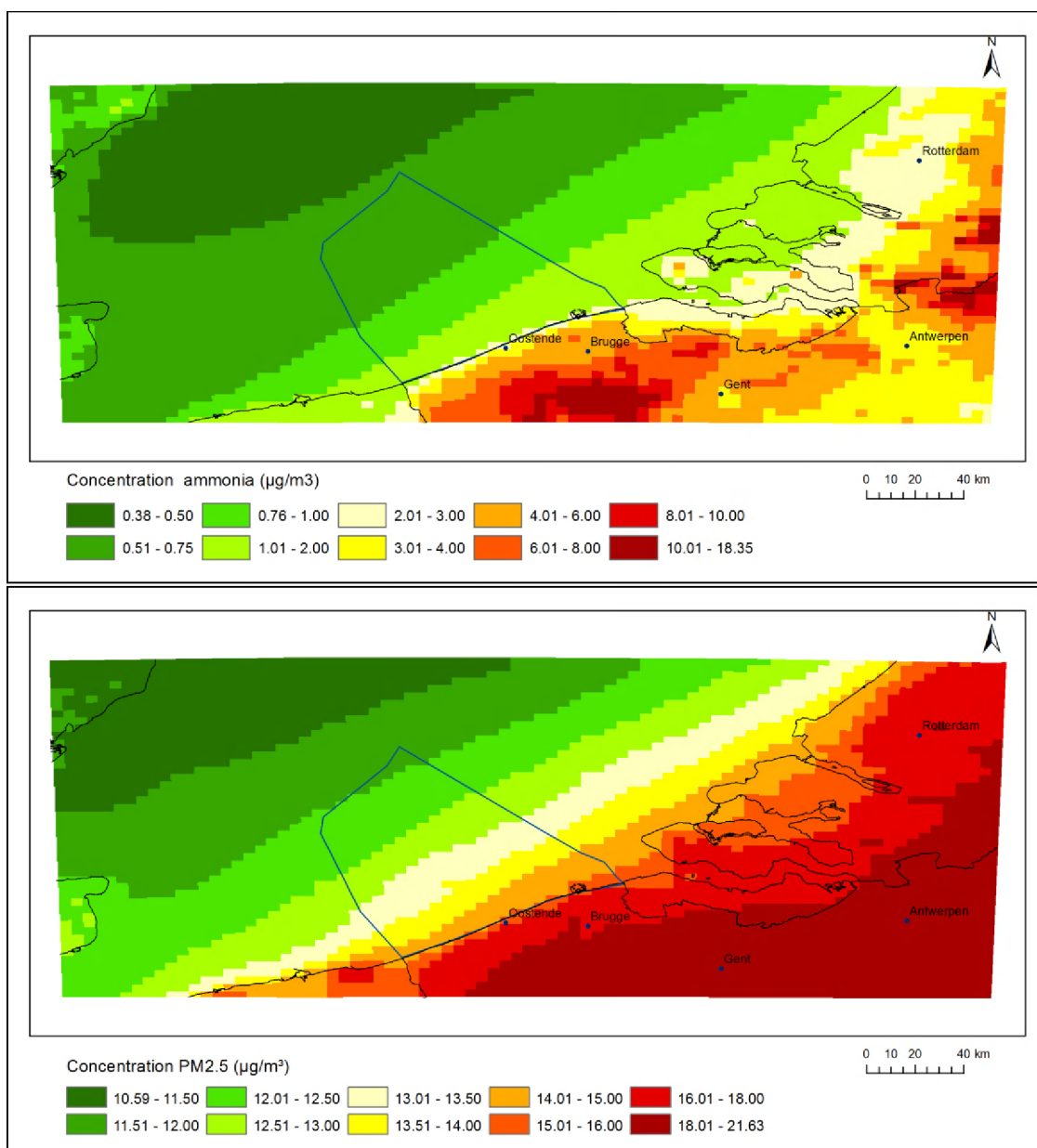
Figure 61. Concentration maps of NH₃ (above) and PM₂.₅ (below) for the base year

3.5.2. Deposition of air pollutants

The following figures show the annual mean total deposition (the sum of dry and wet deposition) for the base year for several relevant pollutants.

Figure 62 shows the deposition of total nitrogen, reduced nitrogen and the deposition of the nitrogen originating from shipping emissions alone. It becomes clear that the deposition above land is significantly higher than the deposition above sea. Two main factors are responsible for this difference: the distribution of the concentration of the relevant nitrogen containing compounds and the difference in deposition velocity of those compounds above land and marine water surfaces. The first can be attributed to the location of the NH₃ emissions from agricultural activities, which is close to the coast in Belgium (e.g., West Flanders as cited above).
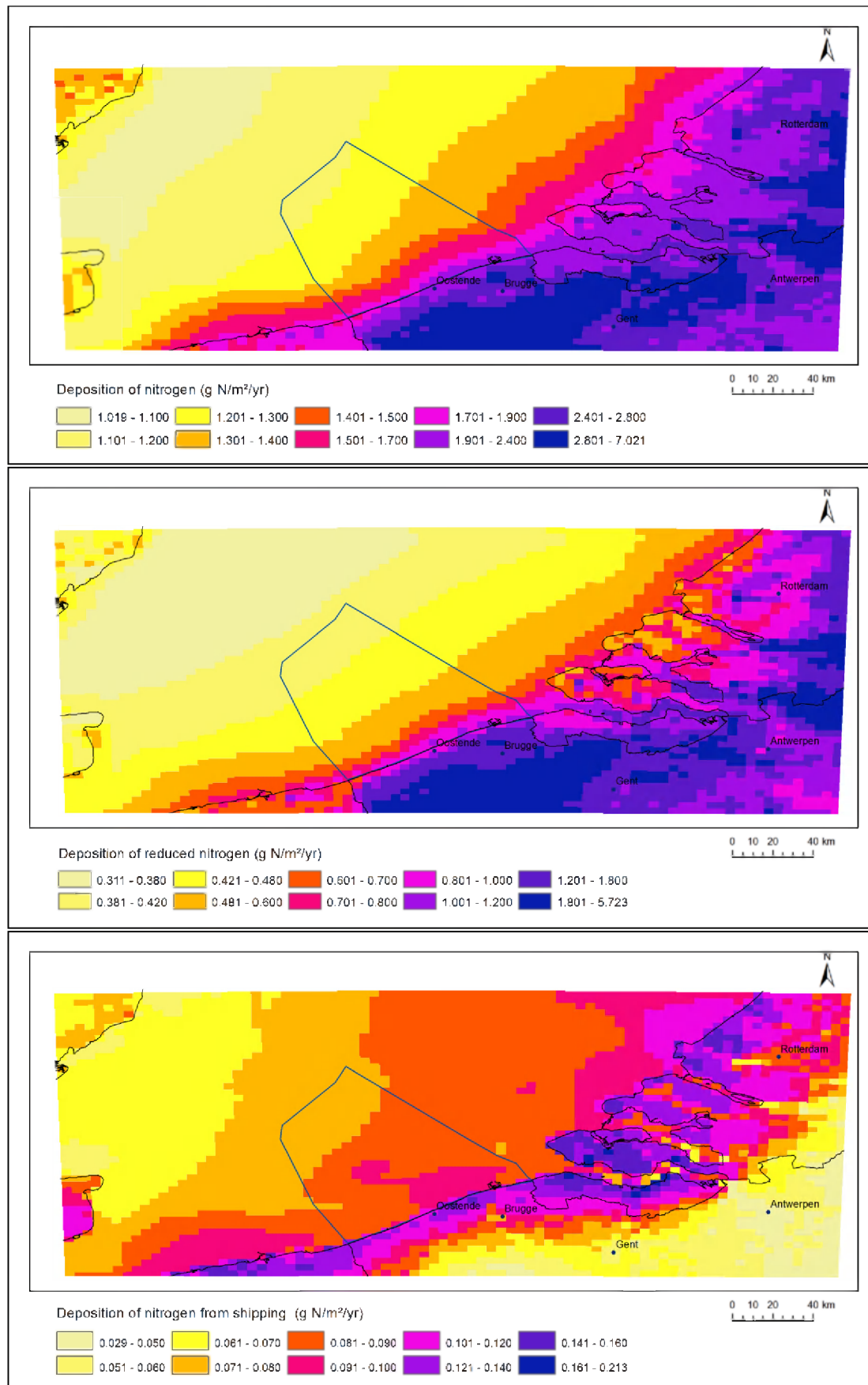
Figure 62. Deposition of total nitrogen (above), reduced nitrogen (middle) and nitrogen due to shipping emissions (below) for the base year

The second factor responsible for the difference in deposition between land and sea is related to the hydrophilic, or hydrophobic character of a compound. For instance, NO_2 is a hydrophobic compound and shows only very limited deposition to sea water, whereas nitric acid (HNO_3) is a highly hydrophilic compound and deposits very fast to sea water.

The third graphic shows the deposition of nitrogen originating from shipping activities which for the largest part occurs either above water, or in the land areas in the vicinity of the coast. In Belgium, the contribution of shipping emissions to the deposition of N drops drastically within a distance of approximately 30 km from the coast.

Figure 63 shows the annual mean deposition of total sulphur for the base year and the deposition of sulphur originating from shipping emissions. The deposition of sulphur compounds from shipping emissions is much more concentrated to the sea areas than the deposition of nitrogen compounds.
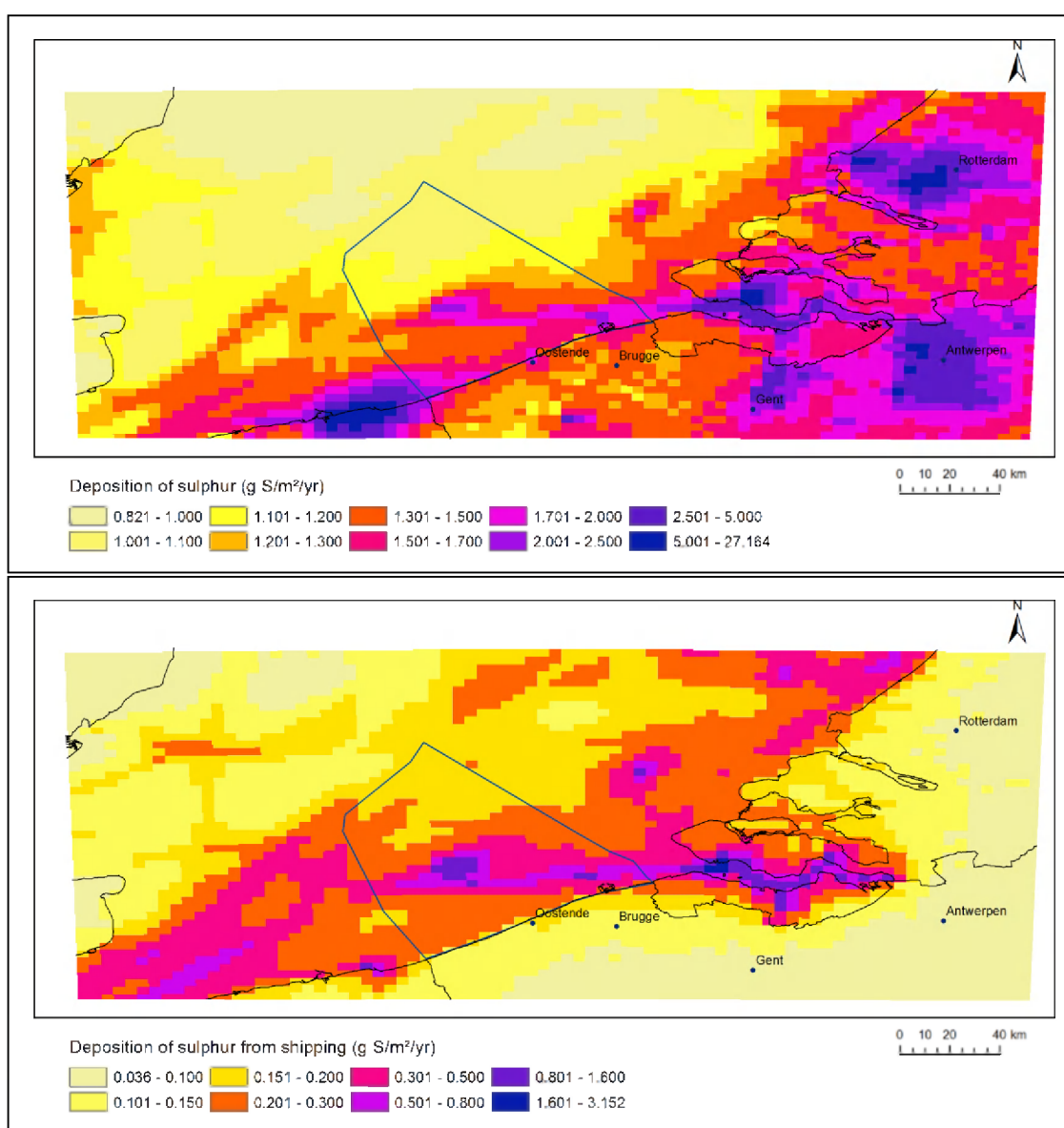

Figure 63. Deposition of total sulphur (above) and sulphur due to shipping emissions (below)

3.5.3. Relative contribution of shipping emissions

The following figures show the relative (%) annual mean contribution of shipping emissions to the deposition of the most relevant compounds for the base year.

Figure 64 shows the relative contribution of shipping emissions to the deposition of nitrogen compounds. It becomes obvious that shipping emissions contribute significantly to the deposition of nitrogen compounds only above sea. Above land, too many other sources are present. The second graphic shows an interesting result. The deposition of reduced nitrogen actually decreases in the presence of shipping emissions. This result can be explained in the following way: only ammonia and thus ammonium compounds (e.g., ammonium nitrate) contribute significantly to the deposition of reduced nitrogen compounds. Ammonia, however, is not originating from shipping emissions, but rather from animal husbandry. The deposition velocity of NH_3 to sea water is high, resulting in a quite large amount of ammonia deposition to the sea. However, in the presence of shipping emissions, the ammonia reacts with sulphuric acid, originating from the oxidation of SO_2 from the shipping emissions, to form ammonium sulphate. However, the deposition velocity of ammonium sulphate is lower than the one of ammonia itself. Hence, due to the transformation of ammonia to ammonium sulphate, the deposition of reduced nitrogen to the Belgian Continental Shelf decreases in the presence of shipping emissions.

If we focus on which nitrogen components are actually contributing to the deposition (Figure 65), we can see that this is mainly nitric acid (HNO_3). When all contributions are considered, we notice that contribution from reduced nitrogen (NH_3 and NH_4^+) is about 38 % of the total deposition and nitrogen dioxide (NO_2) constitutes a negligible fraction of only 2 %, which is less than the 3 % for peroxyacetylnitrate (PAN). When we consider only the deposition due to shipping emissions the part due to reduced nitrogen becomes only 3 %, which is in the same order as the contribution from NO and less than the 10 % due to NO_2. Ships are obviously not contributing to NH_3 deposition as this compound is not emitted by ships, they also do not contribute to the deposition of PAN, but in line with what has been observed in Figure 62, actually, decrease the deposition of reduced nitrogen components.
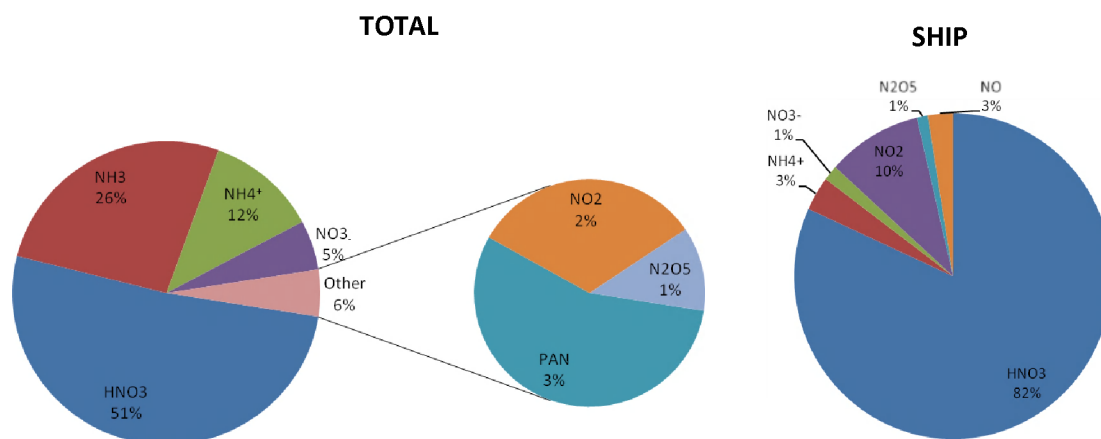

Figure 64. Speciated contribution of all sources (total on the left) and shipping emissions alone to the nitrogen deposition
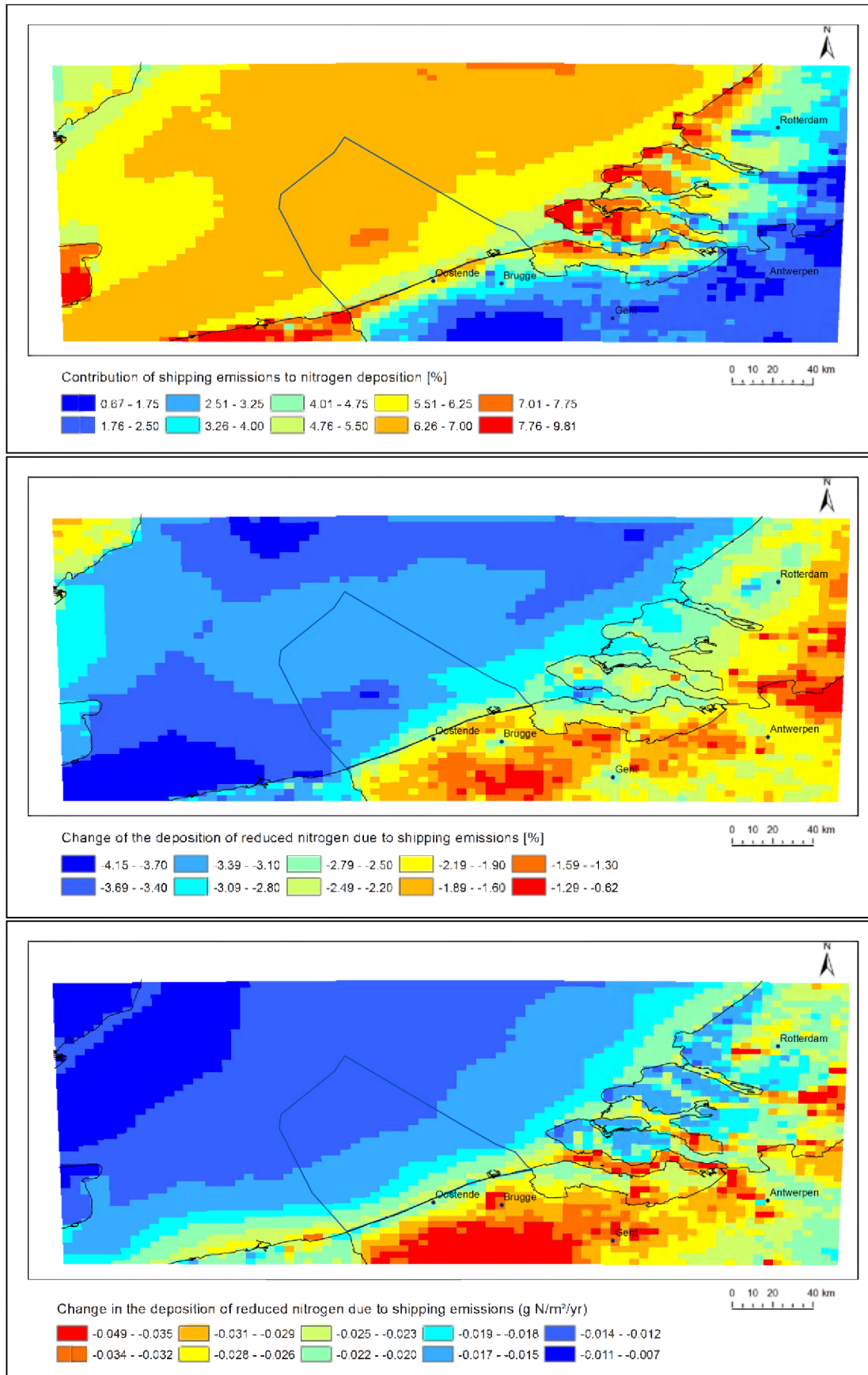
Figure 65. Contribution of shipping emissions to the deposition of nitrogen (above), reduced nitrogen (middle) and change in deposition of reduced nitrogen due to shipping emissions (below) for the base year

Figure 66 shows the contribution of shipping emissions to the deposition of sulphur compounds. Compared to the shipping emission contribution to the nitrogen deposition this is clearly more significant and the main shipping routes can easily be seen on the figure.
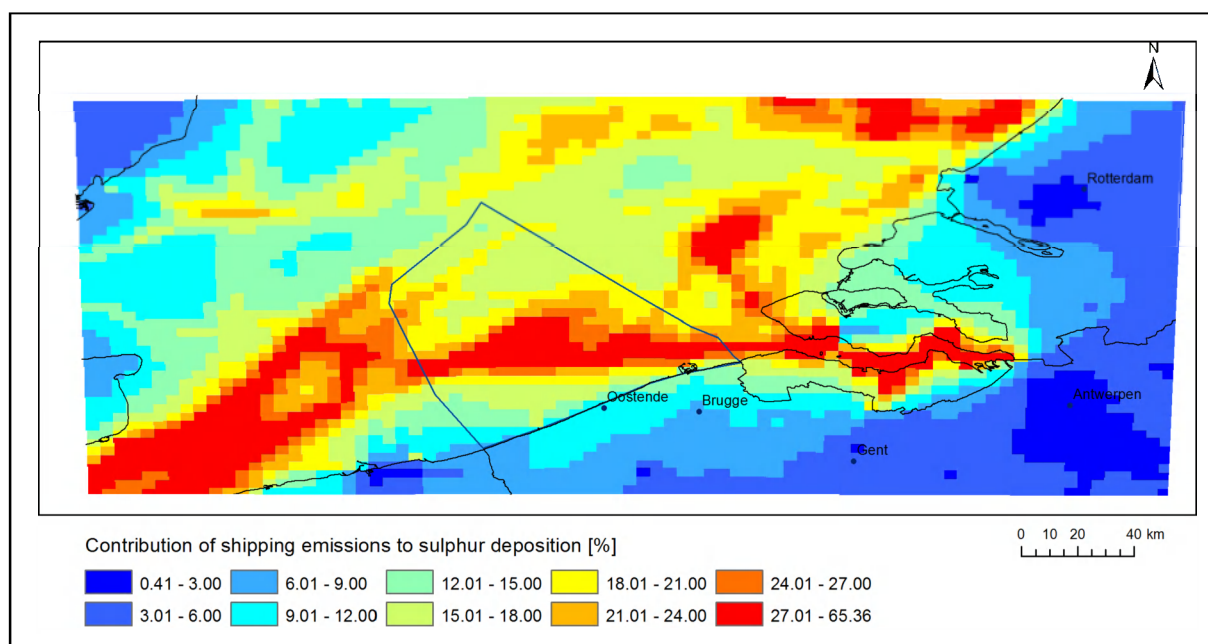

Figure 66. Contribution of shipping emissions to the deposition of sulphur for the base year

3.6. Results for the shipping emission scenarios 2012 and 2020 for the classical pollutants

In this chapter, the results of the calculations for the shipping emission scenarios are presented. For these scenarios, shipping emission projections had been created for the years 2012 and 2020, taking into account today's legislation. More specifically, these scenarios start from the assumptions of a drastic reduction in SO_2 emissions, due to the status of the North Sea as a SECA, but of only minor NOx emission reductions because the North Sea will most probably not become an ECA by 2020.

3.6.1. Deposition of air pollutants and contribution of shipping emissions

Figure 67 shows the contribution of shipping emissions to total sulphur deposition for the two shipping scenarios 2012 and 2020. If we compare these two maps with the map for the base year (Figure 66) we can clearly see the significant reduction in the contribution of the shipping sector to the deposition of sulphur to the BCS in the two scenarios in comparison to the base year. Hence, the planned reductions of the sulphur content of marine fuels to 1 % m/m in 2012 and 0.1 % in 2020 would result in significant reductions of the contribution of shipping emissions to the deposition of sulphur compounds in the Southern Bight of the North Sea and the neighboring coastal areas.

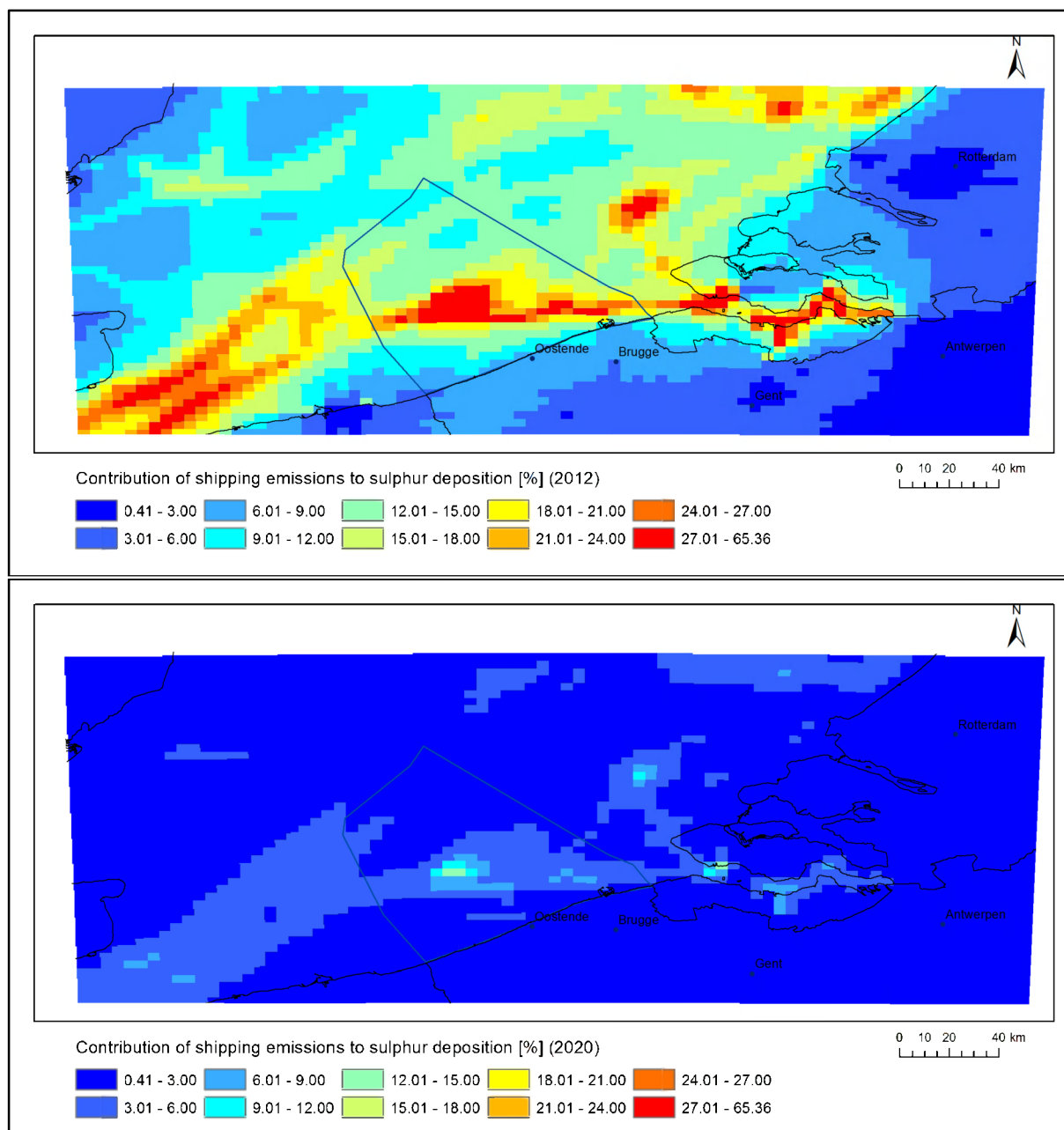Figure 67. Contribution of shipping emissions to the deposition of sulphur for the scenarios 2012 (above) and 2020 (below)

Figure 68 shows the contribution of shipping emissions to the deposition of nitrogen in the scenario 2020. If we compare this result with the contribution of shipping emissions to the deposition of nitrogen for the base year (Figure 65 above), we can see an increase in the contribution for the 2020 scenario.
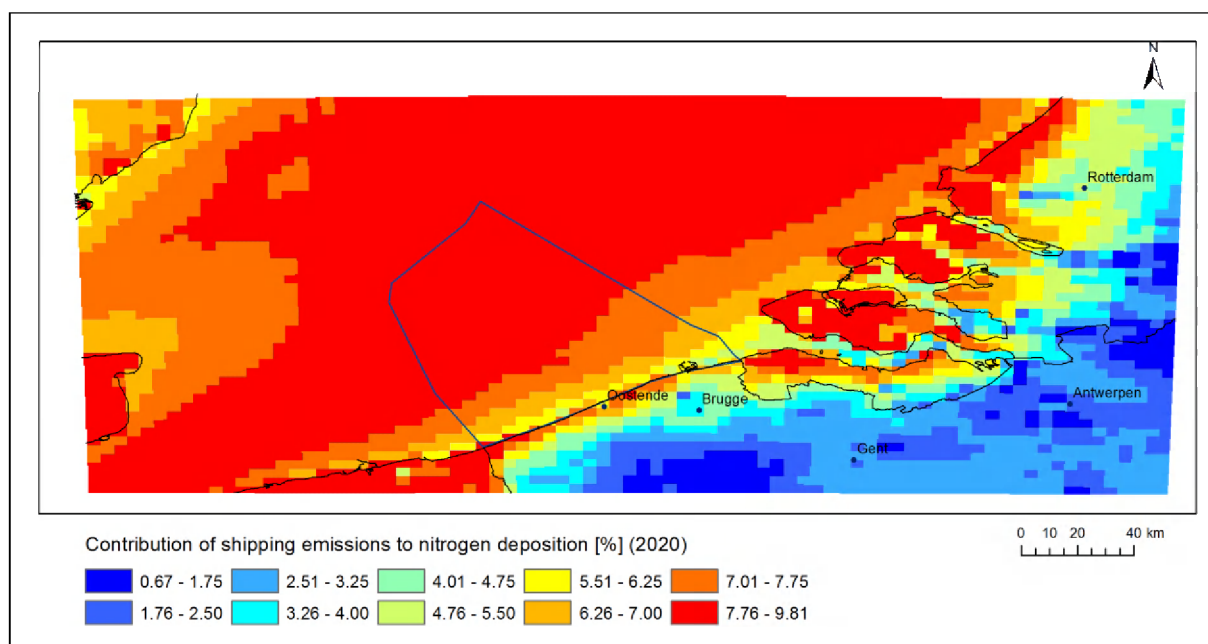
Figure 68. Contribution of shipping emissions to the deposition of nitrogen for the scenario 2020

3.6.2. Overview of the results

Table 30 shows an overview of the annual total deposition of N- and S-components to the Belgian Continental Shelf for the base year and for the 2012 and 2020 shipping scenarios. The total deposition (i.e., from all sources), deposition from shipping emissions and contribution of shipping emissions to total deposition to the BCS is shown.

Table 30. Overview of the annual total deposition of N- and S-components to the Belgian Continental Shelf for the base year and for the 2012 and 2020 scenarios: deposition from all sources, deposition from shipping emissions and contribution of shipping emissions to total deposition to the BCS

Component	Scenario	Total (kTon)	Ship (kTon)	Ship/total (%)
N	reference	4.81	0.29	6.1
	2012	4.75	0.31	6.5
	2020	4.32	0.33	7.6
S	reference	4.71	1.08	22.8
	2012	4.15	0.72	17.3
	2020	2.78	0.09	3.3

As far as the nitrogen compounds are concerned, we can see a decrease in total deposition especially in the 2020 scenario, whereas the deposition originating from shipping emissions slightly increases. This is rather surprising as the NOx emissions from ships decrease for the 2020 scenario by some 10 % compared to the reference situation. An explanation for this is that the atmosphere in the model domain seems to be more oxidizing due to a decrease of the emissions in general, which results in a larger contribution of nitric acid (Figure 69) to the total deposition. This is also confirmed by the average ozone concentrations, which are more than 2 $\mu g/m^3$ higher for the 2020 scenario in the BCS area. Due to this combination of a decreasing total and an

increasing shipping related deposition, the shipping contribution increases from 6.1 % in the base year to 7.6 % in the scenario 2020 (Table 30).
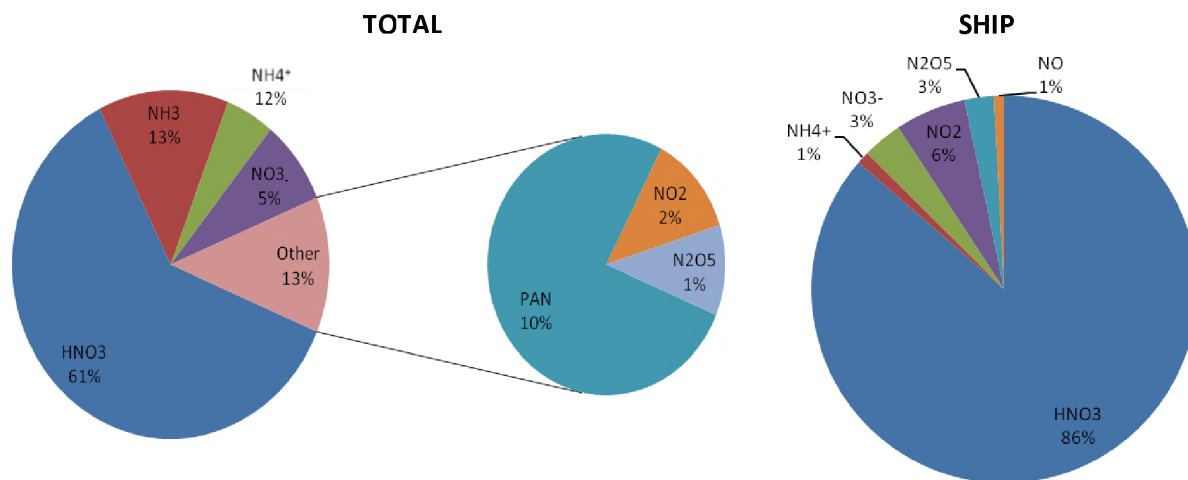

Figure 69. Speciated contribution of all sources (total on the left) and the shipping emissions alone to the nitrogen deposition for the scenario 2020

Concerning the sulphur components, the situation is very different from the one for the nitrogen components. Both in the scenario 2012 and, especially, in the scenario 2020, we can observe a significant decrease in total deposition, a very strong decrease in deposition due to shipping emissions, and hence, also a strong decrease in the contribution of shipping emissions to the deposition of sulphur to the BCS. This contribution decreases from 22.8 % in the base year to 17.3 % in the scenario 2012 and decreases even further to 3.3 % for the scenario 2020. It has to be stressed that this scenario assumes the use of diesel oil with a mass fraction of 0.1 % S for shipping activities on the North Sea.

3.7. Results for the base year for heavy metals and PAHs

3.7.1. Concentrations of heavy metals and PAHs

Figure 70 shows as an example the annual mean concentration of benzo[a]pyrene (B[a]P) for the base year for the 3 km x 3 km AURORA domain. The concentrations of benzo[b]fluoranthene (B[b]F) and benzo[k]fluoranthene (B[k]F) have also been calculated. The map shows a gradient with higher concentrations above land and lower concentrations above the sea, due to the fact that the main emission sources are located on land and shipping emissions are low in comparison to land-based emissions.

Figure 71 shows the concentration maps for the two heavy metals calculated in this study, i.e. the maps for cadmium and for lead. Also for these two compounds, concentrations above land are much higher than above the North Sea, already showing that the contribution of shipping emissions is relatively low.
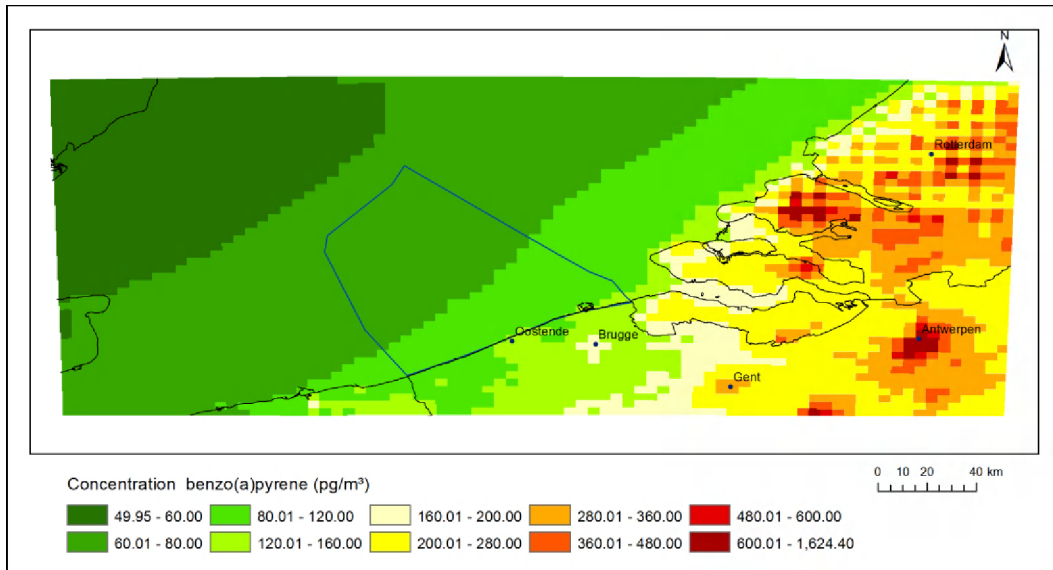
Figure 70. Concentration of benzo[a]pyrene for the 3 km x 3 km domain for the base year
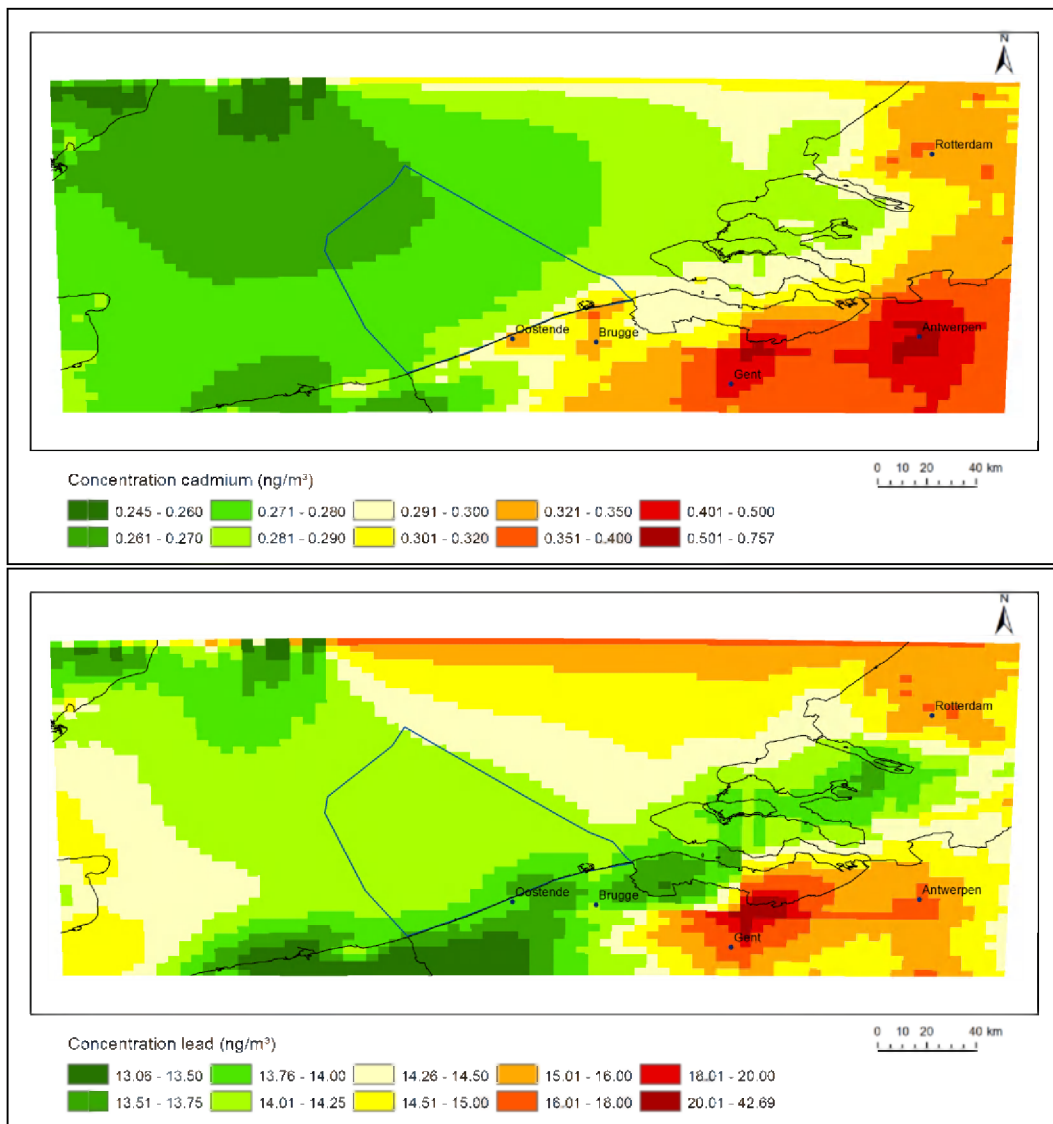

Figure 71. Concentrations of cadmium (above) and lead (below) for the base year

3.7.2. Contribution of shipping emissions to the deposition of heavy metals and PAHs

Figure 72 shows the map for the contribution of shipping emissions to the deposition of B[a]P for the base year. From this map, the contribution of the shipping emissions can clearly be seen. Much higher contributions have been calculated for the main shipping route in the BCS and for the Western Scheldt. Total contributions, however, remain relatively low with the maximum contribution to B[a]P deposition of 3.4 %, due to shipping emissions.
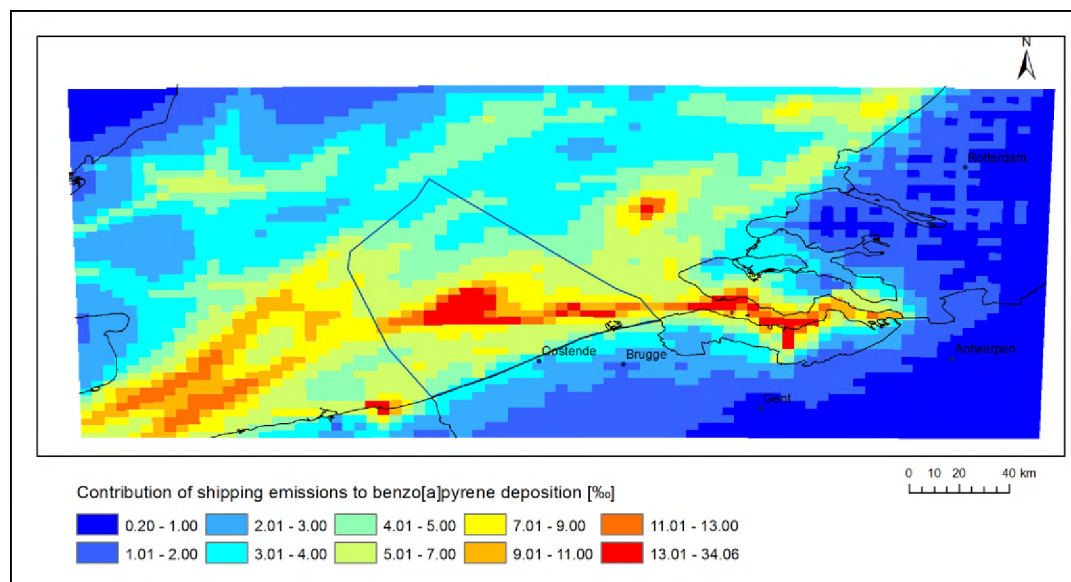
Figure 72. Contribution of shipping emissions to the deposition of B[a]P for the base year

Figure 73 shows the maps for the contribution of shipping emissions to the deposition of cadmium(Cd) and lead(Pb) in the 3 km x 3 km resolution domain. For both heavy metals, the influence of shipping emissions to the deposition is clearly visible, although the contributions stay low with maximum values of 1.3 % for Cd and 0.1 % for Pb.

Table 31 shows an overview of the annual total deposition of the studied PAHs and heavy metals to the Belgian Continental Shelf for the base year. The modelled deposition from all sources, the deposition from shipping emissions and the contribution of shipping emissions to total deposition to the BCS are shown. If we integrate over the entire BCS, the contribution of shipping emissions to the deposition of the selected PAHs and heavy metals stay low with values between 7 ‰ and 0.2 ‰.
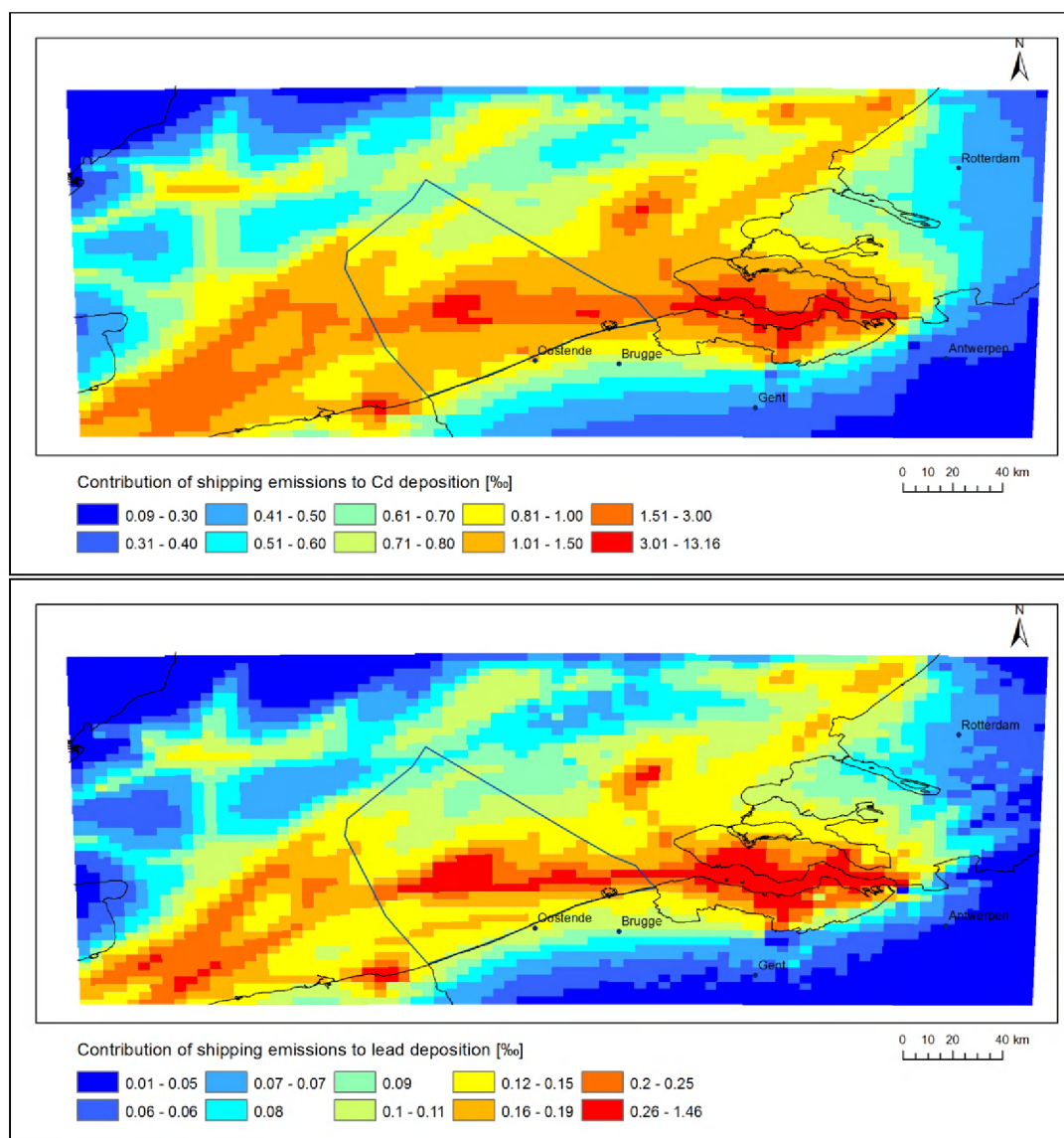
Figure 73. Contribution of shipping emissions to the deposition of Cd (above) and Pb (below)

Table 31. Overview of the annual total deposition of the studied PAHs and heavy metals to the Belgian Continental Shelf for the base year: deposition from all sources, deposition from shipping emissions and contribution of shipping emissions to total deposition for the BCS

Pollutant	Total (kg)	Ship (kg)	Ship/total (‰)
B[a]P	67	0.47	7.0
B[b]F	124	0.51	4.1
B[k]F	72	0.16	2.2
Cd	362	0.50	1.4
Pb	19390	3.11	0.2

Conclusions

The present study provides interesting insights into the ship emission activities on the Belgian Continental Shelf (BCS), the contribution of shipping emissions to air pollutant concentrations and into the contribution of shipping emissions to the deposition of air pollutants to the sea. Considerable progress has been achieved in three fields, according to WP1-3 of the present project.

In the first place, the analytical methodology elaborated and applied in the framework of the present project has been found to be suitable to evaluate the gaseous and aerosol pollutant content of marine air over the shipping routes and background sites. Onboard sampling with the assistance of high/low volume samplers, fast response, on-line monitors (e.g., air-pointer, black carbon monitor) and laboratory analysis has been proven to be well applicable to characterize several ship-emission related pollutants over marine areas.

The measurements of NO_x and SO_2 with a high resolution in space and time have been carried out onboard research vessels travelling in the Belgian marine waters. The observations provide us with valuable data concerning the spatial distribution of pollutant concentrations, showing highly fluctuating concentrations and large gradients when the ship moves around. Additionally, these data are valuable for the validation of the employed methodology for setting up shipping emissions for the BCS and for the calculations of air pollutant concentrations with air quality models.

Overall, the mass distribution for size-segregated aerosols over the Belgian North Sea is obvious; increased atmospheric levels of fine, medium and coarse particulates are experienced, mostly localized at/near marine areas with high ship traffic density, e.g., international shipping lanes, pilot stations, and entrances to large harbours. However, the air levels of the particulates show a fast drop when diverting from these areas towards marine background areas. Similar observations have been made for the distribution pattern of black carbon over the Belgian Continental Shelf during the sampling cruises.

Regarding the elemental content of size-segregated particulate matter, Cl and S dominate in the marine and coastal aerosols. However, Cl was mostly present in the medium and coarse aerosol fractions, while S and K (particularly originating from fuel burning over marine areas) was mainly obtained in the fine and the medium aerosol fractions. Comparing to these elements, lower, but still considerable contribution of Si, K, Ca and Fe was generally observed in the three aerosol fractions, with higher K levels in the finer fractions. The other elements detected were found at trace amounts in the samples. Typical tracers of the heavy fuel emission, e.g., V and Ni, were mostly observed in the fine aerosol fraction, while other trace metals, like Mn, Cu, Zn and Pb were present in the fine and/or medium particulate fractions. As a general observation, the elemental content of the size-segregated aerosols is lower at the sea-side (coastal background site) than over the marine areas with high traffic intensity. However, it should be mentioned that sea salt (mostly as Cl) contributes considerably to this enhanced elemental content of aerosols.

The atmospheric concentrations of HNO_2, HNO_3 and NH_3 acquired in this study indicate a higher gaseous pollutant content of air over the main international and the W-E shipping routes and nearby surrounding sites than those observed at either the marine or the coastal background site. The increase of the concentration of these gaseous pollutants nearby the ship routes generally varied considerably and it highly depended on the atmospheric conditions (wind speed, wind direction, fog events, temperature inversion, radiation intensity, etc.).

The water-soluble (ionic) components of three fractions size-segregated aerosols i.e., PM_1, $PM_{2.5-1}$ and $PM_{10-2.5}$ have also shown site-specific variation. The coarse particles were mostly dominating over the medium and the fine particulate. Coarse aerosols were present in the form of sea salt as Na^+, Cl^-, and Mg^{2+}, but NO_3^- and SO_4^{2-} were also observed at enhanced levels, as compared to finer aerosol fractions. The lower sized-aerosol fractions mostly consisted of NH_4^+ salts of NO_3^- and SO_4^{2-}, which are mostly products of secondary atmospheric processes. The distribution of ionic aerosol species also varied spatially. High concentrations of NO_3^-, SO_4^{2-} and NH_4^+ aerosols were observed over the main international and W-E shipping lanes and marine anchoring stations. The aerosol samples have shown increased concentrations of ionic pollutants (e.g., secondary nitrate and sulphate aerosols), as well as aged sea salt. Interestingly, a reverse trend of total mass distribution could be encountered at fog events, when the finer aerosols showed higher ionic pollutant content than the coarse particulates.

Eleven PAH compounds have been identified in the sampled PM. Benzo(bjk)fluoranthene was dominant amongst all PAHs, followed by chrysene and pyrene. Seasonally, in general, lower PAH concentrations were found in October and May months (with the exception of May 2010- here however only two samples were available from onboard sampling – due to technical problems/bad weather conditions), than during February and March. This is consistent with the fact that meteorological conditions (less daylight hour, reduced ambient air temperatures thus lower volatilization and photochemical activity) contribute to the higher PAHs levels in winter season.

In the second place, a bottom-up inventory for shipping emissions has been set up using AIS messages. In this way, shipping emissions with a high degree of precision with respect to their real positions could be established. The use of emission factors and activity data gave also confidence in the absolute emission values calculated for the BCS. Because of the fact that air quality models have to be applied to a rather large domain in order to take long-range transport of air pollution into account, shipping emissions and land-based emissions had to be set up for almost the whole of Europe. For such a large domain, AIS data and bottom-up derived shipping emissions are, however, not available. Hence, the bottom-up emissions for the BCS had to be combined with top-down shipping emission estimates for the other European marine areas.

During this combination of bottom-up and top-down emissions, large differences in emission totals were observed between the bottom-up and the top-down shipping emissions. Comparison to other available data sources suggested that the bottom-up emissions generated in this study are more reliable than the emission totals reported for the top-down approaches. Hence, we decided to scale the top-down emission totals to the values of the bottom-up emissions for the BCS. In this way, best emission estimates for the European marine areas were obtained that also included the high-resolution bottom-up emissions for the BCS.

In this way, shipping and land-based emissions were set up for a base year for the classical pollutants, for cadmium and lead and for benzo[a]pyrene, benzo[b]fluoranthene and benzo[k]fluoranthene. For the classical pollutants, emission projections were also set up for two scenarios, i.e., for the year 2012 and for the year 2020. Future legislation with respect to air pollutant emissions for all economic sectors was taken into consideration when creating these emission projections. In the case of the shipping emissions, future decreases of the maximum allowed sulphur content of the fuel have been taken into account.

In the third place, air quality model calculations have been carried out using the shipping emissions created in this project. Via a nesting procedure consisting of four steps, high-resolution (3 km x 3 km) calculations have been carried out for a domain containing the entire BCS. Concentrations of the most important air pollutants and deposition of air pollutants to the BCS

have been calculated. Additionally, the contribution of shipping emissions to the deposition of air pollutants has been investigated.

The modelled concentrations of NO_2 and SO_2 have been validated using the measurements carried out onboard the Zeeleeuw and Belgica research vessels in this project. The validation showed that modelled NO_2 concentrations, especially, for the sampling campaign in March 2010, agreed rather well with the observations made onboard the Zeeleeuw. Considering the fact that the model works with annual total emissions, which have been spread uniformly in time along the shipping routes, a rather good agreement with the observations is not evident. The latter are after all heavily influenced by the emissions of individual ships that were travelling at the moment the measurements had been carried out. The emissions from these individual ships are probably not representative for the mean emissions for that location. Nevertheless, observations and model results for NO_2 agreed surprisingly well for the March 2010 campaign. The agreement for SO_2 was not as good as for NO_2 but still fairly good so that we can conclude that, using the shipping emissions created for the 3 km x 3 km model domain, the AURORA model succeeds in representing the NO_2 and SO_2 concentrations above the BCS quite reliably. At the same time we can conclude that the created shipping emissions are obviously quite close to reality. This confirms our choice to scale the top-down emissions for the marine areas outside the BCS to the emissions derived via the bottom-up approach. It is also a clear indication that the top down shipping emissions, which are normally used in this type of modeling, are at least questionable and should be improved.

Total deposition of nitrogen and sulphur to the BCS originating from shipping and other emissions have been calculated, as well as the contribution of the shipping emissions to total deposition values. The comparison of the results for the base year with those for the scenarios 2012 and 2020 show the (potential) benefits of future emission reductions in the shipping sector. A reduction of the sulphur content of shipping fuel would indeed result in a significant decrease of the deposition of sulphur to the BCS and in a decrease of the contribution of shipping emissions to the deposition of sulphur from 23 % in the base year to 3 % in 2020. With respect to the deposition of nitrogen to the BCS no drastic changes in NOx shipping emissions are currently realistic for the North Sea, whereas a significant decrease of NOx emissions for the land-based sources is projected. Hence, the contribution of ship emission to the deposition of nitrogen to the BCS will increase in the future with high probability, unless additional measures are taken to reduce NOx emissions from the shipping sector.

Finally, the contribution of shipping emissions to the deposition of B[a]P, B[b]F, B[k]F, Cd and Pb to the BCS has been calculated. Only low contributions were found especially for the heavy metals, indicating that the influence of land-based sources is predominant for these components. However, it has to be mentioned that the uncertainty on the emissions of those compounds is rather large.

The experimental results and model observations all show a fairly good agreement between the distribution of inorganic and organic pollutant load of the Belgian Continental Shelf. The acquired deposition fluxes along shipping lanes and close proximity are commensurable with those observed at terrestrial areas, and of riverine inputs. This fact puts more emphasis on the importance of monitoring of ship-emission related marine air pollution and its legislation by authorities concerned.

Acknowledgements

References

Balzani Lööv J., Alföldy B., Lagler F., Cavalli F., Putaud J.P., Borowiak A., Bencs L., Horemans B., Van Grieken R., Pintér Csordás A., Hjorth J.(2010) Chemical characterisation of particulate and gaseous emission of seagoing vessels. Poster, presented on the 2010 International Aerosol Conference (IAC 2010), Helsinki, Finland, August 29 - September 3. 2010.

Bartnicki J., Fagerli H. (2006) Atmospheric Nitrogen in the OSPAR Convention Area in the period 1990-2004, EMEP/MSC-W Technical Report 4/2006, Oslo, ISSN 0804-2446.

Bencs L.,Ravindra K., de Hoog J., Rasoazanany E.O., Deutsch F., Bleux N., Berghmans P., Roekens E., Krata A., Van Grieken R., (2008) Mass and ionic composition of atmospheric fine particles over Belgium and their relation with gaseous air pollutants, Journal of Environmental Monitoring, 10, 1148-1157.

Charnock H. 1955 Wind stress on a water surface. Quarterly Journal of the Royal Meteorological Society, 81, 639–640.

Brown A.S., Butterfield D.M., Brown R.J.C., Hughey P., Whiteside K.J., Goddard S.L. (2011) Annual Report for 2010 on the UK PAH Monitoring and Analysis Network, Report to the Department of Environment, Food and Rural Affairs; the Northern Ireland Department of Environment; the Welsh Government and the Scottish Government

Chen T. H. et al. (1997) Cabauw experimental results from the project for intercomparison of land-surface parameterization schemes. Journal of Climate, 10, 11941215.

Cooper D.A., Peterson K., Simpson D. (1996) Hydrocarbon, PAH and PCB emissions from ferries: A case study in the Skagerak – Kattegat – Öresund region, Atmospheric Environment, 30, 2463-2473.

Corbett J.J., Winebrake J.J., Green E.H., Kasibhatla P., Eyring V., Lauer A. (2007) Mortality from ship emissions: A global assessment, Environmental Science and Technology, 41, 8512-8518.

de Leeuw G., Skjøth C.A., Hertel O. et al. (2003) Deposition of nitrogen into the North Sea. Atmospheric Environment 37 (Suppl. 1), 145–165.

DCMR (2008) EMISSIONS 2008: NETHERLANDS CONTINENTAL SHELF, PORT AREAS AND OSPAR REGION II, Final Report, Report No: 23502.620_B/3.

De Meyer P., Maes F., Volckaert A. (2008) Emissions from international shipping in the Belgian part of the North Sea and the Belgian seaports, Atmospheric Environment, 42, 196-206.

De Ridde K., Lefebre F., Adriaensen S., Arnold U., Beckroege W., Bronner C., Damsgaard O., Dostal I., Dufek J., Hirsch J., IntPanis L., Kotek Z., Ramadier T., Thierry A., Vermoote S., Wania A., Weber C. (2008) Simulating the impact of urban sprawl on air quality and population exposure in the German Ruhr area. Part II: development and evaluation of an urban growth scenario. Atmospheric Environment, 42, 7070-7077.

Deutsch F., Vankerkom J., Janssen L., Lefebre F., Mensink C., Fierens F., Dumont G., Roekens E. (2008a) Extension of the EUROS integrated air quality model to fine particulate matter by coupling to CACM/MADRID 2, Environmental Modeling & Assessment 13, 431-437.

Deutsch F., Mensink C., Vankerkom J., Janssen L. (2008b) Application and validation of a comprehensive model for PM10 and PM2.5 concentrations in Belgium and Europe, Applied Mathematical Modelling 32, 1501-1510.

Deutsch F., Janssen L., Vankerkom J., Lefebre F., Mensink C., Fierens F., Dumont G., Roekens E. (2008c) Modelling changes of aerosol compositions over Belgium and Europe, Int. J. of Environment and Pollution 32, 162-173.

Deutsch F., Vankerkom J., Janssen L., Janssen S., Bencs L., Van Grieken R., Fierens F., Dumont G., Mensink C. (2008d) Modelling concentrations of airborne primary and secondary PM10 and PM2.5 with the BelEUROS-model in Belgium, Ecological Modelling 217, 230-239.

Deutsch F., Veldeman N., Vanherle K., Lodewijks P., Duerinck J., Janssen L., Campling P., Janssen S. (2011) Beoordeling beleidsopties luchtvervuiling internationale scheepvaart, Tijdschrift Lucht 7, 30-33 (in Dutch).

Evans M.C., Campbell S.W., Bhethanabotla V. et al. (2004) Effect of sea salt and calcium carbonate interactions with nitric acid on the direct dry deposition of nitrogen to Tampa Bay, Florida. Atmospheric Environment 38, p. 4847-4858.

Fowler D., Pilegaard K., Sutton M.A. et al. (2009) Atmospheric composition change: Ecosystems-Atmosphere interactions. Atmospheric Environment 43, p. 5193-5267.

Gallagher M.W., Beswick K.M., Coe H. (2001) Ozone dry deposition to coastal waters. Quarterly Journal of the Royal Meteorological Society 127, 539–558.

Gery, M. W., G. Z. Whitten, J. P. Killus, Dodge M.C. (1989), A photochemical kinetics mechanism for urban and regional computer modeling, Journal of Geophysical Research, 94(D10), 12925– 12956.

Horemans B., Krata A., Buczynska A.J., Dirtu A.C., Van Meel K., Van Grieken R., Bencs L. (2009) Major ionic species in size-segregated aerosols and associated gaseous pollutants at a coastal site on the Belgian North Sea, Journal of Environmental Monitoring, 11, 670-677.

Kanda M. (2007) Progress in urban meteorology: A review. Journal of the Meteorological Society of Japan 85b, p. 363-383.

Klein L.M. 2002. Influence of coastal atmospheric processes on nitrogen input in coastal regions. Ph.D. Thesis, Fachbereich Geowissenschaften, University of Hamburg, Germany, 96pp.

Lefebvre W., Vercauteren J., Schrooten L., Janssen S., Degraeuwe B., Maenhaut W., de Vlieger I., Vankerkom J., Cosemans G., Mensink C., Veldeman N., Deutsch F., Van Looy S., Peelaerts W., Lefebre F. (2011) Validation of the MIMOSA-AURORA-IFDM model chain for policy support: Modeling concentrations of elemental carbon in Flanders. Atmospheric Environment, 45, 6705-6713.

Maes J., Vliegen J., Van de Vel K., Janssen S., Deutsch F., De Ridder K., Mensink C. (2009) Spatial surrogates for the disaggregation of CORINEAIR emission inventories, Atmospheric Environment 43, 1246-1254.

Mensink C., De Ridder K., Lewyckyj N., Delobbe L., Janssen L., Van Haver P. (2001) Computational aspects of air quality modelling in urban regions using an optimal resolution approach (AURORA). Large-Scale Scientific Computing – Lecture Notes in Computer Science, 2179, 299-308.

Nenes A., Pandis S.N., Pilinis C. (1998) ISORROPIA: A new thermodynamic equilibrium model for multiphase multi-component inorganic aerosols, Aquatic Geochemistry, 4, 123-152.

Pryor S.C., Barthelmie R.J. (2002) Particle dry deposition to water surfaces: processes and consequences. Marine Pollution Bulletin 41, p. 220-231.

Rendell A.R., Ottley C.J., Jickels T.D., Harrison R.M., 1993. The atmospheric input of nitrogen species to the North Sea. Tellus B 45, 53–63.

Rojas A.L.P., Venegas L.E. (2009) Atmospheric deposition of nitrogen emitted in the Metropolitan Area of Buenos Aires to coastal waters of de la Plata River. Atmospheric Environment 43, p. 1339-1348.

Schlunzen K.H. (2002) Simulation of transport and chemical transformations in the atmospheric boundary layer—review on the past 20 years developments in science and practice. Meteorologische Zeitschrift, 11, 303–313.

Schlunzen H. K., Mayer E.M.I. (2007) Impacts of meteorological situations and chemical reactions on daily dry deposition of nitrogen into the southern North Sea. Atmospheric Environment, 41, 289-302.

Spolnik Z., Belilov K., Van Meel K., Adriaenssens E., De Roeck F., Van Grieken R. (2005) Optimization of measurement conditions of an energy dispersive X-ray fluorescence spectrometer with high-energy polarized beam excitation for analysis of aerosol filters. Applied Spectroscopy, 59, 1465-1469.

Van de Vel K., Mensink C., De Ridder K., Deutsch F., Maes J., Vliegen J., Aloyan A., Yermakov A., Arutyunyan V., Khodzher T., Mijling B. (2008) Air-quality modelling in the Lake Baikal region, Environmental Monitoring and Assessment 165, 665-674.

Viaene P., Janssen L., Jongen S., Veldeman N., Celis D., Lefebre F. (2010) Atmosferische depositie van probleemstoffen voor de waterkwaliteit: ruimtelijke spreiding, VITO-report 2010/RMAR/0151, study by order of the Flemish Environment Agency (in Dutch).

Walcek C.J. (2000) Minor flux adjustment near mixing ratio extremes for simplified yet highly accurate monotonic tracer advection, Journal of Geophysical Research, 105, 9335-9348.

Yarwood, G., Rao S., Yocke M., Whitten G.Z., 2005, Updates to the Carbon Bond Mechanism: CB05 Report to the U.S. Environmental Protection Agency RT-04-00675, 246 pp.

Zilitinkevich S.S., Mironov D. (1996) A multi-limit formulation for the equilibrium depth of a stably stratified boundary layer. Boundary-Layer Meteorology 81, p. 325-351.

Zilitinkevich S.S., Grachev A.A., Fairall C.W. (2001) Scaling Reasoning and Field Data on the Sea Surface Roughness Lengths for Scalars. Journal of Atmospheric Sciences, 58, 320-325.